UNIVERSITY
OF MICHIGAN
MAR 6
1958
MAR 1958
PHYSICS
LIBRARY

Journal of Research

of the

National Bureau of Standards

FEBRUARY 1958

VOLUME 60 NUMBER 2

U. S. DEPARTMENT OF COMMERCE
Sinclair Weeks, Secretary
NATIONAL BUREAU OF STANDARDS
A. V. Astin, Director

FEBRUARY • 1958
VOLUME • 60
NUMBER • 2

JOURNAL OF RESEARCH
of the
NATIONAL BUREAU OF STANDARDS

The National Bureau of Standards

Functions and Activities

The functions of the National Bureau of Standards are set forth in the Act of Congress, March 3, 1901, as amended by Congress in Public Law 619, 1950. These include the development and maintenance of the national standards of measurement and the provision of means and methods for making measurements consistent with these standards; the determination of physical constants and properties of materials; the development of methods and instruments for testing materials, devices, and structures; advisory services to Government Agencies on scientific and technical problems; invention and development of devices to serve special needs of the Government; and the development of standard practices, codes, and specifications. The work includes basic and applied research, development, engineering, instrumentation, testing, evaluation, calibration services, and various consultation and information services. A major portion of the Bureau's work is performed for other Government Agencies, particularly the Department of Defense and the Atomic Energy Commission. The scope of activities is suggested by the listing of divisions and sections on the inside of the back cover.

Publications

The results of the Bureau's work take the form of either actual equipment and devices or published papers. These papers appear either in the Bureau's own series of publications or in the journals of professional and scientific societies. The Bureau itself publishes three monthly periodicals, available from the Government Printing Office: The Journal of Research, which presents complete papers reporting technical investigations; the Technical News Bulletin, which presents summary and preliminary reports on work in progress; and Basic Radio Propagation Predictions, which provides data for determining the best frequencies to use for radio communications throughout the world. There are also five series of nonperiodical publications: The Applied Mathematics Series, Circulars, Handbooks, Building Materials and Structures Reports, and Miscellaneous Publications.

Information on the Bureau's publications can be found in NBS Circular 460, Publications of the National Bureau of Standards ($1.25) and its Supplement ($0.75), available from the Superintendent of Documents, Government Printing Office, Washington 25, D. C.

Order all publications from the Superintendent of Documents
U. S. Government Printing Office, Washington 25, D. C.

Use of funds for printing this publication approved by the Director of the Bureau of the Budget (May 14, 1956)

Journal of Research of the National Bureau of Standards Vol. 60, No. 2, February 1958 Research Paper 2824

Energy Spectra of Cascade Electrons and Photons[1]

Charles A. Olson [2] and Lewis V. Spencer

The equations for the energy spectra of electrons and photons in a cascade shower are written in a form suitable for numerical applications with accurate cross sections. Trial calculations were carried out to check the feasibility of a step-by-step numerical integration procedure similar to that used successfully at low energies in noncascade problems. Numerical results were obtained for lead by using a monoenergetic source of electrons at 360 mc^2 and extreme relativistic cross-sectional forms, which assume complete screening. The method was designed to permit the determination of cascade-shower spectra, spatial distributions, and directional distributions that are exact in the sense that the main limiting factor is the accuracy with which the cross sections are known. The numerical results of the trial calculations were found to agree with previously published results based on more restrictive methods of analysis.

1. Introduction

High-energy electrons and photons dissipate their energy by generating secondary electrons and photons. The complex radiation arising in this manner from a high-energy electron or photon source is called a cascade shower. Most attempts to describe this phenomenon have used approximations that are valid only at very high energies, i. e., in the extreme relativistic range; and the results have only limited applicability in a broad range of lower energies where the cascade phenomenon is still of importance. At these lower energies realistic calculations must be largely numerical because the accurate cross-sectional forms are too complicated to permit analytic transformations.

In this paper a calculational procedure which applies without restrictions on cross-sectional forms, and which has been used in noncascade problems, is adapted to the cascade situation. It should provide an adequate way of describing cascade-shower spectra in any energy range. Because the equations are part of a linked set of moment equations, which describe also spatial and directional distributions, and possibly fluctuations, the procedure in this paper may eventually form the basis for a more complete description of many aspects of the cascade problem.

The equations are applied, in a trial calculation, to the special case of a monoenergetic electron source. Calculations for an electron source are more important than for a photon source for the following reason: If a photon source is assumed, it is possible to calculate the resulting photon spectrum at all energies. This type of calculation has been done many times and offers no difficulty (for an example, see reference [1]).[3] One can then determine by simple quadrature the electron spectrum generated by this photon spectrum. The whole cascade spectrum of electrons and photons, except for the initial photon component already determined, can then be determined by appropriate superposition of solutions for monoenergetic electron sources. Thus, calculations for a monoenergetic electron source demonstrate that the main difficulty blocking a complete numerical analysis of the cascade problems is removed.

For the initial calculation, extreme relativistic cross-sectional forms that assume complete screening are used. They include the same types of singularity as the exact cross sections and therefore provide a meaningful trial run. Also they are quite similar to the cross-sectional forms used in earlier applications of conventional cascade theory; so they make possible a direct check with previously published results.

[1] This work was supported by the Office of Naval Research and the Atomic Energy Commission.
[2] Submitted to the University of Maryland in partial fulfillment of the requirements for the M. S. degree.
[3] Figures in brackets indicate the literature references at the end of this paper.

2. Interactions Involved in Cascade Showers

The two types of interactions that predominate in the development of cascade showers are bremsstrahlung and pair production. In a bremsstrahlung interaction a high-energy electron or positron, under the influence of a nuclear or electronic field, generates a photon. In pair production a high-energy photon in the electromagnetic field of a nucleus or electron gives up all its energy to generate an electron and a positron. The combination of these two processes results in the creation of photons, electrons, and positrons in increasing numbers at lower energies.

At all energies below the extreme relativistic range, there are additional effects that influence the development of the showers. There are energy losses due to atomic interactions that slow down the electrons more or less continuously along their path. Some of these interactions result in secondary electrons with high energies, i. e., knock-on electrons. Compton scattering also contributes some high-energy electrons to the shower, but at low energies it is of primary importance through its influence on the photon spectrum. The photoelectric effect and photonuclear interactions have cross sections that are much smaller than the other interactions at all cascade-shower energies, though the former is of importance below shower energies.

3. Discussion of Earlier Work

An excellent discussion of the lines along which the mathematical description of the cascade phenomenon has been developed can be found in a book by B. Rossi [2]. Because the procedural methods of this paper are directed mainly toward a solution of the cascade problem at low energies where accurate cross-sectional forms are needed, comments here on earlier work will be restricted to developments pertinent to these lower energies.

The first attempt to describe a low-energy cascade spectrum was made by Arley [3]. He neglected interactions that slow down the electrons, i. e., ionization losses, above the critical energy;[4] and he further neglected bremsstrahlung and the generation of secondary electrons by all processes at energies below the critical energy. His results as compared with more recent calculations are low by a factor of 3 or 4.

Tamm and Belenky [4] have obtained a much more accurate solution by an analytic method, using asymptotic cross-sectional forms for bremsstrahlung and pair production, assuming continuous ionization loss and neglecting the Compton effect and knock-on electrons. Their solution has proved to be more accurate than was at first expected, considering the approximations. Friedman [5] has discussed their solution at length and computed a first correction term. This correction term never exceeded 4.5 percent of the original solution in the case that Friedman considered.

Perhaps the most satisfactory treatment of the energy-spectra problem for low energies has been given by Richards and Nordheim [6]. They have used reasonably accurate representations for all important interactions, but they treat small radiation and ionization losses as continuous, thus incurring an error of up to 8 percent, according to their own estimates. They obtain results by numerical integration for energies from ½ to 10 times the critical energy. Their results are not absolute and do not describe the spectra near the initial energy. To obtain more complete spectra, it is necessary to normalize their equations to a solution valid at high energies, and they have used the results of Rossi and Greisen [7] for this purpose.

All these calculations are difficult to generalize to a more accurate treatment of all the different interactions, and hence there is a need for a new approach that will permit use of arbitrarily accurate cross sections.

4. Analytic Treatment of the Problem

In this section equations will be derived for the energy spectra of electrons and photons. No distinction is made between positrons and electrons, the two being considered as having

[4] The critical energy in a given material is the energy at which the radiation losses of an electron equal the ionization losses.

identical cross sections and combining to make up an "electron" spectrum. The differential energy spectrum for electrons will be represented by $I(E)dE$, which is the track length traveled by all electrons in the energy range E to $E+dE$. $H(\alpha)d\alpha$ represents the photon spectrum similarly.[5] In all cases energies are in units of mc^2, and the electron energies include the rest energy.

To set up equations in terms of $I(E)$ and $H(\alpha)$, a time-independent source is assumed. Physically, this means a continuous cascade in which the average number of electrons, positrons, and photons at any given energy remains constant with time. The equations will be derived in a general form, and considerations of the interactions and cross-sectional forms will be reserved for a separate section.

Continuity equations for $I(E)$ and $H(\alpha)$ can be written as follows:

$$\int_E^\infty dE' k^{es}(E',E) I(E') = s^{eg}(E) + \int_E^\infty d\alpha' k^{eg}(\alpha',E) H(\alpha') \tag{1}$$

$$\int_\alpha^\infty d\alpha' k^{ps}(\alpha',\alpha) H(\alpha') = s^{pg}(\alpha) + \int_\alpha^\infty dE' k^{pg}(E',\alpha) I(E'), \tag{2}$$

where

$k^{es}(E',E)$ is the total probability per unit path length traveled for an electron of energy E' to undergo an interaction that removes it from the energy range above E,

$k^{eg}(\alpha',E)$ is the total probability per unit path length traveled for a photon of energy α' to generate an electron of energy greater than E,

$s^{eg}(E)$ is the total source strength for generating electrons with energies greater than E, and

$k^{ps}(\alpha',\alpha)$, $k^{pg}(E',\alpha)$, and $s^{pg}(\alpha)$ are similar quantities with the photon and electron roles reversed.

Note that the superscripts refer to "electron scattering," "photon generating," etc., although strictly speaking the interactions include types other than scattering. Physically, eq (1) states that for a time-dependent source the rate at which electrons are removed from the energy range above E is equal to the rate at which electrons come into the energy range above E. Equation (2) has the same meaning for photons.

Equations (1) and (2) completely define $I(E)$ and $H(\alpha)$ for specified sources; however, these equations as they stand are not very suitable for numerical work. It is advantageous to make further transformations suggested by the nature of the variations of spectra and cross sections. The particular choice given here is based largely on numerical and analytic exploratory calculations that are not sufficiently pertinent to the main discussion to warrant a detailed description, but some general arguments to justify this choice are given below.

$I(E)$ may vary rapidly if $s^{eg}(E)$ is discontinuous (i. e., if the source is concentrated at some energy), as for example, in the case of figure 1 in reference [8]. A more slowly varying function on which to base a step-by-step numerical integration is

$$F(E) = \int_E^\infty dE' I(E'),$$

which gives the track length traveled by all electrons while their energy is above E. The function $H(\alpha)$ may also be singular if the source function $s^{pg}(\alpha)$ is discontinuous, but photon cross sections permit the removal of such singularities by iteration (see, for example, reference [9]). It is therefore not necessary to utilize an integral form of the photon spectrum.

Equation (1) could be rewritten in terms of $F(E)$ by partial integration, but this results in the differentiation of $k^{es}(E',E)$, which is already singular as E' approaches E. A further transformation is needed to make the equation more tractable, namely integration of all terms of eq (1). With regard to eq (2), $k^{ps}(\alpha',\alpha)$ and $k^{pg}(E',\alpha)$ are integrals of nonsingular cross sections. It is therefore possible, and in fact advantageous, to accompany the partial integration of the last term in eq (2) with a *differentiation* of all terms in the equation.

[5] $I(E)$ and $H(\alpha)$ are in the units g cm^{-2}(Mc^2)$^{-1}$ sec^{-1}. These are track-length units referring to a source of one electron. The dimensions of $I(E)$ and $H(\alpha)$ change to those of flux if the source is 1 electron per gram per second.

Applying these transformations we obtain for the left side of eq (1)

$$\int_E^\infty dE' \int_{E'}^\infty dE'' k^{es}(E'',E') I(E'') = \int_E^\infty dE' I(E') \int_E^{E'} dE'' k^{es}(E',E'')$$

$$= \int_E^\infty dE' F(E') \frac{\partial}{\partial E'} \int_E^{E'} dE'' k^{es}(E',E'').$$

The other term in the integration by parts, $-F(E')\left[\int_E^{E'} dE'' k^{es}(E'E'')\right]\Big|_E^\infty$, is zero at both limits.

Equation (1) thus becomes

$$\int_E^\infty dE' K^{es}(E',E) F(E') = S^{eg}(E) + \int_E^\infty d\alpha' K^{eg}(\alpha',E) H(\alpha'), \tag{3}$$

where

$$K^{es}(E',E) = \frac{\partial}{\partial E'} \int_E^{E'} dE'' k^{es}(E',E''),$$

$$K^{eg}(\alpha',E) = \int_E^{\alpha'} dE' k^{eg}(\alpha',E'),$$

$$S^{eg}(E) = \int_E^\infty dE' s^{eg}(E').$$

Equation (2) becomes

$$\mu(\alpha) H(\alpha) - \int_\alpha^\infty d\alpha' K^{ps}(\alpha',\alpha) H(\alpha') = S^{pg}(\alpha) + \int_\alpha^\infty dE' F(E') K^{pg}(E',\alpha), \tag{4}$$

Note that the other term on the right side,

$$\frac{\partial}{\partial \alpha}\{F(E') k^{pg}(E',\alpha)|_{E'=\alpha}^\infty\},$$

obtained after integration by parts, is zero at both limits.

The various quantities in (4) are defined as follows:

$$\mu(\alpha) = k^{ps}(\alpha,\alpha) \tag{4a}$$

is the total photon interaction probability per unit path length for photons at energy α.

$$K^{ps}(\alpha',\alpha) = \frac{\partial k^{ps}(\alpha',\alpha)}{\partial \alpha} = NZ\sigma(\alpha',\alpha), \tag{4b}$$

where $\sigma(\alpha',\alpha)$ is the photon differential scattering cross section per electron, and N is the number of atoms per gram.

$$K^{pg}(E',\alpha) = -\frac{\partial^2 k^{pg}(E',\alpha)}{\partial E' \partial \alpha} = \frac{\partial}{\partial E'} N\sigma(E',\alpha), \tag{4c}$$

where $\sigma(E',\alpha)$ is the cross section per atom for producing radiation.

$$S^{pg}(\alpha) = -\frac{\partial s^{pg}(\alpha)}{\partial \alpha} \tag{4d}$$

s the photon source strength at α.

5. Interactions and Cross Sections

Equations (3) and (4) as derived in section 4 make no reference to specific interactions or cross-sectional forms, and consequently this choice can be adapted to the specific nature of each problem. In terms of the interactions discussed in section 2, the functions K may be written

$$K^{es}(E',E)=K_{\text{bremsstrahlung losses}}+K_{\text{atomic interactions}},$$

$$K^{eg}(\alpha',E)=K_{\text{pair production}}+K_{\text{Compton electrons}},$$

$$K^{ps}(\alpha',\alpha)=K_{\text{Compton photons}},$$

$$K^{pg}(E',\alpha)=K_{\text{bremsstrahlung photons}},$$

$$\mu(\alpha)=\mu(\alpha)_{\text{pair production}}+\mu(\alpha)_{\text{Compton photons}}+\mu(\alpha)_{\text{absorption}}.$$

At this point accurate cross-sectional forms could be introduced in the equations, but an examination of their suitability can be made with simplified forms similar to whose used by earlier investigators. Specifically, (a) extreme relativistic cross sections are used, (b) complete screening is assumed, and (c) the rest mass of the electron has been neglected insofar as it influences the limits of the integrals. Detailed cross sections are given in appendix 1. The K functions derived from these cross-sectional forms are

$$K^{es}(E',E)=N4\bar{\varphi}\left\{\left[-\frac{1}{3}-\frac{4}{3}\ln(1-\eta)+\frac{4}{3}(1-\eta)-\frac{1}{6}\eta^2-\frac{1}{3}\eta^3\right]\ln 183Z^{-\frac{1}{3}}\right.$$
$$\left.-\frac{1}{18}-\frac{1}{9}\ln(1-\eta)+\frac{1}{9}(1-\eta)-\frac{\eta^2}{18}\right\}+NZ\frac{3}{4}\varphi_T\frac{1}{E'}\left[\frac{2\eta-1}{(1-\eta)}\right],$$

where $\eta=E/E'$;

$$K^{eg}(\alpha',E)=N8\bar{\varphi}\alpha'\left\{\left[\frac{7}{18}-\frac{7}{9}\eta+\frac{1}{2}\eta^2-\frac{2}{9}\eta^3+\frac{1}{9}\eta^4\right]\ln 183Z^{-\frac{1}{3}}-\frac{1}{108}+\frac{\eta}{54}-\frac{\eta^3}{54}\right.$$
$$\left.+\frac{\eta^4}{108}\right\}+NZ\frac{3}{8}\varphi_T\left[(1-\eta)\left(\ln E+\ln\frac{1-\eta}{\eta}+\ln 2-\frac{1}{2}\right)+\frac{1}{2}\eta^2-\frac{1}{6}\eta^3-\frac{1}{3}\right],$$

where $\eta=E/\alpha'$;

$$K^{ps}(\alpha',\alpha)=NZ\frac{3}{8}\varphi_T\frac{1}{\alpha^2}(\eta^3+\eta),$$

where $\eta=\alpha/\alpha'$;

$$K^{pg}(E',\alpha)=N4\bar{\varphi}\frac{1}{\alpha^2}\left[\left(-\frac{4}{3}\eta^2+2\eta^3\right)\ln 183Z^{-\frac{1}{3}}-\frac{1}{9}\eta^2\right],$$

where $\eta=\alpha/E'$; and

$$\mu(\alpha)=N4\bar{\varphi}\left[\frac{7}{9}\ln 183Z^{-\frac{1}{3}}-\frac{1}{54}\right]+NZ\frac{3}{8}\bar{\varphi}_T\frac{1}{\alpha}\left[\ln 2\alpha+\frac{1}{2}\right].$$

6. Numerical Treatment of the Problem

In determining a convenient system for the numerical integration, we note that the functions K depend primarily on ratios between the two energies involved. We wish to take advantage of this scaling property by choosing integration steps of equal length in the logarithm of this energy ratio. This choice of integration mesh has the additional advantages that one can integrate over an enormous energy range with comparatively few steps, and that a cross-sectional tabulation can be made that is applicable to widely different energy ranges.

The numerical integration is performed by Simpson's rule, using modifications of the familiar $(\frac{1}{3}, \frac{4}{3}, \frac{2}{3}, \frac{4}{3}, \frac{1}{3})\Delta$ set of weights to make the rule apply also to an odd number of intervals.

The integrals were computed essentially as follows:

$$\int dE' K^{es}(E',E)F(E') = \int d(\ln E')E'K^{es}(E',E)F(E')$$

$$= \sum_{i=0}^{n} \omega'_{in} E_i K^{es}(E_i,E_n)F(E_i)$$

$$= \sum_{i=0}^{n} \omega_{in} K^{es}(E_i,E_n)F(E_i).$$

Note that the integration weights ω_{in} decrease in size as the energy decreases. More details are given in appendix 2.

Despite the transformations discussed in section 4, the function $K^{es}(E',E)$ in eq (3) is still singular. However, this singularity causes no difficulty if one writes the integral in the following manner:

$$\int_E^\infty dE' K^{es}(E',E)F(E') = \int_E^\infty dE' K^{es}(E',E)[F(E')-F(E)] + F(E)\int_E^\infty dE' K^{es}(E',E).$$

Note that the first term on the right is no longer singular and can be integrated numerically. The last term can be evaluated without difficulty by integrating the singular parts of $K^{es}(E',E)$ analytically. Notice also that as $E' \to E$, the first integrand is finite, approaching the limit $A[\partial F(E)/\partial E]$, where $A = \lim_{E' \to E}(E'-E)K^{es}(E',E)$. This term is very small and needs to be evaluated only approximately. A three-point numerical differentiation formula, described in appendix 2, was adopted for this purpose, the corresponding weights being denoted by a_i. By utilizing these devices, we represent the first integral of eq (3) as the sum of terms

$$F(E_n)[\mathscr{K}^{es}(E_n) - \sum_{i=0}^{n-1} \omega_{in} K^{es}(E_i,E_n) + Aa_n] + \sum_{i=0}^{n-1}[\omega_{in} K^{es}(E_i,E_n) + Aa_i]F(E_i),$$

where $\mathscr{K}^{es}(E) = \int_E^\infty dE' K^{es}(E',E)$. Note that a_i is zero except for $i=n,\ n-1,\ n-2$.

If the functional form of $K^{es}(E',E)$ is that given in section 5,

$$\mathscr{K}^{es}(E) = N4\bar{\varphi}E_0\left\{\left[-\frac{1}{3}-\frac{4}{3}(1-\eta)\ln(1-\eta)+\frac{4}{3}(1-\eta)+\frac{1}{6}\eta^2+\frac{1}{6}\eta^3\right]\ln 183Z^{-1/3} - \frac{1}{18}\right.$$

$$\left. -\frac{1}{9}(1-\eta)\ln(1-\eta)+\frac{1}{9}(1-\eta)+\frac{\eta^2}{18}\right\} + NZ^2\frac{3}{4}\varphi_T \ln\frac{\eta(1-\eta)E_0}{\bar{Q}},$$

where $\eta = E/E_0$, and E_0 is the highest energy of the source of electrons and photons. For a discussion of the choice of the cutoff value $\bar{Q}$, see reference [8]. In this paper it has been evaluated as follows:

$$\bar{Q} = \frac{1}{2}\left(\frac{I_0 Z}{mc^2}\right)^2 \frac{e}{E_0^2 - 1} = 4.9214 \times 10^{-11},$$

where $I_0 = 13.5$ ev.

The function $K^{pg}(E',\alpha)$ in eq (4) is not singular, but the exact expression varies rapidly as $E' \to \alpha$. This can easily be taken into account by using addition-subtraction as before:

$$\int_\alpha^\infty dE' K^{pg}(E',\alpha)F(E') = \int_\alpha^\infty dE' K^{pg}(E',\alpha)[F(E')-F(E)_{E=\alpha}] + F(E)_{E=\alpha}\int_\alpha^\infty dE' K^{pg}(E',\alpha).$$

Written as a sum, this term becomes

$$F(E_n)[\mathscr{K}^{pg}(\alpha_n)-\sum_{i=0}^{n-1}\omega_{in}K^{pg}(E_i,\alpha_n)]+\sum_{i=0}^{n-1}\omega_{in}K^{pg}(E_i,\alpha_n)F(E_i),$$

where $\mathscr{K}^{pg}(\alpha)=\int_{\alpha}^{\infty}dE'K^{pg}(E',\alpha)$. If the functional form of $K^{pg}(E',\alpha)$ is that given in section 5,

$$\mathscr{K}^{pg}(\alpha)=N4\bar{\varphi}\alpha^{-1}\left[\left(\frac{4}{3}-\frac{4}{3}\eta+\eta^2\right)\ln 183Z^{-1/3}+\frac{1-\eta}{9}\right],$$

where $\eta=\alpha/E_0$.

Equations (3) and (4) can now be written in their final form for numerical evaluation:

$$F(E_n)=\frac{1}{C^e(E_n)}\left[-\sum_{i=0}^{n-1}W_{in}^{es}F(E_i)+\sum_{i=0}^{n-1}W_{in}^{eg}H(\alpha_i)+S^{eg}(E_n)\right] \tag{5}$$

$$H(\alpha_n)=\frac{1}{C^p(\alpha_n)}\left[F(E_n)D^{pg}(\alpha_n)+\sum_{i=0}^{n-1}W_{in}^{pg}F(E_i)+\sum_{i=0}^{n-1}W_{in}^{ps}H(\alpha_i)+S^{pg}(\alpha_n)\right], \tag{6}$$

where

$$\left.\begin{aligned}
W_{in}^{es}&=\omega_{in}K^{es}(E_i,E_n)+Aa_i,\\
W_{in}^{eg}&=\omega_{in}K^{eg}(\alpha_i,E_n),\\
W_{in}^{pg}&=\omega_{in}K^{pg}(E_i,\alpha_n),\\
W_{in}^{ps}&=\omega_{in}K^{ps}(\alpha_i,\alpha_n),\\
C^e(E_n)&=\mathscr{K}^{es}(E_n)-\sum_{i=0}^{n-1}\omega_{in}K^{es}(E_i,E_n)+Aa_n,\\
C^p(\alpha_n)&=\mu(\alpha_n)-\omega_{nn}K^{ps}(\alpha_n,\alpha_n),\\
D^{pg}(\alpha_n)&=\mathscr{K}^{pg}(\alpha_n)-\sum_{i=0}^{n-1}W_{in}^{pg}.
\end{aligned}\right\} \tag{7}$$

These seven functions depend only on cross-sectional forms, and they are evaluated separately prior to the main calculation. Note that eq (5) depends on $F(E_i)$ and $H(\alpha_i)$ but not on $H(\alpha_n)$, while eq (6) depends on $F(E_n)$ and on $F(E_i)$ and $H(\alpha_i)$. Therefore, eq (6) must be determined after eq (5) at each step in the integration. The problem of how to start the calculation is taken up in the next section.

7. Special Solution Near E_0

$F(E)$ and $H(\alpha)$ must vanish at the highest energy, E_0. It would be possible to use eqs (5) and (6), with the cross-sectional forms that have been listed, to solve for the spectra near E_0. But it was found more convenient and accurate to do a separate calculation because the solution near E_0 has certain special features. In particular, we note that (1) for small energy losses it is always possible to use extremely simple cross-sectional forms, (2) the linkage between the electron and photon equations can be simplified because the higher cascades have negligible influence in this energy region, and (3) it is possible, though not necessarily desirable, to seek analytic solutions.

Because even an analytic development leads to a numerical integration, it appeared most expeditious to employ eq (3), with the simplifications just mentioned and a finer integration spacing, to develop a solution in this region. In particular, for an electron-generated cascade, the term for generating electrons from photons and the term $A[\partial F(E)/\partial E]$ are very small and can be neglected. The remaining functions K can be written in the approximate form:

$$K^{es}(E',E)=\frac{A}{E'-E}-B\ln\frac{E'-E}{E_0}+C,$$

$$\mathscr{K}^{es}(E)=A\ln\frac{E_0-E}{Q}-B(E_0-E)\ln\frac{E_0-E}{eE_0}+C(E_0-E),$$

where A, B, and C are constants (see appendix 1).

The quantities (7) were tabulated at $E_0\times 2^{-m/6}$, where $m=\frac{1}{8},\frac{1}{4},\frac{1}{2},1$. This spacing required a special set of weights; but otherwise the evaluation in this special case is carried out by using the appropriate form of eq (5) in a manner similar to the main calculation. Results of this special solution not only give the solution near E_0 but also permit a more accurate evaluation of the integrals in eq (3) for $\alpha',E'\geq E_0\times 2^{-1/6}$. In this energy region the use of Simpson's rule with $2^{-1/6}$ spacing is not really a good enough approximation because $F(E)$ has large nonquadratic variations.

8. Calculations

The calculations in this paper are based on a monoenergetic source of 1 electron per second at 360 mc^2 in lead. Results were first obtained for the special solution near E_0. The main calculation, extending down to 5.6 mc^2, was carried out in two parts, using the mesh $E_0\times 2^{-m/6}$ to the energy $\frac{1}{4}E_0$ and the mesh $E_0\times 2^{-m/3}$ from that energy to $E=5.6\ mc^2$.

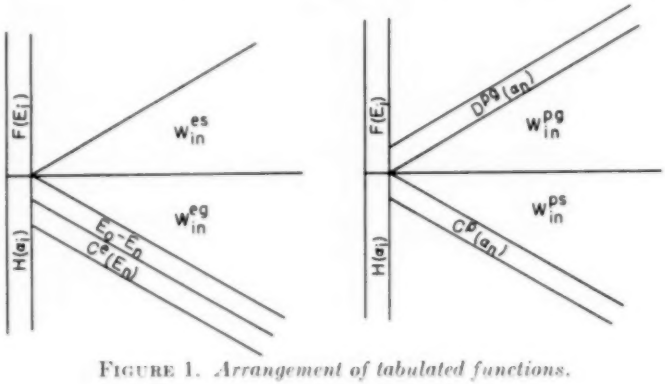

FIGURE 1. *Arrangement of tabulated functions.*

The calculation was facilitated by arranging a triangular tabulation of the four W's and a linear tabulation of the C's and D in a form shown in figure 1. Most of the work went into tabulating K functions and W's, the final computation being carried out in a few hours. The results are given in table 1.

Any error had the effect of introducing an oscillation in the final computation, with alternate points being too high and too low. The integration procedure appeared stable in that such oscillations tended to damp out slowly rather than to magnify. By plotting the results it was possible to use these oscillations to find errors. The final sequence of numbers is smooth, i. e., nonoscillatory, to better than 1 percent, which may indicate that the integration procedure introduced errors no larger than this, although the possibility that errors may have piled up at low energy is not excluded.

TABLE 1. *Results*

E	$F(E)$	$H(\alpha)$	E	$F(E)$	$H(\alpha)$	E	$F(E)$	$H(\alpha)$
360.0	0	0	160.4	5.26	0.0409	28.4	22.4	1.44
354.8	0.751	.....	142.9	5.92	.0537	22.5	26.8	2.20
349.8	.980	.....	127.3	6.52	.0693	17.9	31.4	3.27
339.8	1.35	0.00488	113.4	7.31	.0901	14.2	36.5	4.80
320.7	1.76	.00652	101.0	7.97	.115	11.3	41.6	6.85
285.7	2.47	.00985	90.0	8.91	.148	8.93	47.9	10.1
254.6	3.05	.0135	71.4	10.5	.235	7.09	53.8	13.8
226.8	3.61	.0180	56.7	13.0	.384	5.63	60.3	19.2
202.0	4.14	.0238	45.0	15.6	.601			
180.0	4.71	.0314	35.7	18.9	.944			

9. Discussion of Results

The results in table 1 are plotted in figures 2 and 3, where they are compared with the results of Richards and Nordheim [6] and calculations based on the analytic solution given by Rossi and Greisen [7]. (See appendix 3 for a discussion of the normalization.) For the comparatively low initial energy considered here, the equations of Rossi and Greisen are only accurate in a very limited energy region around 130 mc^2. At lower energies, as pointed out by Richards and Nordheim [6], a more accurate representation of the interaction probabilities is necessary. The Richards and Nordheim numerical calculation was based on more accurate cross-sectional forms, but their results are normalized to those of Rossi and Greisen at 131 mc^2. Thus, near that energy, the significant comparison is with Rossi and Greisen. At lower energies, due to differences in the cross-sectional functions involved, the three curves go apart. At energies near E_0 no comparable calculations have been found. Thus the only energy region where close agreement between the spectra calculated in this paper and those given by the other authors could be expected is from $\frac{1}{2}$ to $\frac{1}{4}E_0$. In this region the agreement is shown in figures 2 and 3 to be quite good.

Through a consideration of the specific cross-sectional forms used in the three calculations, some further comparisons are possible at lower energies. For example, the spectra of Rossi and Greisen indicate a larger number of electrons and a smaller number of photons than reported in this paper. This is caused mainly by the cross section for pair production, which is significantly lower under the complete screening approximation than the asymptotic form used by Rossi and Greisen. Thus, in the calculations in this paper, low-energy photons do not generate as many electrons, and there results a decrease in $F(E)$ and an increase in $H(\alpha)$ relative to Rossi-Greisen. The spectra of Richards and Nordheim indicate a much larger number of electrons and photons at low energies. Although this must be traceable similarly to a difference in cross sections, the reasoning is not as straightforward in this case.

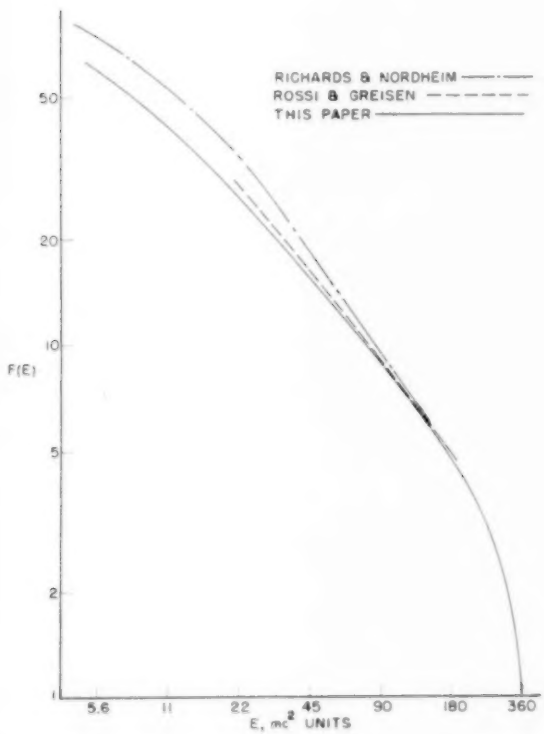

FIGURE 2. *Comparison of $F(E)$ with previous results.*

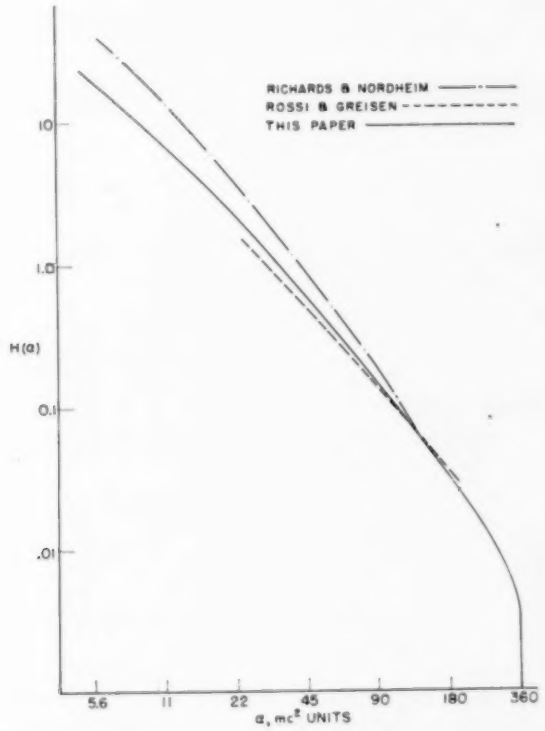

FIGURE 3. *Comparison of $H(\alpha)$ with previous results.*

10. Final Comments

The agreement as to general trends and as to absolute magnitude near $\frac{1}{2}E_0$ demonstrates the feasibility of the calculational procedure developed in this paper. Logically, the next step is to introduce accurate cross-sectional forms into the equations to obtain more accurate spectra. Alternatively, one could move immediately toward a solution of the spatial and directional distributions. This would involve computing the higher moments in the linked set of equations of which these spectra form the zeroth moment (for an example of this, see reference [10]).

11. Appendixes

Appendix 1. Cross-Sectional Forms

The following detailed cross-sectional forms were used to derive the functions K discussed in section 5.

Bremsstrahlung losses [11]:

$$\sigma_b(E',E)=4\bar{\varphi}\,\frac{1}{E'}\left(\frac{\eta}{1-\eta}\right)\left[\left(\frac{1+\eta^2}{\eta}-\frac{2}{3}\right)\ln 183Z^{-\frac{1}{3}}+\frac{1}{9}\right],$$

where $\eta=E/E'$.

Electron atomic interactions [8]:

$$\sigma_M(E',E)=\frac{3}{4}\,\varphi_T\,\frac{1}{E'^2}\left[\frac{1}{(1-\eta)^2}+\frac{1}{\eta^2}\right],$$

where $\eta=E/E'$.

Pair production (either electron or positron) [11]:

$$\sigma_{pp}(\alpha',E)=8\bar{\varphi}\,\frac{1}{\alpha'}\left[\left(\frac{4}{3}\,\eta^2-\frac{4}{3}\,\eta+1\right)\ln 183Z^{-\frac{1}{3}}-\frac{1}{9}\,\eta(1-\eta)\right],$$

where $\eta=E/\alpha'$.

Compton electrons:

$$\sigma_{ce}(\alpha',E)=\frac{3}{8}\,\varphi_T\,\frac{1}{\alpha'^2}\left[\frac{\alpha'}{\alpha'-E+1}+\frac{\alpha'-E+1}{\alpha'}\right].$$

Compton photons:

$$\sigma_c(\alpha',\alpha)=\frac{3}{8}\,\varphi_T\,\frac{1}{\alpha'^2}\left[\frac{\eta^2+1}{\eta}\right],$$

where $\eta=\alpha/\alpha'$.

Bremsstrahlung photons [11]:

$$\sigma_{bp}(E',\alpha)=4\bar{\varphi}\,\frac{1}{\alpha}\left[\left(\frac{4}{3}-\frac{4}{3}\,\eta+\eta^2\right)\ln 183Z^{-\frac{1}{3}}+\frac{1-\eta}{9}\right],$$

where $\eta=\alpha/E'$.

The cross-sectional constants were evaluated as follows:

$$\varphi=\frac{Z^2r_0^2}{137}\,\frac{Z+1}{Z}=3.9435 \text{ barns}, \qquad Z=82;$$

and

$$\varphi_T=\frac{8}{3}\,\pi r_0^2=0.6652 \text{ barn}.$$

The constants A, B, and C in the special solution near E_0 (section 7) are obtained from the expression for $K^{es}(E',E)$; they are coefficients of the terms proportional to $E^{-1}(1-\eta)^{-1}$, $-\ln(1-\eta)$, and 1, respectively, in the limit $E,E'\to E_0$:

$$A=NZ\frac{3}{4}\varphi_T=0.1189$$

$$B=N4\bar{\varphi}\left[\frac{4}{3}\ln 183Z^{-\frac{1}{3}}+\frac{1}{9}\right]=0.2339$$

$$C=N4\bar{\varphi}\left[-\frac{5}{6}\ln 183Z^{-\frac{1}{3}}-\frac{1}{9}\right]-\frac{3}{4}NZ\varphi_T\frac{2}{E_0}=-0.1487.$$

Appendix 2. Integration and Differentiation Weights

To obtain the integration weights ω_{in} used in connection with eqs (5) and (6), the following formulas were used:

$$\int_{x_0-\Delta}^{x_0+\Delta}dxf(x)\approx\frac{\Delta}{3}\left[f(x_0+\Delta)+4f(x_0)+f(x_0-\Delta)\right]$$

$$\int_{x_0}^{x_0+\Delta}dxf(x)\approx\frac{\Delta}{12}\left[5f(x_0+\Delta)+8f(x_0)-f(x_0-\Delta)\right],$$

$$\int_{x_0-\Delta}^{x_0+2\Delta}dxf(x)\approx\frac{3\Delta}{4}\left[f(x_0+2\Delta)+3f(x_0)\right],$$

where $f(x)$ is a function that varies slowly for x in the region of integration.

For differentiation the weights a_i were determined by using the following formula:

$$\frac{\partial F(_n)}{\partial E_n}=F(E_n)\left[\sum_{i\neq n}\frac{1}{E_n-E_i}\right]+\sum_{i\neq n}F(E_i)\left[\frac{\prod_{j\neq i}(E_n-E_j)}{\prod_{j\neq i}(E_i-E_j)}\right].$$

Appendix 3. Normalization of Previous Results

The following results were obtained by using a table of calculations given by Richards and Nordheim [6].

E	$F(E)=69.86F_{RN}(E)$	$H(\alpha)=5.329g(K)$
131	6. 43	0. 0639
91. 8	9. 08	. 171
65. 6	12. 6	. 384
39. 3	21. 0	1. 12
26. 2	30. 0	2. 61
19. 7	37. 7	4. 74
13. 1	49. 6	10. 7
6. 56	71. 3	34. 1

The normalization factors arise in the following manner:

$$69.86=\left[0.437\times\frac{184}{6.7}\right]\times\text{density of lead (11.005)}\times\text{radiation length (0.529)}$$

$$5.329=69.86\times\text{energy conversion factor }\frac{1}{13.11}.$$

For a discussion of the factor in square brackets, see reference [6].

The following results were obtained by using the equations of Rossi and Greisen [7] under "approximation B":

E	$F(E)=5.822Z_{\pi}(E_0,E)$	$H(\alpha)=2.975z_{\gamma}(E_0,W)$
180	4. 77	0. 0348
90	9. 02	. 132
45	16. 4	. 482
22. 5	28. 5	1. 70

The normalization factors arise in the following manner:

$$5.822=\text{density of lead } (11.005)\times\text{radiation length } (0.529),$$

$$2.975=5.822\times mc^2\ (0.511).$$

12. References

[1] H. Brysk, Phys. Rev. **96,** 419 (1954).
[2] B. Rossi, High energy particles, chap. 5 (Prentice-Hall, Inc., New York, N. Y., 1952).
[3] N. Arley, Proc. Roy. Soc. (London) [A] **168,** 519 (1938).
[4] I. Tamm and S. Belenky, J. Phys. USSR **1,** 177 (1939); Phys. Rev. **70,** 660 (1946).
[5] F. L. Friedman, Tech. Rept. 31, Laboratory for Nuclear Science and Engineering, MIT (1949).
[6] J. A. Richards and L. W. Nordheim, Phys. Rev. **74,** 1106 (1948).
[7] B. Rossi and K. Greisen, Rev. Mod. Phys. **13,** 240 (1941).
[8] L. V. Spencer and U. Fano, Phys. Rev. **93,** 1172 (1954).
[9] U. Fano, L. V. Spencer, and M. Berger, Penetration and diffusion of X-rays, Handbuch der Physik (to be published).
[10] L. V. Spencer and U. Fano, J. Research NBS **46,** 446 (1951) RP2213.
[11] W. Heitler, The quantum theory of radiation, 2d ed. (Oxford Univ. Press, London, 1944).

WASHINGTON, May 15, 1957.

Journal of Research of the National Bureau of Standards Vol. 60 No. 2, February 1958 Research Paper 2825

Observer Differences in Color-Mixture Functions Studied by Means of a Pair of Metameric Grays

Kenneth L. Kelly

The Granville metameric gray panels have served to characterize the color vision of observers in an approximate but useful way. Thus, the 39 observers studied, and the four color-mixture functions were classed into five groups according to their indicated amounts of ocular pigmentation. These panels were also used to measure the correlation of lens and macular pigmentations with observer age, sex, and eye and hair colors. Of the three sets of color-mixture functions intended to refer to 2° field observation, the 1931 Commission Internationale de L'Éclairage standard observer agrees best. These data thus afford no basis for supplanting the 1931 Commission Internationale de L'Éclairage standard observer with either the Judd "j" or the 1955 Stiles' 2° color-mixture functions. The 1955 Stiles' 10° functions, however, agree fairly well.

1. Introduction

The standard observer and coordinate system, now widely used in the interpretation of spectrophotometric and colorimetric data, were recommended in 1931 by the CIE (the Commission Internationale de L'Éclairage) for this purpose so that all subsequent data would be expressed in the same tristimulus system and would therefore be immediately comparable. This system was based on the work done by Guild and by Wright in England and until recently has proved quite satisfactory. However, it was reported to fail in several instances to account correctly for the differences in color between two samples whose spectrophotometric curves differ in the short wavelength end of the spectrum, especially below 420 mμ.

These reported failures resulted in much discussion looking toward a possible revision of this standard observer and led Judd to suggest in 1951 a modified set of color-mixture functions based on the data of Wright and Guild combined with the standard luminosity function modified below 460 mμ according to luminous-efficiency data by Gibson-Tyndall, Wald, Weaver, Thomson, and Ishak. Now Dr. W. S. Stiles of the National Physical Laboratory in England has undertaken the first careful direct determination of the color-mixture functions of average normal observers which the standard observer should represent.

In these discussions, use of a field size larger than the 2° field used for the 1931 standard observer has been advanced to accord more closely with viewing conditions in industry. Dr. Stiles is therefore making his measurements with both 2° and 10° fields and has already reported color-mixture data for a pilot group of 10 observers whose average age is about 31 yr [8].[1]

In 1949, Walter Granville, then of the Container Corp. of America, painted several metameric gray panels to illustrate the possible effect of angular subtense on color matching [2]. Two of these were chosen for the work herein reported; a nearly nonselective gray produced by a mixture of white and black pigments called the simplex gray (No. 1), and a selective gray produced by a mixture of yellow, green, purple, and white pigments called the complex gray (No. 8). Figure 1 and table 1 show the spectral directional reflectances of these two grays obtained on the General Electric recording spectrophotometer.

According to the 1931 standard observer, the complex gray will appear greener in daylight (source C) than the simplex, and the reverse will be true when source A (color temperature 2,854°K, representative of incandescent lamp light) is used. The same effect results from changing the angular subtense of the sample from 10° to 2°; the retinal area stimulated first will include the macula and also a portion of the surrounding retina, and second will lie inside the macula only. This change from 10° to 2° will have an effect at least partly analogous to placing a yellow filter (macular pigment) in front of the eye for the 10° condition and, thus should have somewhat the same effect as reducing the color temperature of the source.

The purpose of the present study is to establish a criterion by means of which it will be possible to determine whether any set of color-mixture functions gives predictions of the character of the color difference between the Granville grays in accord with observers known to have normal vision by the ac-

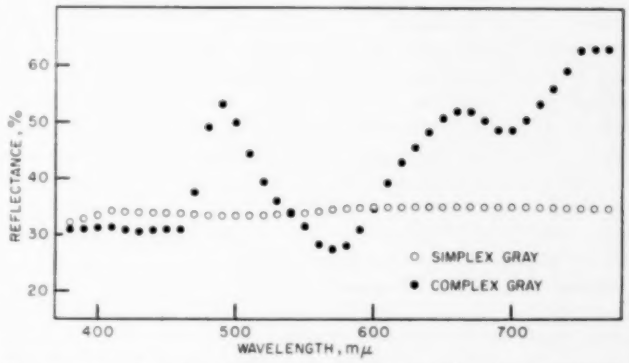

FIGURE 1. *Spectrophotometric curves of the two metameric Granville grays.*

[1] Figures in brackets indicate the literature references at the end of this paper.

TABLE 1. *Spectral directional reflectances of the two Granville grays*

Wavelength	Simplex (No. 1)	Complex (No. 8)
380	[a] 0.317	[a] 0.305
390	[a] .324	[a] .307
400	.331	.309
410	.338	.310
420	.337	.304
430	.336	.301
440	.335	.305
450	.334	.306
460	.334	.316
470	.332	.373
480	.331	.488
490	.330	.528
500	.330	.497
510	.331	.441
520	.331	.391
530	.332	.357
540	.334	.337
550	.336	.311
560	.338	.289
570	.342	.281
580	.343	.287
590	.345	.306
600	.346	.342
610	.347	.389
620	.347	.425
630	.347	.452
640	.347	.480
650	.347	.504
660	.348	.517
670	.347	.516
680	.347	.500
690	.348	.484
700	.348	.483
710	.348	.502
720	.347	.528
730	.346	.556
740	.346	.589
750	.345	.626
760	[a] .344	[a] .627
770	[a] .343	[a] .627

[a] Extrapolated.

TABLE 2. *The spectral transmittances and change in reciprocal color temperature for the daylight filters used*

Wavelength	Davis-Gibson "C"	Filter G90A 2.13 mm	Davis-Gibson plus G90A	Filter No. 8331	Davis-Gibson plus No. 8331
mμ					
380	[a] 0.69	[a] 0.751	0.5182	[a] 0.47	0.32
390	[a] .71	[a] .774	.5495	[a] .59	.42
400	.7268	.7967	.5790	.685	.498
410	.7501	.8096	.6050	.712	.534
420	.7475	.7800	.5830	.656	.490
430	.7180	.7585	.5446	.617	.443
440	.6923	.7279	.4821	.555	.368
450	.5836	.6982	.4075	.498	.291
460	.5090	.6647	.3383	.440	.224
470	.4557	.6345	.2891	.388	.177
480	.4056	.6029	.2445	.344	.140
490	.3532	.5777	.2040	.309	.109
500	.2956	.5551	.1641	.280	.0828
510	.2479	.5323	.1320	.254	.0630
520	.2178	.5088	.1108	.228	.0497
530	.2027	.4805	.0974	.199	.0403
540	.1961	.4602	.0902	.179	.0351
550	.1891	.4547	.0860	.172	.0325
560	.1765	.4600	.0812	.176	.0311
570	.1600	.4560	.0730	171	.0274
580	.1420	.4310	.0612	.150	.0213
590	.1250	.3950	.0494	.119	.0149
600	.1115	.3805	.0424	.109	.0122
610	.1015	.3750	.0381	.103	.0105
620	.0940	.3650	.0343	.094	.0088
630	.0880	.3498	.0308	.083	.0073
640	.0825	.3318	.0274	.072	.0059
650	.0779	.3207	.0250	.066	.0051
660	.0724	.3217	.0233	.068	.0049
670	.0684	.3330	.0228	.072	.0049
680	.0634	.3493	.0221	.078	.0049
690	.0584	.3618	.0211	.083	.0048
700	.0534	.3646	.0195	.082	.0044
710	.0489	.3626	.0177	.080	.0039
720	.0444	.3569	.0158	.076	.0034
730	.0404	.3509	.0142	.073	.0029
740	.0369	.3463	.0128	.068	.0025
750	.0344	.3418	.0118	.067	.0023
760	[a] .033	[a] .337	.0111	[a] .066	.0022
770	[a] .032	[a] .333	.0107	[a] .064	.0020
Δ μrd	202.5	77.9	280.4	187.5	390.0

[a] Extrapolated.

cepted tests. In particular, this criterion is to be applied to the four sets of color-mixture functions already mentioned.

2. Experimental Method

The experiment consisted of placing the two gray panels side by side in a nearly vertical position illuminated by CIE source A and viewing them through a Davis-Gibson (CIE) C filter prepared in February 1955. The spectral transmittances of this filter determined in July 1956 at the start of the observations are given in table 2. The observer was asked to stand at a line that would cause the retinal image of the two panels to subtend a 10° angle and to disregard the Maxwell spot [7] if present. First he was to describe the color of the simplex gray with respect to that of the complex gray and then, as the operator reduced the voltage on the lamp and thereby its color temperature, to note when neither panel appeared redder or greener than the other. The voltage of the source at this point was recorded along with the observer's age, sex, and hair and eye colors. Observers not passing the 5th Edition Ishihara Tests for Colour Blindness were eliminated.

The observer was then asked to step back to another line from which the retinal image would subtend an angle of 2° and the experiment was repeated. The combination of source and Davis-Gibson filter resulted in a maximum color temperature of 6,750° K, but for those observers requiring a source of higher color temperature, one or more measured blue daylight glasses (table 2) were used with the Davis-Gibson filter. Therefore, by varying the voltage on the lamp and by using combinations of these filters, color temperatures could be obtained from 1,800° K up and, indeed, it was found that some sources bluer than a source corresponding to infinite color temperature were required. The voltage and filter combinations were noted for each red-green balance point for each observer and the corresponding reciprocal color temperatures were determined from table 3 by subtracting the change in microreciprocal degrees Kelvin (μrd) produced by the filter combination from the reciprocal color temperature of the bare lamp.

TABLE 3. *Color temperature (θ) in ° K of the lamp, and the reciprocal color temperature in μrd of the lamp and the lamp with one or more of the daylight filters against voltage on the lamp*

Voltage	Θ of lamp alone	$10^6/\Theta$ of lamp	$10^6/\Theta$ of lamp and Davis-Gibson filter	$10^6/\Theta$ of lamp and Davis-Gibson with G90A	$10^6/\Theta$ of lamp and Davis-Gibson with 8331	$10^6/\Theta$ of lamp and Davis-Gibson with G90A and 8331
36.0	1800	556	353	275	166	88
42.7	1900	526	324	246	137	58
49.9	2000	500	298	220	110	32
57.6	2100	476	274	196	86	8
66	2200	455	252	174	65	−13
75	2300	435	233	154	45	−33
84	2400	417	214	137	27	−51
94	2500	400	198	119	10	−68
104	2600	385	182	104	−5	−83
115	2700	370	168	90	−20	−98
126	2800	357	155	77	−33	−111
133	2854	350.4	148	70	−40	−118

3. Red-Green Balance Points for the Four Color-Mixture Functions

The red-green balance points for the four color-mixture functions were determined by first computing the chromaticity coordinates for the two gray panels for each of the functions for three Planckian sources (277, 221, and 191 μrd), for nine Planckian sources (666, 571, 500, 488, 486, 444, 400, 350, and 308 μrd) combined with the Davis-Gibson "C" filter ($\Delta 10^6/\Theta = 202$ μrd), and for the same Planckian sources combined with the double filter Davis-Gibson "C" plus G90A ($\Delta 10^6/\Theta = 280$ μrd). These data were plotted on the (x,y)-chromaticity diagram and fall close to the Planckian locus.

It was noted that the direction of the straight line connecting each pair of points as well as the distance between them (indicative of color difference) varies regularly with the correlated color temperature of the energy reflected by the simplex gray regardless of whether the computation is based on a Planckian source or on a Planckian source modified by the single or the double filter. Figure 2 shows the Planckian locus and 10 of the 21 pairs of computed points plotted on the (x,y)-diagram for the CIE standard observer. Note that near 300 μrd the simplex gray is seen by this observer as greener than the complex, whereas at source C (148 μrd), the reverse is true.

The red-green balance points for the two Stiles color-mixture functions were easily determined because they each predicted that under a certain one of the illuminants the two gray panels would be a chromaticity match; that is, the chromaticity points for them were found not to be significantly different. The reciprocal color temperature of the source satisfying this condition for the Stiles' 2° color-mixture functions is 210 μrd, while that for the Stiles' 10° color-mixture function is 267 μrd.

The other two color-mixture functions predict that at the red-green balance point there will be a residual yellow-blue difference. Therefore it was necessary to establish some criterion to determine when the red-green difference equals zero. The

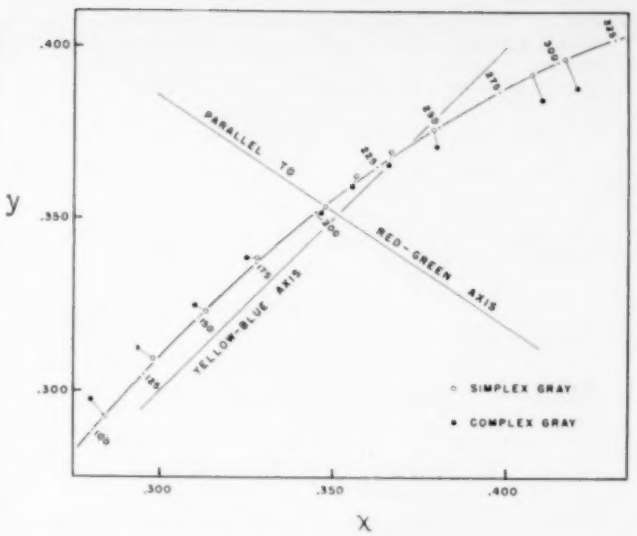

FIGURE 2. *Illustration of the change in relative position and distance apart of the CIE (x,y)-points of the Granville grays as the color temperature of the source is changed.*

first criterion used in determining the corresponding reciprocal color temperature of source was that the line joining the chromaticity points of the two grays be parallel to the yellow-blue axis on the (x,y)-diagram. This axis, having an inclination of 45°, was drawn between the 476 and 578 mμ points on the spectrum locus. These are the proposed centers of the yellow and blue segments of the boundary of real colors on this diagram [6]. The corresponding values of reciprocal color temperature of source satisfying this criterion for the 1931 CIE and 1951 Judd "i" color-mixture functions are 192 and 202 μrd, respectively.

The second criterion used in determining the corresponding reciprocal color temperature of source was that the line joining the chromaticity points of the grays be perpendicular to the red-green axis on a uniform chromaticity scale diagram [4]. This axis was drawn from the 508 mμ point on the spectrum locus to the intersection of the line drawn through the 493 mμ point and the "C" illuminant point with the line connecting the red and violet ends of the spectrum locus. These are the proposed centers of the red and green segments of the boundary of real colors on the (x,y)-diagram [6].

A perpendicular to this axis was drawn through the "C" illuminant point and was found to intersect the spectrum locus at 567 mμ. This perpendicular was transferred to the (x,y)-diagram by drawing it also through the "C" illuminant point and the 567 mμ point on the spectrum locus. The angle of inclination of this perpendicular is found to be 66.5° and the corresponding values of the reciprocal color temperature of source satisfying this criterion for the two color-mixture functions are 206 and 213 μrd, respectively. Table 4 summarizes the values of reciprocal color temperature computed by these criteria to correspond to these balance points for the four sets of color-mixture functions.

TABLE 4. *Values of reciprocal color temperature of red-green balance points for the four color-mixture functions by different criteria*

Color-mixture functions	Reciprocal color temperature of source in μrd yielding red-green balance	
	By chromaticity match	
Stiles' 2°	210	
Stiles' 10°	267	
	Parallel to Y-B axis	Perpendicular on UCS triangle to R-G axis
1931 CIE	192	206
1951 Judd "f"	202	213

4. Results and Discussion

Table 5 contains the individual data for the 39 observers studied with their descriptions of the two panels and the reciprocal color temperature of their red-green balance points. Note that observer 39 was able to obtain a match at the 10° position but that it was not possible to run the lamp at a sufficiently high color temperature for him to obtain a match at the 2° position, presumably due to his very heavy ocular pigmentation.

Because the image of a 2° field falls wholly within the macula, the 2°-field results depend both on the macula and on the lens pigmentations. Likewise, since the image of a 10° field covers the macula and a large region of the surrounding retina of which the area of the macula represents about 10 percent, the 10°-field results depend only on the lens pigmentation provided the observers disregard the Maxwell spot as instructed. Also, the difference between the two may be taken as a measure of the macular pigmentation on the assumption that the spectral sensitivities of the receptors apart from pigmentation are the same throughout the 10° field [7].

The degree of pigmentation of an observer is indicated by his red-green balance point. By this interpretation, Stiles' 10° average observer (balance point at 267 μrd, see table 4) would be the least pigmented of the four.

TABLE 5. *Observer initials, age, sex, eye, and hair color, descriptions of colors of gray panels illuminated by source C at the 10° and 2° positions, and reciprocal color temperature of source required by each observer for red-green balance at both positions and the difference between them*

Observer		Sex and age	Eye color	Hair color	Color of simplex relative to complex		Reciprocal color temperature of match point		
					10°	2°	10°	2°	Difference
1	DBJ	M55	blue	brown	red	green	204	91	113
2	KLK	M45	hazel	brown	red	green	238	103	135
3	GWH	F56	brown	brown	red	green	179	47	132
4	MRF	M27	hazel	dark brown	pink	pink	278	196	82
5	CAD	M44	blue	brown	red	green	196	84	112
6	MMB	F39	blue	dark brown	red	green	213	132	81
7	LEB	M51	dark brown	black	slightly pink	green	213	78	135
8	THP	M41	blue	blond	pink	green	256	149	107
9	IN	M38	blue	red	pink	green	200	110	90
10	CDC	M21	hazel	auburn	pink	green	238	84	154
11	------	F50	hazel	brown	pink	slightly pink	256	189	67
12	HKH	M39	blue	blond	pink	pink	250	179	71
13	FCB	M62	blue	brown	pink	green	172	118	54
14	RTV	M34	blue	brown	red	green	222	135	87
15	RWC	M46	blue	brown	pink	green	213	71	142
16	WAH	M29	dark brown	black	pink	green	263	182	81
17	GHL	M34	dark brown	black	pink	pink	286	213	73
18	WHA	M47	blue	brown	match	green	189	65	124
19	RLM	F44	brown	dark brown	pink	green	238	159	79
20	WRD	M42	brown	brown	pink	match	227	149	78
21	ECW	M48	brown	brown	pink	green	222	175	47
22	BPG	F37	dark brown	dark brown	lavender	green	227	127	100
23	WBF	F23	brown	brown	pink	pink	256	164	92
24	SAC	F19	brown	brown	lavender	lavender	270	208	62
25	JJ	F29	blue	brown	red	match	278	154	124
26	CAL	F25	hazel	light brown	lavender	match	250	170	80
27	RPT	M53	blue	brown	match	green	95	−14	109
28	HJK	M52	brown	brown	match	green	170	2	168
29	VIB	F42	dark brown	dark brown	pink	slightly pink	256	175	81
30	KSG	M66	blue	brown	green	green	91	−40	131
31	RD	M68	blue	brown	green	green	130	−28	158
32	WLH	M21	hazel	blond	red	green	233	110	123
33	WFM	M36	blue	blond	red	green	196	29	167
34	PI	F18.5	hazel	brown	pink	pink	278	170	108
35	JCS	M28	green	blond	pink	pink	270	161	109
36	TOT	M38	brown	light brown	pink	pink	263	192	71
37	RS	M56	blue	brown	red	green	196	84	112
38	JWL	M31	dark brown	black	pink	pink	256	182	74
39	CB	M77	blue	brown	green	green	−118	<−118	------
Averages	------	41.3	------	------	------	------	214	<114	>100

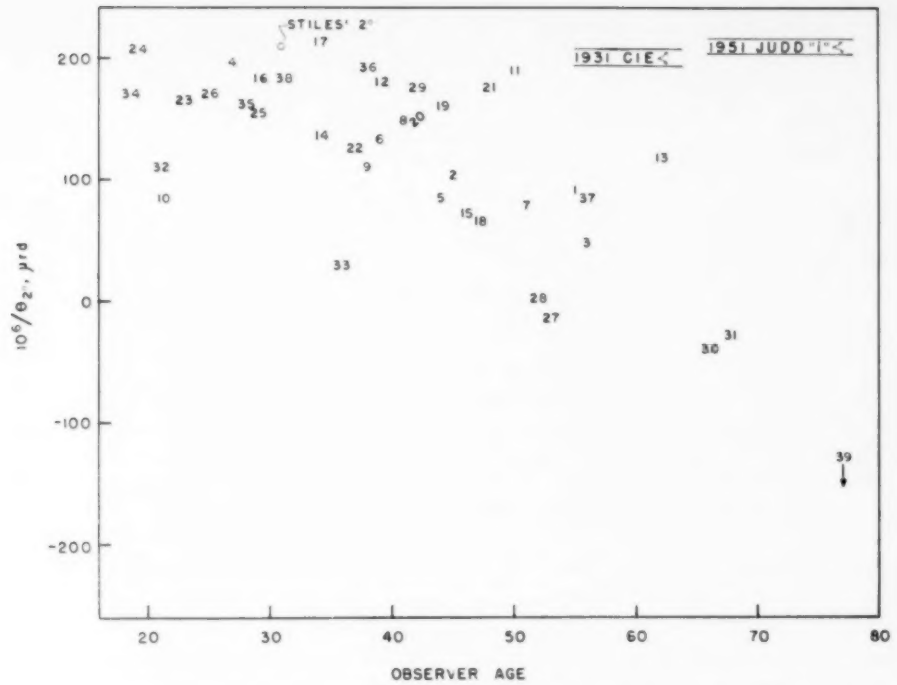

FIGURE 3. *Reciprocal color temperature of source required in a 2° field by 39 observers to produce red-green balance between the Granville grays plotted against observer age.*

Note the tendency of older observers to require lower reciprocal color temperatures. This tendency suggests that the amount of lens and macular pigmentations combined increases with age.

In figure 3, the reciprocal color temperature ($10^6/\Theta_2$) of the 2° red-green balance points for the 39 observers studied (see table 5) are plotted with observer number against observer age. Since no age has been given for the 1931 CIE and 1951 Judd "i" color-mixture functions, the spread in reciprocal color temperatures required by them for red-green balance as given in table 4, are indicated by a pair of lines which should extend across the graph but have been shown as short sections only to avoid complicating the figure. Stiles gives the average age of his pilot group of 10 observers as 31. It may be seen from figure 3 that only four of the 39 observers studied seem to have less pigmentation than the 1931 CIE standard observer, only two less than the 1951 Judd "i" (both of these on the basis of yellow-blue criterion) and only one less than the Stiles' 2° color-mixture functions by this test. It also indicates that the CIE and Judd color-mixture functions both correspond to very young observers in regard to balance point for the Granville grays.

The rank correlation (Spearman's) between $10^6/\Theta_2$ for red-green balance and age of the observers at the 2° position is 0.60 with an uncertainty of plus or minus 0.22, the uncertainty being 4.9 times the probable error. Thus, it is suggested that there is a poor but significant correlation of lens and macular pigmentations with age. Figure 4 shows the correlation of $10^6/\Theta_{10}$ with age; the rank correlation is better being 0.76 plus or minus 0.13. This correlation is attributable to the known increase in lens pigmentation with age. Here again, there are only six observers apparently less pigmented than Stiles' 10° color-mixture functions. From figure 5 it will be noted that there is no correlation of macular pigmentation with age, the rank correlation being −0.145 plus or minus 0.61. Also, there is no significant correlation of macular or lens pigmentations with either eye color or hair color.

From table 5 and figures 3, 4, and 5, it is possible to classify the oberservers and the four color-mixture functions into five groups, depending on their amounts of ocular pigmentation. From table 5, it will be seen that certain observers describe the simplex gray as redder than the complex at both the 10° and 2° positions. These are the young observers and those tentatively considered to have the least ocular pigmentation and constitute group 1. Those in group 2 apparently have a little more pigmentation and so call the simplex redder at the 10° position but a match at the 2° position. Group 3, comprising the majority of the observers, contains those who call the simplex redder at the 10° position and greener at the 2° position. With more pigmentation, the observers in group 4 call the simplex a match at the 10° position and greener at the 2° position. The most heavily pigmented observers, and these contain the oldest observers, call the simplex greener at both positions. Thus, these groups are called red-red, red-match, red-green, match-green, and green-green. The same grouping may be made with respect to the color temperature or reciprocal color temperature of the red-green balance points at the 10° and 2° positions. The three criteria for the five groups are

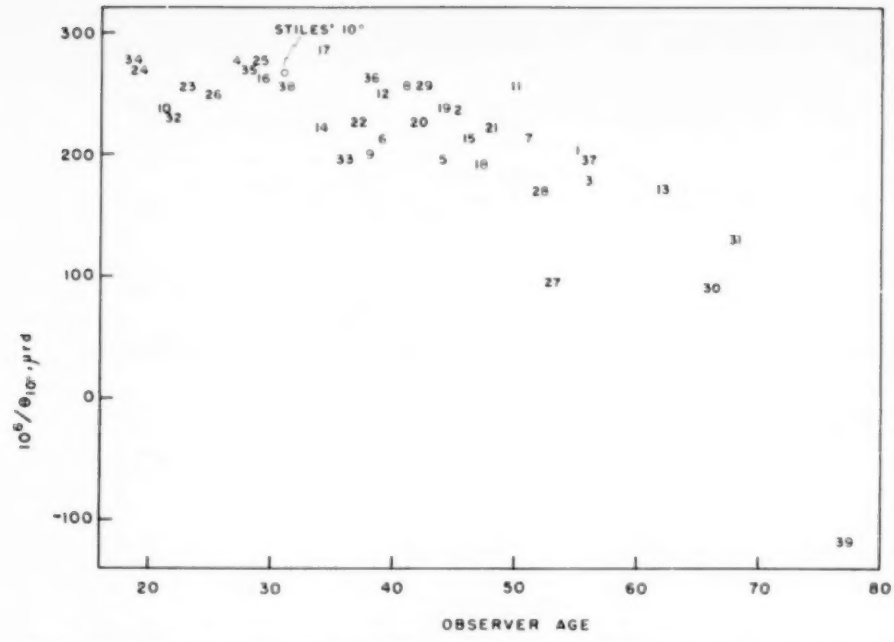

FIGURE 4. *Reciprocal color temperature of source required in a 10° field by 39 observers to produce red-green balance between the Granville grays plotted against observer age.*

Note that older observers require lower reciprocal color temperatures. This result is ascribed to the known increase in lens pigmentation with age.

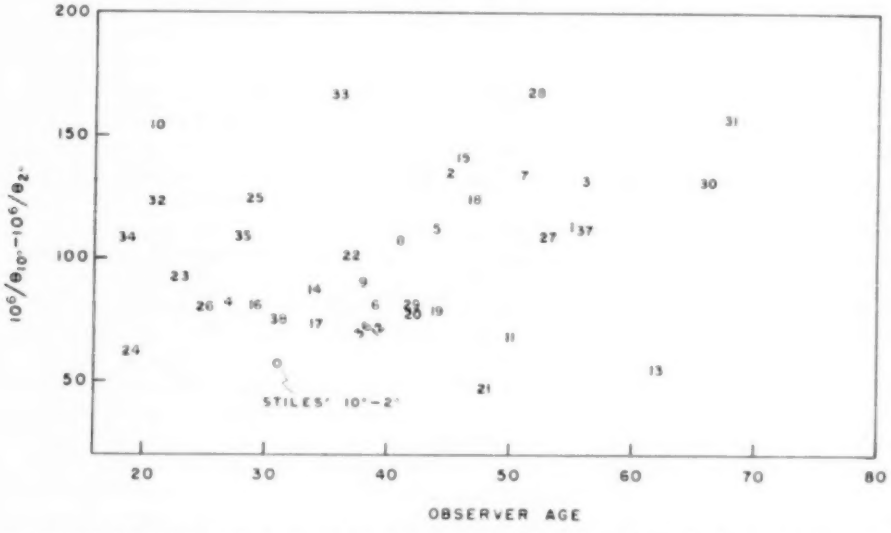

FIGURE 5. *Difference between the reciprocal color temperatures required for 10° and 2° fields by 39 observers to produce red-green balance between the Granville grays.*

On the assumption that the spectral sensitivities, apart from macular pigmentation, of the receptors are invariant over the whole central 10° of the retina, this difference is a measure of the amount of macular pigmentation. Note that there is no evidence of change in amount of macular pigmentation with age.

shown in table 6. According to this classification, all four color-mixture functions fall into the red-red group of very lightly pigmented observers with the CIE the most heavily pigmented and the Stiles' 10° the least.

5. Conclusions

The reciprocal color temperature of the source required to produce red-green balance between the Granville grays has been found to vary widely from one observer of normal color vision to another, and determination of this value of reciprocal color temperature for any one observer serves to characterize his color vision in an approximate but useful way. The value of reciprocal color temperature required in a 10° field for red-green balance of the Granville grays is dependent on the amount of yellow pigmentation in the lens of the observer's eye, and is tentatively taken as a measure of this pigmenta-

TABLE 6. *Classification of observers into five groups according to indicated ocular pigmentation as shown by their description of the simplex gray relative to the complex gray for source C, and alternatively by the color temperature and reciprocal color temperature of source required to make neither gray redder or greener than the other*

Observer group	Simplex relative to complex		Color temperature of source at match point	Reciprocal color temperature of source at match point
	10°	2°		
red-red	red	red	$\Theta_{10°} < \Theta_{2°} < 6{,}750°$	$148 < 10^6/\Theta_{2°} < 10^6/\Theta_{10°}$
red-match	red	match	$\Theta_{10°} < 6{,}750° = \Theta_{2°}$	$10^6/\Theta_{2°} = 148 < 10^6/\Theta_{10°}$
red-green	red	green	$\Theta_{10°} < 6{,}750° < \Theta_{2°}$	$10^6/\Theta_{2°} < 148 < 10^6/\Theta_{10°}$
match-green	match	green	$\Theta_{10°} = 6{,}750° < \Theta_{2°}$	$10^6/\Theta_{2°} < 148 = 10^6/\Theta_{10°}$
green-green	green	green	$6{,}750° < \Theta_{10°} < \Theta_{2°}$	$10^6/\Theta_{2°} < 10^6/\Theta_{10°} < 148$

tion. Similarly, the value of reciprocal color temperature required in a 2° field for red-green balance of the Granville grays is dependent both on lens pigment and on macular pigment, and the difference in these two values (value for 2° field minus value for 10° field) is tentatively taken as a measure of the macular pigmentation of the observer.

The tentative measure of lens pigmentation afforded by the Granville grays correlates well with the age of the observer, but the tentative measure of macular pigmentation shows no correlation with age. Neither measure shows significant correlation with eye color or hair color, but a tendency, significant at about the 15 percent level of confidence, was found for female observers to have less pigmented eyes than male observers of the same age.

The reciprocal color temperatures of source required by four sets of color-mixture functions for red-green balance of the Granville grays have been computed and found to be higher than the average value for 39 actual observers with normal color vision. Of the three sets of color-mixture functions intended to refer to 2°-field observation, the 1931 CIE standard observer agrees best. These data thus afford no basis for supplanting the 1931 CIE standard observer either with the Judd "i" color-mixture functions or the 1955 Stiles' 2° color-mixture functions for a pilot group of 10 observers.

With respect to these observations on the Granville grays, the Stiles' 1955 data for 2° viewing does not fulfill the requirement recommended in 1955 by the CIE [1] that any revision of the "standard observer for colorimetry should represent average normal vision, adjusted as for an observer 30 years of age", but the data for 10° viewing are fairly satisfactory in this regard.

6. References

[1] Comm. Internationale de L'Éclairage, Compt. rend., Zurich, p. II, sec. 1.3.1. (1955).

[2] W. C. Granville and D. B. Judd, Metameric color and the macular pigment, J. Opt. Soc. Am. **39**, 632A (1949).

[3] A. E. Jacobsen, Non-adaptability of the ICI system to some near-whites which show absorption in the far-blue region of the spectrum, J. Opt. Soc. Am. **38,** 442 (1948).

[4] D. B. Judd, A Maxwell triangle yielding uniform chromaticity scales, J. Research NBS **14,** 41 (1935) RP756; J. Opt. Soc. Am. **25,** 24 (1935).

[5] D. B. Judd, A comparison of direct colorimetry of titanium pigments with their indirect colorimetry based on spectrophotometry and a standard observer, J. Research NBS **43,** 227 (1949) RP2024; J. Opt. Soc. Am. **39,** 945 (1949) with errata in **40,** 52 (1950).

[6] K. L. Kelly, Color designations for lights, J. Research NBS **31,** 271 (1943) RP1565; J. Opt. Soc. Am. **33,** 627 (1943).

[7] J. C. Maxwell, On the unequal sensibility of the foramen centrale to light of different colours, Reports British Association, p. 12 (1856).

[8] W. S. Stiles, Interim report to the Comm. Internationale de L'Éclairage, Zurich (1955) on the National Physical Laboratory's investigation of colour-matching (1955), Optica Acta **2,** 168 (1955).

WASHINGTON, June 7, 1957.

Journal of Research of the National Bureau of Standards Vol. 60, No. 2, February 1958 Research Paper 2826

Precise Evaluation of Surface Area With Indirectly Calculated Dead Space

William V. Loebenstein

The determination of surface area from nitrogen adsorption data obtained at low temperature by volumetric methods is subject to several errors. One error that becomes especially serious when the surface area is small is associated with the calibration of the dead space with helium. This error is large because the volume of adsorbed gas is calculated as a small difference between two comparatively large quantities.

A statistical method of successive approximations has been developed for calculating the dead space. The latter is obtained as that quantity necessary to yield the best agreement with the known isotherm equation. This procedure fixes the value of V_m (directly proportional to the surface area). The procedure also provides an estimate of the experimental error associated with the over-all determination.

1. Introduction

Adsorption of vapors at temperatures near their boiling points provides the most convenient means for determination of the surface areas of finely divided or porous solids. In volumetric apparatus, which is most commonly used, the amount of adsorbed gas is the difference between that admitted to the sample container and that remaining in the dead space. The latter is the void space between or within the solid particles plus the volume of the connecting tubing.

The precision with which a dead space calibration is normally made using helium is fairly well limited by the equipment and does not depend upon the surface area of the sample. The effect of this limitation of precision upon the measurement of the volume of gas (nitrogen, for example) adsorbed is especially serious when the surface area is relatively small. This is because the amount of gas adsorbed is calculated as the small difference between two large quantities. Indeed, the uncertainty in the measurement resulting from the dead space calibration is greater than that of all other factors which contribute to the over-all error of the surface area determination. It is difficult to express this fact using rigorous mathematical language because the surface area evaluation results from the parameters of a least-square line assumed to represent all of the points. No simple relationship exists between the over-all error and the errors associated with the determination of the individual points, especially since an error in the dead space actually destroys the linearity of the plotted curve.

Anyone who has made surface area determinations in the conventional manner can calculate from his own data the percentage change in surface area resulting from an error of, say, one percent in the dead space. The author has found that this error exceeded 100 percent for a sample of glass beads whose area was of the order of 0.2 m^2/g as measured with N_2 at 90° K. Normally, of course, the careful technician would in such a case make sufficient replicate determinations of the dead space to insure that its precision was appreciably better than one percent.

In routine determinations where the isotherm equation is known from previous experience, the dead space need not be experimentally obtained. The surface area can be found by assigning a value for the dead space that will allow the experimental measurements to fit the known isotherm. This paper describes a procedure of successive approximations by which this is accomplished. The conservative technician may always prefer to determine the helium calibration directly. He can use the resultant dead space value as a starting point which may then be "refined" according to the technique described here. It is unnecessary to continue the refinement beyond the point in the calculations where the error of the dead space ceases to be the dominant factor contributing to the over-all error of the surface area determination.

It is fortunate that the adsorption isotherms which apply to a large number of materials measured at or near the boiling point of the adsorbate are expressible in one linear form or another. These are represented by the well known "Free Surface" equation of Brunauer, Emmett, and Teller [1][1] (BET) (eq 1), and by the equally familiar Langmuir equation (eq 2).

$$p/[V(p_0-p)]=[(C-1)/(V_mC)]\ p/p_0+1/(V_mC) \quad (1)$$

$$p/V=p_0/(V_mB)+p/V_m, \quad (2)$$

p = pressure attained when adsorption and desorption processes are at equilibrium,
p_0 = vapor pressure,
V = volume of gas adsorbed STP,
B, C = constants (under conditions of the experiment) related to the energy of adsorption, and
V_m = a constant equal to the volume of gas (STP) required to cover the surface to the extent of one molecular layer.

[1] Figures in brackets indicate the literature references at the end of this paper.

2. Determination of the Dead Space Factor Z

The volume of adsorbed gas may be calculated from measurements as follows:

$$V=k\,[N-(fp/R)\,Z] \tag{3}$$

where N is the total number of moles of gas admitted to the adsorption tube and the quantity $(fp/R)Z$ represents the moles which remain in the gaseous state in equilibrium with the adsorbed phase. The factor f corrects for the nonideal behavior of a real gas at low temperatures. It is usually expressed as $(1+\alpha p)$ where α is a constant [2] depending upon the particular gas and its temperature. The quantity R is the gas constant in appropriate units; Z is the ratio of the dead space volume to the absolute temperature; and the proportionality constant k converts the moles of gas adsorbed to milliliters per gram at STP. The problem then is to choose a value of Z by trial so that with the measured values of N and p the best fit to the known isotherm equation is obtained.

It is customary in using the BET isotherm equation to plot $p/[V(p_o-p]$ as Y against p/p_o as X. The resulting graph is linear and may be written as follows:

$$Y=a+bX \tag{4}$$

where the intercept a and the slope b depend only on C and V_m. It should be noted that $1/V_m=a+b$. The surface area is determined by multiplying V_m by a packing factor characteristic of the gas adsorbed and of the temperature at which the isotherm was carried out.

The best value of Z in eq (3) is obtained when the resulting values for the gas adsorbed obey eq (4). It is not possible to determine Z with sufficient precision by graphical means alone, hence an analytical method was developed. This was achieved by considering eq (4) as a special case of the more general empirical equation

$$Y=a+bX+cX^2 \tag{5}$$

The least square value for the added parameter c can be determined and the value assumed for Z adjusted to make this coefficient approach zero.

The least square solution [2] for the coefficient c is

$$c=\frac{Sx^2Sx^2y-Sx^3Sxy}{Sx^2Sx^4-(Sx^3)^2} \tag{6}$$

[2] The following nomenclature is used throughout this paper:

X, Y are the individual points.
n = number of points,
$\bar{X}=(\Sigma X)/n$; $\bar{Y}=(\Sigma Y)/n$,
$x=X-\bar{X}$; $y=Y-\bar{Y}$,
$Sx^2=\Sigma X^2-(\Sigma X)^2/n$,
$Sy^2=\Sigma Y^2-(\Sigma Y)^2/n$,
$Sxy=\Sigma XY-(\Sigma X)\,(\Sigma Y)/n$
$Sx^3=\Sigma X\cdot X^2-(\Sigma X)\,(\Sigma X^2)/n$
$Sx^2y=\Sigma X^2Y-(\Sigma X^2)\,(\Sigma Y)/n$, and
$Sx^4=\Sigma X^2\cdot X^2-(\Sigma X^2)^2/n$

The denominator of eq (6) contains only terms [3] in x and, hence, is independent of Z and need not be determined. The numerator is designated by $F_{(Z)}$

$$F_{(Z)}=Sx^2Sx^2y-Sx^3Sxy \tag{7}$$

As each successive choice of Z is made, the value of Y is computed for each experimental point and $F_{(Z)}$ evaluated from eq (7). If the new $F_{(Z)}$ is nearer zero than the last, the new choice has then resulted in an improvement in linearity.[4]

The question may arise as to how far this procedure need be carried before the results can be considered acceptable. This can be answered in terms of the experimental error as measured by the random scatter of the points. This is discussed in the next section of this paper. A standard deviation $s_{(1/V_m)}$ attributable to random scatter is relatively insensitive to small changes in Z. On the other hand, the value of $1/V_m$ may be extremely sensitive to changes in Z. Consider, therefore, two values of Z that produce corresponding values of $F_{(Z)}$, both greater than and less than zero, respectively. Two sets of values for Y may be determined and from these, two values of $1/V_m$. If the difference between these latter two is small compared with $s_{(1/V_m)}$, estimated from either set, no further improvement in Z can be justified by the data.

3. Estimate of Experimental Error

The preceding section was concerned with the contribution of the error of the dead space to the over-all variability of the results. When this is sufficiently reduced, the variability that remains is a measure of the scatter of the experimental points.

The errors associated with the regression parameters a and b may be readily calculated. Furthermore, an equation may be derived [3, 4, 5] for the standard deviation of the sum of a and b. The result may be written

$$s^2_{(1/Vm)}=s^2_{y\cdot x}[1/n+(1-\bar{X})^2/Sx^2]. \tag{8}$$

The term $s^2_{y\cdot x}$ is evaluated as follows [5, 6]

$$(n-3)s^2_{y\cdot x}=Sy^2-(Sxy)^2/Sx.^2 \tag{9}$$

Confidence limits in $1/V_m$ may be determined by inserting "student-t" values into the relationship

$$\pm l(1/V_m)=[s_{(1/V_m)}]\;[t_{(n-3)}]. \tag{10}$$

[3] Pressure (or relative pressure), which is taken as the independent variable, is assumed to be measured without error. While this is not strictly true, the assumption is permissible since these errors are probably very small as compared with those for derived quantities such as the volume of gas adsorbed, which appears in the ordinate. Furthermore, the errors in Y are assumed to be completely random and normally distributed about a mean of zero.

[4] The quantity $F_{(Z)}$ (as it passes through zero) has a positive slope (with respect to Z). An estimate of the magnitude of this slope from previous choices aids in the selection of Z.

[5] The quantity $(n-3)$ is preferred here as a more conservative estimate of the number of degrees of freedom than $(n-2)$. This is because the data have been utilized for the determination of three parameters instead of the usual two.

[6] In computing $s_{y\cdot x}$ from eq (9), rounding off by dropping of digits should be postponed until the end of the operation, otherwise serious errors may be introduced.

Hence, the confidence interval surrounding V_m (which is proportional to the surface area) is given as

$$\frac{1}{1/V_m+l(1/V_m)} \lessgtr V_m \lessgtr \frac{1}{1/V_m-l(1/V_m)}. \qquad (11)$$

The 95-percent confidence limits are implied if not otherwise stated. In layman's language this means that the interval determined by the stated limits will, on the average, bracket the correct value of $1/V_m$ 95 percent of the time. The appropriate "student-t" values may be found in any elementary textbook on statistical methods.

The method outlined will now be applied to a 24.4188 g sample of Pitch Coke (Koppers Co.) which was found to have a surface area of 1.6 m^2/g. Table 1 summarizes the adsorption measurements using nitrogen at 90° K for which the BET free-surface equation was known to apply. The values in the second column of table 1 were determined with use of eq (3) to express V in terms of Z. Values of some of the quantities used in this example are $k=917.32$ ml/mole; $R=6.236\times10^4$ (mm Hg) (ml) $(\text{mole})^{-1}$ $(°\text{K})^{-1}$ $f=1+3.3\ p\times10^{-5}$; and 2,715 mm $\lessgtr p_0 \lessgtr$ 2,722 mm.

TABLE 1. *Adsorption measurements of N_2 at 90° K on Pitch Coke (Koppers Co.)*

Relative pressures (X)	$\frac{p}{V(p_o-p)}$ [V expressed in terms of Z by eq (3)]
0.0869	(1.1700)/[9.367—(42.670)Z]
.1411	(1.7909)/[12.469—(62.366)Z]
.1765	(2.3364)/[14.942—(78.231)Z]
.1972	(2.6769)/[16.290—(87.508)Z]
.2182	(3.0430)/[17.893—(96.916)Z]
.2341	(3.3322)/[18.870—(104.080)Z]
.2540	(3.7118)/[20.375—(113.057)Z]
.2679	(3.9887)/[21.243—(119.425)Z]

The geometry of the adsorption vessel furnishes a means to estimate the first values to be ascribed to Z. After a few trials the choice of Z was narrowed down to within 0.135 and 0.137 for which $F_{(Z)}$ was less than zero and greater than zero, respectively. An estimate of the standard deviation was made according to eq (8) and the results are entered in table 2.

It can be seen from table 2 that the difference between the two values for $1/V_m$ for the first comparison amounts to more than three times the estimate of $s_{(1/V_m)}$. This means that further improvement in Z should be made in order that the limiting factor in the precision of the experiment be the random scatter of the points. It is significant that if the dead space had been calibrated directly, and the results obtained were 12.15 and 12.33 ml for duplicate determinations, the agreement would have been considered acceptable. Yet these values correspond to 0.135 and 0.137 for Z which has just been shown to have too wide a spread to be acceptable.

TABLE 2. *Results of successive approximations*

	1st comparison			2d comparison		
Z	0.135	-----	0.137	0.1362	-----	0.1363
$F_{(Z)}\times10^5$	−.022	-----	+.012	−.006	-----	+.002
$1/V_m$	2.686	-----	2.850	2.782	-----	2.791
$\Delta(1/V_m)$	-----	0.164	-----	-----	0.009	-----
$s_{(1/V_m)}$	0.047	-----	0.051	0.049	-----	0.049
$\pm l_{(1/V_m)}$	-----	-----	-----	.1264	-----	.1269

Upon further refinement of the computations by successive approximations, the spread in Z was decreased to fall within 0.1362 and 0.1363 and the results are also summarized in table 2. The difference between the values of $1/V_m$ has now been diminished to an acceptable value of 0.009 since this is only about one-fifth the standard deviation of $1/V_m$. Hence, there is no need for further refinement. The average of the acceptable values of $1/V_m$ is 2.786 with 95-percent confidence limits of ±0.1267. This corresponds to a surface area of

$$1.656^{+0.080}_{-0.072}\ m^2/g.$$

4. Application to the Langmuir Equation

The development is simpler in the event that the isotherm applicable to the data is the Langmuir equation (eq 2) where now $1/V_m=b$. The quantity p/v when plotted as a function of p results in a straight line providing the correct dead space is used. The experimental error is obtained by the same reasoning that was used in the previous section. Equation (9) is equally applicable for determining $s^2_{y.x}$. However, instead of eq (8), the corresponding relationship is

$$s^2_{(1/V_m)}=s^2_{y.x}/Sx^2. \qquad (12)$$

The remainder of the treatment for this case is exactly the same as that already described.

5. Discussion

The effect of an error in the dead space upon the determination of the volume of gas adsorbed becomes especially serious whenever the amount of adsorbed gas is small compared with the unadsorbed gas. Indeed, the uncertainty in the measurement of the dead space can overshadow the unreliability of all other factors which contribute to the over-all error in V_m. This error can be decreased appreciably by a different choice of experimental conditions designed to increase the adsorption. The use of krypton as the adsorbate at liquid nitrogen temperatures has become increasingly popular in this connection especially where the surface areas to be measured are extremely small (i. e. of the order of 100 cm^2/g).

The technique described in this paper is not proposed as an alternative to the use of krypton, but rather as a supplement. It can be applied to isotherms obtained with krypton as well as with

nitrogen or any other gas for that matter, as long as the isotherm equations are applicable. For many practical reasons [7] it is desirable to use nitrogen in preference to krypton where at all possible. The limiting criterion should be whether sufficient precision is obtainable using nitrogen based upon the scatter of the adsorption points alone.

It is a common experience in many laboratories to repeat adsorption measurements because many of the points fail to conform to the BET isotherm equation. Small errors in the dead space could account for such failures, especially when the volume adsorbed is small. For such cases the technique of this paper is of considerable value.

There may be reasons for discrepancies existing between measurements of dead space and their correct values other than the usual limitations in the precision of the experimental observation. Helium may itself be adsorbed upon certain materials [8] at the temperature of the dead space calibration. Also, probably more commonly than realized, adsorbents may have an appreciable volume within pores larger than that of the helium molecule, but smaller than nitrogen. This would give rise to a molecular-sieve phenomenon that might alter the dead space obtained from a helium calibration.

The most reliable estimate of surface area is obtained by taking the arithmetical mean of several independent determinations. In this way, chance variations even among samples can be averaged out. Such a procedure for as few as two determinations can seldom be justified economically. The only practical alternative is to make a single determination. Hence, it is especially important to select a representative sample and to employ an analytical technique which leads to results of the highest precision that the data are capable of yielding. An estimate of this precision is also very desirable. It is believed that the present work accomplishes these ends.

Obviously, the calculations are somewhat more time consuming with the proposed technique than with the conventional method of determining dead space. The time saved by elimination of the dead space calibration partially compensates for the additional time required for the calculations.

The more experimental points taken within the applicable pressure range of the isotherm equation, the better one is able to distinguish between experimental error and incorrect dead space. However, a large number of points is time consuming, and increases the possibility of introducing errors due to undetected changes in experimental conditions. While it is beyond the scope of this paper to determine rigorously the minimum number of points required, it is felt from experience that about eight is a practical compromise.

The helium calibration employed in the conventional method for surface area determination sometimes poses a problem not universally encountered. The limited availability of helium in many areas could act as an effective deterrent for its use, particularly where surface area measurements are of a rountine nature. For these localities a technique such as that described in this paper should be especially attractive.

6. References

[1] S. Brunauer, P. H. Emmett, and E. Teller, J. Am. Chem. Soc. **60,** 309 (1938).

[2] W. V. Loebenstein and V. R. Deitz, J. Research NBS **46,** 51 (1951) RP2174.

[3] W. E. Deming, Statistical adjustment of data, p. 167 (John Wiley & Sons, 1943).

[4] F. D. Rossini and W. E. Deming, J. Wash. Acad. Sci. **29,** 416 (1939).

[5] S. S. Wilks, Mathematical statistics, p. 158 (Princeton Univ. Press, 1943).

Washington, August 26, 1957.

[7] 1. Highly sensitive differential pressure measuring techniques are required since all the adsorption points must fall within the pressure range of 0.2 to 0.6 mm where the BET isotherm is valid.

2. Long periods of time are required before equilibrium is attained at each adsorption pressure.

3. Thermal transpiration (thermo-molecular diffusion) effects become so pronounced that special calibration is required to correct for this phenomenon.

[8] A polymer carbon described by F. H. Winslow, W. O. Baker, N. R. Pape, and W. Matreyek, J. Polymer Sci. **16,** 101 (1955) adsorbed 3 cm³ of helium per g even at 30° C. The surface area of this sample (nearly 600 m²/g) was determined from its nitrogen adsorption at 90° K. The absolute error of the dead space was quite large because of the appreciable adsorption of helium at that temperature. The relative effect of this error upon the surface area was negligible, however, because of the very large adsorption of nitrogen as compared with the unadsorbed gas in equilibrium with it.

Journal of Research of the National Bureau of Standards Vol. 60, No. 2, February 1958 Research Paper 2827

Sample Calculations of Gamma-Ray Penetration Into Shelters: Contributions of Sky Shine and Roof Contamination [1]

Martin J. Berger and James C. Lamkin

An approximate method is presented for calculating the penetration of gamma radiation in shelters. Sample calculations, for an assumed source energy of 1 million electron volts, are given for the following problems: (1) Dose rate inside houses and underground shelters whose roofs are covered with radioactive fallout, and (2) dose rate in open holes due to reflected radiation (sky shine) from fallout contamination on the surrounding ground. A detailed examination is made of the dependence of the dose rate in a shelter on the shape of the shelter, and on the position of the detector within the shelter. The estimated accuracy of the calculations is ±30 percent.

1. Introduction

The shielding against gamma radiation provided by shelters, houses, and similar structures is of considerable practical interest. The experimental data on this problem are usually obtained under complex circumstances, so that they are difficult to interpret. It is desirable, therefore, to obtain some theoretical understanding of the shielding problem. Calculations with the required accuracy (say 30 to 50%) appear feasible, and are perhaps easier than experimental determinations.

The well-developed semianalytic theory of the penetration and diffusion of gamma radiation [1,3] [2] treats only infinite homogeneous media, and is thus not directly applicable to the problem under consideration which involves more complicated boundary conditions. Yet the theory provides the foundations on which the calculations can be carried out. It would be possible, but rather laborious, to take the boundary conditions into account by means of random sampling (Monte Carlo). Another approach appears more promising—the adaptation of infinite-medium results to realistic conditions through a suitable schematization.

It is the purpose of this paper to explore one such schematization that can be applied to calculations of *shielding against fallout radiation*. In this schematization, the radiation dose inside a shelter is computed as a suitable weighted integral over the angular distribution of the radiation dose in an infinite medium. The present paper contains only pilot calculations. More extensive and systematic calculations are now in progress as part of a National Bureau of Standards program of shelter evaluation, carried out under the auspices of the Federal Civil Defense Administration.

[1] Work supported by the Federal Civil Defense Administration.

[2] Figures in brackets indicate the literature references at the end of this paper.

2. Schematization

The nature of the schematization can be most easily explained by applications to specific problems. Generalization to other situations is then straightforward. Figure 1 illustrates the schematization to be employed for three typical situations that will form the basis for our discussion.

2.1. Underground Shelter With Roof Covered by Fallout

The shelter roof and the surrounding ground are assumed to be covered with radioactive material that constitutes a *plane isotropic source of gamma radiation* of constant strength per unit area, which emits gamma rays uniformly in all directions.

Simplification 1. Different materials of low average atomic number, such as air, concrete, earth, or water, have nearly the same gamma-ray mass attenuation coefficients. Provided that all distances from the source are expressed in units of mass per unit area, it is therefore a good approximation to replace the combination air-concrete (or earth) by a concrete medium that is infinite and homogeneous, except that it contains an air cavity (the inside of the shelter).

Simplification 2. In order to reach a detector somewhere inside the shelter, radiation must penetrate varying amounts of concrete or earth, depending on its path. Radiation coming through the ceiling has the least amount of material to traverse and is therefore least attenuated. There are two types of paths on which photons could reach the detector through the floor. They can detour the shelter to come up from below, but in this case the attenuation is so strong that the contribution of the detoured photons is negligible. There is also the more important possibility for photons to enter the shel-

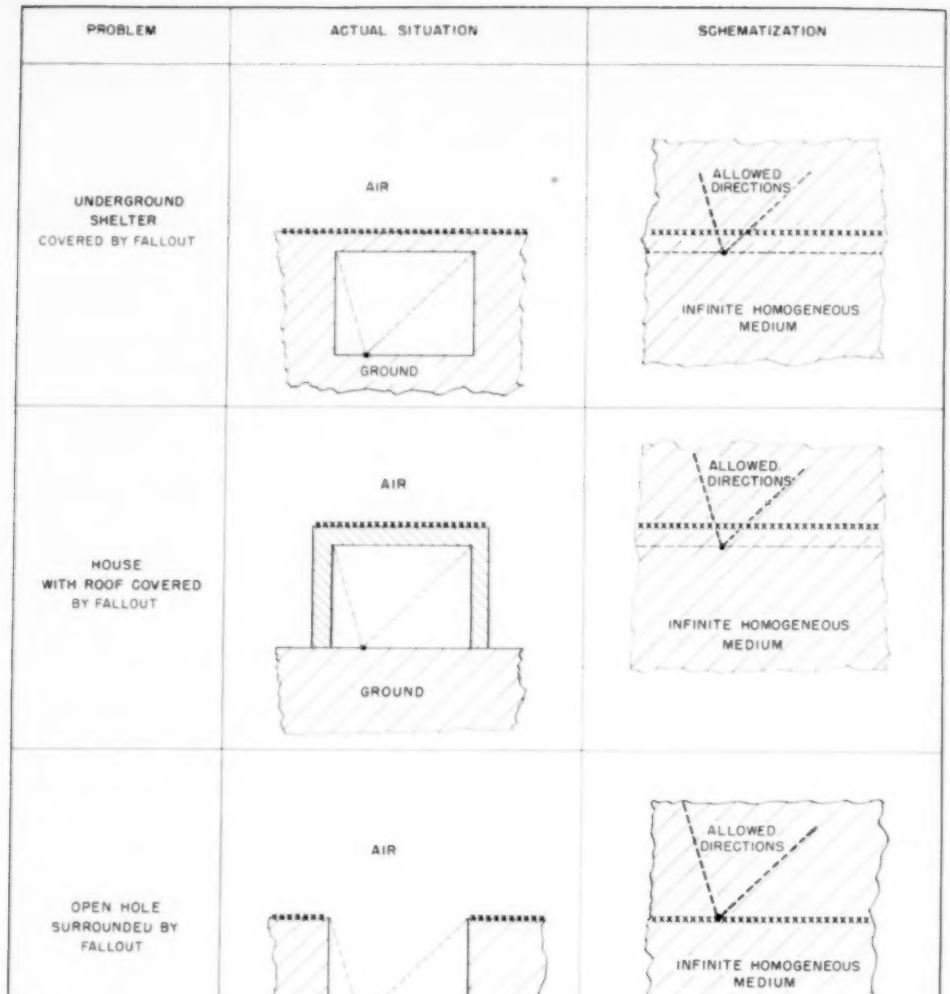

FIGURE 1. *Schematization.*

ter through the ceiling, to penetrate into the floor (or side walls) and then to be backscattered. Some radiation will also penetrate to the detector through the side walls of the shelter. But because of the small size of a mean free path in concrete or earth (a few inches) only a small side-wall region near the ceiling can make a nonnegligible contribution, resulting in an effective ceiling area somewhat larger than the true ceiling area. Both the backscattering correction and the side-wall penetration correction are small. They are briefly discussed in sections 6.1 and 6.2 but are omitted from the initial schematization. It will be a good first approximation to consider only radiation entering through the ceiling. The mean free path in air is of the order of several hundred feet, and is very large compared to the shelter dimensions. The radiation thus travels in a straight line inside the shelter and can reach a detector only if its direction of motion lies within the solid angle subtended by the ceiling with respect to the detector. This solid angle is indicated in figure 1 by the label "allowed directions." The notion of "allowed directions" will be formalized later through the introduction of an "angular response function."

Summary of the Calculation. The calculation consists of the following steps: (1) Replacement of the air-shelter complex by an infinite concrete medium; (2) computation of the amount and angular distribution of the radiation in such a medium, at a distance from an infinite plane isotropic source equal to the thickness of the shelter roof; (3) computation of the

angular response function for a specific shelter-detector configuration; (4) computation of the total amount of radiation received by the detector, by an integral over the angular distribution weighted by the angular response function; and (5) corrections to account for additional radiation reaching the detector through the side walls, and by the reflection from interior surfaces of the shelter.

2.2. House With Roof Covered by Fallout

As indicated in figure 1, the schematization for this problem is essentially the same as for the previous problem. A number of points require comment, however.

(1) The contamination now is confined to the roof so that the plane-isotropic source is *finite*. Yet the situation is practically equivalent to that of an underground shelter underneath an infinite contaminated plane. Note that in the underground shelter, fallout from regions other than that directly above the roof does not contribute appreciably to the dose, because of the large amount of intervening earth.

The equivalence is, of course, only approximate. To illustrate the order of magnitude of the error involved, one may consider the following point. In the schematization, approximately 10 to 15 percent of the energy emitted by the source is reflected back toward the roof. In the actual situation, with air above the roof, this reflected radiation would spread laterally, and most of it would come down on the ground surrounding the roof. The reflected radiation assumed incorrectly to be incident on the roof is low in energy and diffuse in direction, so that its penetrating power is much less than that of the source radiation. Hence, the resulting dose-overestimate will only be a few percent.

(2) There is a somewhat better chance than in the case of an underground shelter, that radiation originating on the roof will reach the detector through the side walls. But this radiation consists mainly of photons which after repeated air scattering are incident on the side walls with low energies and therefore are not very penetrating.

(3) If the ground surrounding the house is also covered with fallout, the penetration of radiation through the side walls becomes very important. The numerical details of this case are not worked out in the present paper, but the same schematization could be applied as in the case of a roof contamination, through the introduction of appropriate allowed directions and angular response functions defined with respect to the side walls, or perhaps the windows.

2.3. Open Hole Surrounded by Fallout

Again, the schematization is essentially the same as in 2.1. The detector is now in a position where it cannot "see" the source, i. e., only *scattered* radiation can reach it. This scattered radiation will consist mainly of photons that have gone up into the air and are reflected into the hole by scattering. This radiation component is customarily called *sky shine*. The radiation distributions that must now be used in steps (2) and (4) of the schematized calculation are those pertaining to the *scattered* flux at the source plane.

3. Mathematical Formulation

An isotropic source of gramma radiation is assumed to be located in the plane $z=0$. Let $I_D(z, \theta) \sin \theta d\theta$ denote the dose delivered to a detector in an infinite homogeneous medium at a distance z from the source plane, by photons incident on the detector at angles between θ and $\theta+d\theta$ (with respect to the z-axis). Dose means the quantity technically called "absorbed air dose", i. e., energy dissipated in air, measured in rads (100 ergs/g) [2]. It will be convenient to express the dose distribution in the form

$$I_D(z,\theta)=f(z)g(z,\theta), \tag{1}$$

where $g(z,\theta)$ is an angular distribution normalized to unity:

$$\int_0^\pi g(z,\theta) \sin \theta d\theta=1. \tag{2}$$

The factor $f(z)$ will represent the attenuation of radiation by the roof of thickness z in the problems of the house or underground shelter. For the open hole, one must replace $f(z)$ and $g(z,\theta)$ by quantities $f_s(z)$ and $g_s(z,\theta)$ pertaining to *scattered* radiation.

Let the shelter-detector configuration be such that only a fraction $\psi(\theta)$ of the photons with direction θ can reach the detector. This function is called the angular response function and is further discussed in section 5. The dose $D(z)$ received by the partially shielded detector in the shelter is expressible as the product of three factors:

$$D(z)=Cf(z)\ G(z), \tag{3}$$

where

$$G(z)=\int_0^\pi g(z,\theta)\,\psi(\theta) \sin \theta d\theta, \tag{4}$$

and C is a correction factor taking into account the contribution of radiation penetrating through the side walls or reflected from the interior surfaces. The determination of the geometrical protection factor G is the main objective of this paper.

4. Calculation of the Radiation Field

The standard solution for an infinite homogeneous medium is provided by the moment method [1]. Tabulations based on this method are available from which one can extract information about the dose $f(z)$ from a plane isotropic source [3].[3] The calculation of the angular distribution $g(z,\theta)$ has been described in [4].

The numerical computations of this paper all pertain to a source emitting 1-Mev photons. This source energy is a little higher than the average energy of fallout radiation, but close to the energy

[3] As part of the work sponsored by FCDA, further tabulations, with applications to shelter evaluation, are now being prepared at NBS.

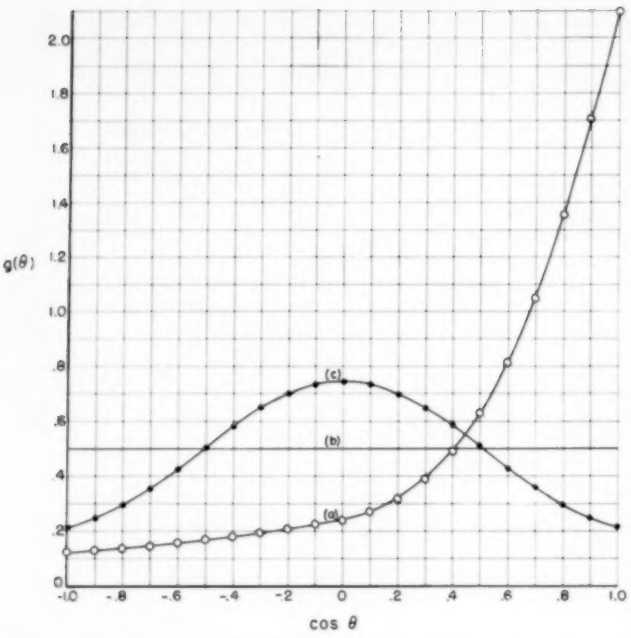

FIGURE 2. *Angular distribution of absorbed air dose from a 1-Mev plane isotropic source in an infinite medium.*

The calculation is for a water medium, but is in very good approximation also applicable to concrete.
(a) $g(z,\theta)$, at a distance $\mu_0 z=4$ from the source plane.
(c) $g_s(z,\theta)$, at the source plane $\mu_0 z=0$ (This distribution represents only the contribution of *scattered* photons.)
The curve (b) represents an isotropic distribution.

of Co^{60}-radiation, which is most suitable for controlled experimentation. The choice was motivated by the ready availability of results for $g(z,\theta)$. In any case, calculations with a 1-Mev source will be sufficient for the illustrative purposes of this paper.

Let $f(z)$ be the dose in an infinite concrete medium at a distance z from a plane isotropic source. The results of a calculation by the moment method can be summarized by the approximate formula

$$f(z)=f_0(z)+f_s(z) \tag{5}$$

with

$$f_0(z)=kE_1(\mu_0 z), \tag{5a}$$

representing the contribution of unscattered radiation, and with

$$f_s(z)=1.04ke^{-0.915\mu_0 z}, \tag{5b}$$

representing the contribution of scattered radiation. The range of validity of (5b) is $0\leq\mu_0 z\lesssim 8$, E_1 is the exponential integral [5], and $\mu_0=0.0635$ cm^2/g is the mass attenuation coefficient for gamma radiation in concrete at the source energy (1 Mev). The constant k determines the source normalization. If the source plane is covered with 1 curie of gamma emitter per square foot, and the dose rate is expressed in rads per hour, the normalization constant has the value

$$k=32.2. \tag{5c}$$

If the fallout is spread over a rough surface, the schematization of the source as a perfect geometric plane is not altogether suitable. A possible alternative schematization consists in assuming that the radioactive material is mixed homogeneously with a thin top layer of the ground of thickness t. In this case, the dose function $f(z)$ must be replaced by

$$f^*(z,t)=\frac{1}{t}\int_z^{z+t} f(z')\,dz'. \tag{6}$$

Three angular distributions are shown in figure 2: (a) $g(z,\theta)$ at a distance $\mu_0 z=4$ (0.897 lb of concrete per square inch); (b) a completely isotropic distribution; and (c) the distribution $g_s(z,\theta)$ for *scattered* radiation only, at the source plane $\mu_0 z=0$. The distribution (a) peaks at $\theta=0°$ and is for use in the problems treated in sections 2.1 and 2.2. The distribution (c) peaks at $\theta=90°$ and is for use in the problem in section 2.3. Both of these distributions pertain to an infinite plane-isotropic source and were calculated according to the method of reference [4]. The distribution (b) is flat (when plotted against cos θ) and has been included as an intermediate case. Together, the three cases span a wide range of possible distributions.

5. Calculation of the Response Function

To each angle θ there corresponds a family of unit vectors $(\sin\theta\cos\varphi, \sin\theta\sin\varphi, \cos\theta)$, indicating possible photon directions. If these unit vectors are required by the schematization to lie within a specified solid angle, then not all values of the azimuth φ are permitted, but only azimuths in a region $A_\theta\leq 2\pi$. The response function is defined as the fraction $\psi(\theta)=A_\theta/2\pi$.

5.1. Cylindrical Geometry

As a simple first example, we consider a shelter in the form of an upright cylinder of height H and radius R, with the detector located at the center of the bottom of the shelter (see fig. 3). The response

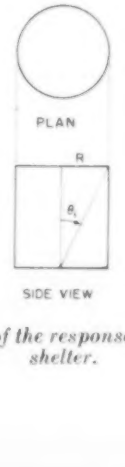

FIGURE 3. *Calculation of the response function for a cylindrical shelter.*

function is in this case particularly simple:

$$\left.\begin{aligned} &0 \leq \theta \leq \theta_1 = \cos^{-1} \frac{H}{\sqrt{H^2+R^2}}, \quad A_\theta = 2\pi, \ \psi(\theta) = 1 \\ &\theta_1 < \theta \leq \pi \qquad\qquad\qquad , A_\theta = 0, \quad \psi(\theta) = 0. \end{aligned}\right\} \tag{7}$$

5.2. Parallelepiped Geometry

We consider a box-shaped shelter of length L, width W, and height H. It can be assumed without loss of generality that $L \geq W$. The response function depends on solid angles, and is thus a function of the shape but not of the absolute size of the shelter. Therefore, we eliminate one parameter by dividing all dimensions of the shelter by L, so that the scaled length is unity, the scaled width is

$$W/L = \epsilon \leq 1, \tag{8}$$

and the scaled height is

$$H/L = h. \tag{9}$$

The construction of the response function is illustrated in figure 4 for a detector in a bottom corner of the shelter.

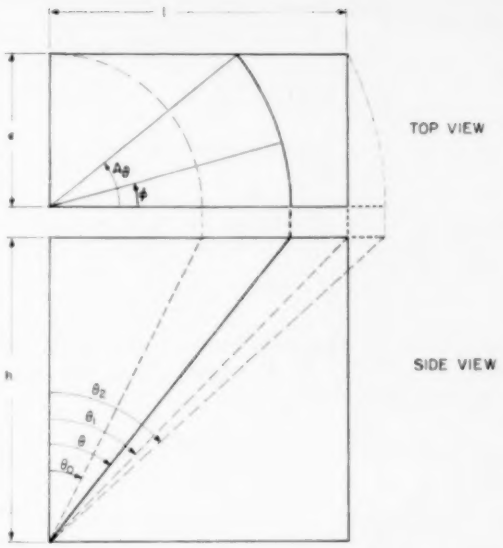

FIGURE 4. *Calculation of the response function for a box-shaped shelter.*

Angular range	Response function, $\psi(\theta,\epsilon,h)$
$0 \leq \theta \leq \theta_0 = \cos^{-1} \frac{h}{\sqrt{h^2+\epsilon^2}}$	1
$\theta_0 < \theta \leq \theta_1 = \cos^{-1} \frac{h}{\sqrt{h^2+1}}$	$\frac{1}{2\pi} \sin^{-1} \left(\frac{\epsilon}{h \tan \theta}\right)$
$\theta_1 < \theta \leq \theta_2 = \cos^{-1} \frac{h}{\sqrt{h^2+\epsilon^2+1}}$	$\frac{1}{2\pi} \sin^{-1} \left(\frac{\epsilon}{h \tan \theta}\right) - \frac{1}{2\pi} \cos^{-1} \left(\frac{1}{h \tan \theta}\right)$
$\theta_2 < \theta \leq \pi$	0

(10)

The response function (10), evaluated with the parameters $\epsilon = 0.5$ and $h = 0.5$, is shown in figure 5.

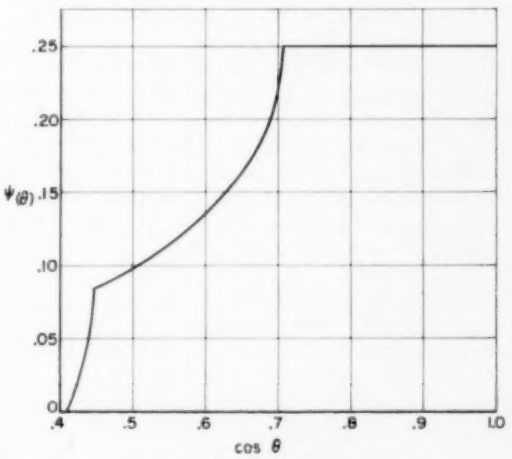

FIGURE 5. *Response function for a detector at a bottom corner of a box-shaped shelter with scaled width (horizontal eccentricity) $\epsilon = 0.5$ and height $h = 0.5$.*

5.3. Combination Rule

Expression (10) can readily be generalized so as to provide the response function for an arbitrary detector location. In the first place, it is to be noted that—within our schematization—the vertical distance of the detector from the shelter ceiling (or top of the open hole) must be assumed as the effective height H. Now consider a detector located at the bottom of the shelter, in a horizontal position P with coordinates $(\alpha,\beta\epsilon)$, as illustrated in figure 6. We now imagine that the shelter is partitioned by two vertical walls (perpendicular to each other), which pass through the point P, and are very thin, but perfect, radiation shields. The detector can then

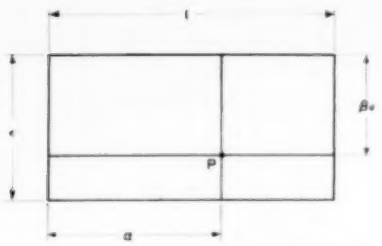

FIGURE 6. *Diagram illustrating the application of the combination rule by which response functions for off-corner positions are calculated.*

be thought of as being located at the corner of each of four adjoining box-shaped shelters with the dimensions listed below.

j	ϵ_j	h_j
1	$\frac{\min(\alpha, \beta\epsilon)}{\max(\alpha, \beta\epsilon)}$	$\frac{h}{\max(\alpha, \beta\epsilon)}$
2	$\frac{\min(1-\alpha, \beta\epsilon)}{\max(1-\alpha, \beta\epsilon)}$	$\frac{h}{\max(1-\alpha, \beta\epsilon)}$
3	$\frac{\min(\alpha, \epsilon-\beta\epsilon)}{\max(\alpha, \epsilon-\beta\epsilon)}$	$\frac{h}{\max(\alpha, \epsilon-\beta\epsilon)}$
4	$\frac{\min(1-\alpha, \epsilon-\beta\epsilon)}{\max(1-\alpha, \epsilon-\beta\epsilon)}$	$\frac{h}{\max(1-\alpha, \epsilon-\beta\epsilon)}$

$0 \leq \alpha \leq 1$, $0 \leq \beta \leq 1$.
$\min(x, y)$ = smaller of x and y.
$\max(x, y)$ = larger of x and y.

The response function ψ_P at point P is

$$\psi_P(\theta) = \sum_{j=1}^{4} \psi(\theta, \epsilon_j, h_j). \tag{11}$$

5.4. Legendre Polynomial Expansion

In order to obtain the geometric protection factor $G(z)$, it is necessary to evaluate the integral in (4) for each distribution $g(z,\theta)$ of interest. When many distributions must be included, this procedure tends to become laborious. It is then convenient to perform a set of standard integrations based on an expansion of the response function into a series of Legendre polynomials:

$$\psi(\theta) = \sum_{l=0}^{\infty} \frac{2l+1}{2} a_l P_l(\cos\theta). \tag{12}$$

The theory of radiation diffusion provides as the most direct result, a similar Legendre polynomial expansion for the angular distribution:

$$g(z,\theta) = \sum_{l=0}^{L} \frac{2l+1}{2} g_l(z) P_l(\cos\theta). \tag{13}$$

As a rule, only the first few harmonics ($l=0, 1, \ldots, L \leq 7$) are at one's disposal, but they suffice to specify $g(z,\theta)$. When (12) and (13) are substituted into (4), it follows from the orthogonality of the Legendre polynomials that

$$G(z) = \sum_{l=0}^{\infty} \sum_{n=0}^{L} \frac{2l+1}{2} a_l \frac{2n+1}{2} g_n(z) \int_0^{\pi} P_l(\cos\theta) P_n(\cos\theta) \sin\theta d\theta \tag{14}$$

$$= \sum_{l=0}^{L} \frac{2l+1}{2} a_l g_l(z).$$

Thus, one can limit oneself to the calculation of the first few response function expansion coefficients

$$a_l = \int_0^{\pi} \psi(\theta) P_l(\cos\theta) \sin\theta d\theta, \; l = 0, 1, \ldots, L. \tag{15}$$

With these coefficients, one is in a position to evaluate $G(z)$ for any angular distribution $g(z,\theta)$ through simple superposition according to (14).

Numerical evaluations of G have been carried out for detectors in various positions in box-shaped shelters, on the basis of the angular distribution functions shown in figure 2. These results apply as follows:

Problem	Angular distribution	Infinite medium dose-rate $\frac{\text{rads/hour}}{\text{curies/foot}^2}$
Underground shelter or house with roof covered by fallout, roof thickness $\mu_0 z = 4$ (0.896 lb of concrete per square inch).	(a)	$f(z) = 0.983$
Isotropic comparison distribution.	(b)	----------
Sky shine (scattered radiation) into open hole.	(c)	$f_s(z) = 33.5$

The results are presented as functions of the following dimensionless parameters:

$$\text{Horizontal eccentricity} = \frac{\text{width}}{\text{length}} = \epsilon \tag{16}$$

$$\text{Vertical eccentricity} = \frac{\sqrt{\text{roof-area}}}{\text{height}} = \frac{\sqrt{\epsilon}}{h} = \tau. \tag{17}$$

The range of parameters considered includes $0 \leq \epsilon \leq 1$ and $0.2 \leq \tau \leq 20$. This appears sufficient for all practical applications.

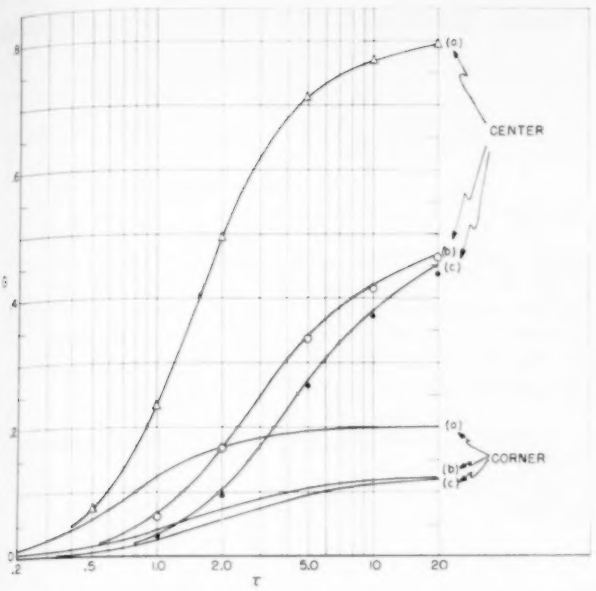

FIGURE 7. *Geometric protection factor versus vertical eccentricity, for fixed horizontal eccentricity* $\epsilon = 1$.

The curves labeled (a), (b), and (c) are based on the use of the corresponding angular distributions in figure 2. The triangles, solid circles, and hollow circles represent results obtained with the response function (7) for a cylindrical shelter.

Figure 7 contains plots of G versus τ, for a shelter with a square cross section ($\epsilon = 1$). Figure 8 contains plots of G versus ϵ, for different fixed values of τ. Results are shown for the detector in a corner, and in a center position ($\alpha = \beta = \frac{1}{2}$). The figures confirm quantitatively what one would expect on the basis of a commonsense estimate. The protection provided by the shelter increases rapidly as τ is increased, but is generally a very slowly varying function of ϵ for fixed τ, except when ϵ has a very small value. Dose rates in the corner are on the order of four times smaller than dose rates in the center. The angular distribution (a) with its strong forward peak gives rise to G-values 2 to 3 times larger than those obtained with the diffuse sky-shine distribution (c), whereas there is little difference between cases (c) and (b).

The question may be asked to what extent the results for the geometrical protection factor are affected by the choice of a rectangular shelter cross section. To obtain a partial answer, calculations were carried out for a detector at the center of a cylindrical shelter, with the use of the response function (7). As can be seen from these values plotted in figure 7, the results thus obtained are, for the same value of τ, practically identical with the results for a detector at the center of a box-shaped shelter with $\epsilon = 1$. This means that the geometric protection factor depends very little on the shape of the cross section. Combined with the previously demonstrated insensitivity of G with respect to the horizontal eccentricity ϵ, this has the following

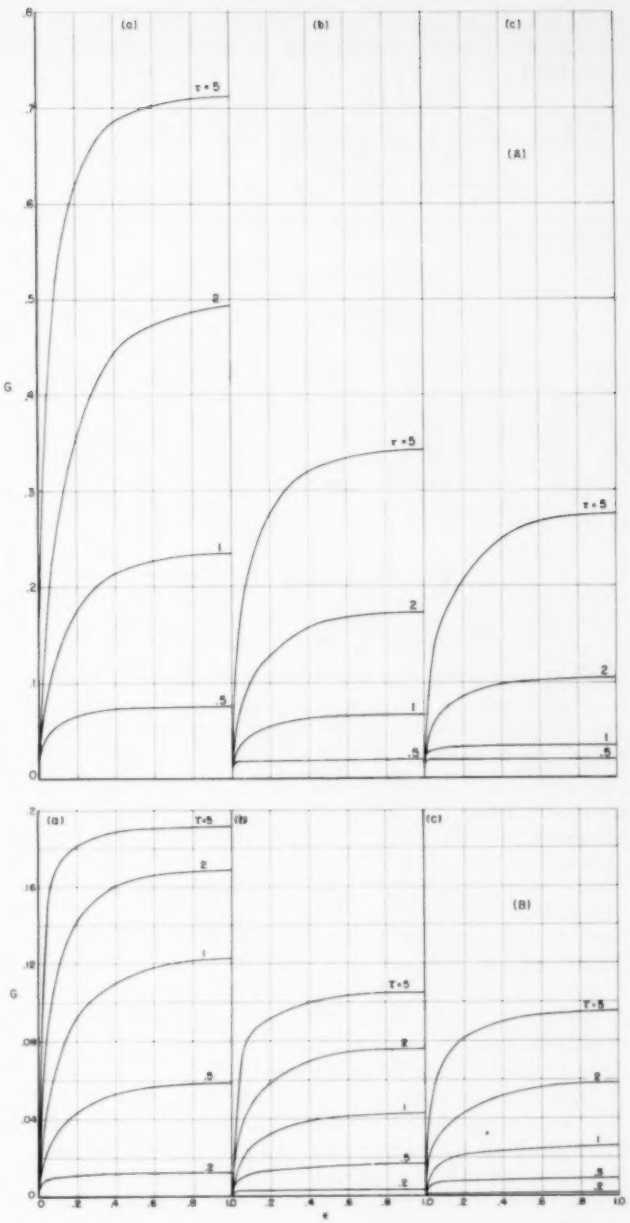

FIGURE 8. *Geometric protection factor versus horizontal eccentricity, for various constant values of the vertical eccentricity.*

The curves labeled (a), (b), and (c) pertain to the corresponding angular distributions of figure 2. (A) Detector in center; (B), detector in corner.

implications: (1) The geometric protection factor at the center of a shelter of any shape is, in good approximation, only a function of the vertical eccentricity τ; (2) under these circumstances, a calculation using the very simple response function (7) will be adequate.

Center and corner values provide upper and lower limits of G. To indicate the transition between the two extremes, a systematic mapping of G is presented

in table 1 for numerous detector positions in the horizontal plane, the shelter being box-shaped with $\epsilon=1$ and $\tau=2$.

TABLE 1. *Geometric protection factor G as a function of the position in the horizontal plane, for a detector in a shelter with horizontal eccentricity $\epsilon=1$ and vertical eccentricity $\tau=2$, calculated for the angular distribution (a) of figure 2*

The position indicators α and β are those defined in figure 6. Note that the ransformations $\alpha\to1-\alpha$, $\beta\to1-\beta$, or $(\alpha\to\beta, \beta\to\alpha)$ leave G unchanged.

β \ α	0. 0	0. 125	0. 25	0. 375	0. 5
0. 0	0. 17	0. 22	0. 26	0. 27	0. 29
. 125	. 22	. 31	. 34	. 37	. 38
. 25	. 26	. 34	. 40	. 43	. 44
. 375	. 27	. 37	. 43	. 47	. 48
. 5	. 29	. 38	. 44	. 48	. 49

6. Corrections, Accuracy

6.1. Penetration Through the Side Walls

This effect has, so far, been investigated only in a limited manner to obtain the order of magnitude of the necessary correction. To simplify the calculations, they were done for a detector at the center of the bottom of a cylindrical cavity. For the case of an underground shelter (the problem in section 2.1), the response function (7) could be amended as follows:

$$\left.\begin{aligned} &\theta_1<\theta\le\frac{\pi}{2},\ \psi(\theta)=\frac{\varphi(z+z')}{\varphi(z)}\,\frac{g(z+z',\theta)}{g(z,\theta)}\\ &\frac{\pi}{2}<\theta\le\pi,\ \psi(\theta)=0 \end{aligned}\right\} \qquad (7')$$

where

$$z'=H-R\cot\theta.$$

The meaning of (7′) is that the surface elements of the side wall contribute to the dose in proportion to the intensity and angular distribution of the radiation at the distance $z=z'$ of the surface elements from the source plane.

Sample calculations have been carried out for a shelter with roof thickness $\mu_0 z=4$, horizontal eccentricity $\epsilon=1$, and a depth of 8 ft. (The side-wall correction differs from the uncorrected response function in that it depends on the absolute size of the shelter.) It was found that for vertical eccentricities

$$\tau=1,\ 2,\ \text{and}\ 4,$$

the increase of the dose is 7, 3, and 1 percent, respectively.

6.2. Backscattering

Some radiation will be scattered toward the detector by reflection from the side walls, floor, and ceiling of the shelter. The order of magnitude of this effect can be estimated roughly on the basis of available Monte Carlo calculations of backscattering. The results of reference [6] suggest a dose increase by approximately 15 percent.

6.3. Over-all Correction and Error Estimate

In the final equation for the dose received by the partially shielded detector,

$$D(z)=Cf(z)G(z), \qquad (3)$$

the factor C, incorporating side-wall and backscattering effects, is estimated to be 1.2. It is further estimated that the factors in (3) have the relative errors $(\delta fG)/fG\approx\pm0.2$ and $(\delta C)/C\approx\pm0.2$, which leads to the following error estimate for D:

$$\frac{\delta D}{D}=\sqrt{\left(\frac{\delta fG}{fG}\right)^2+\left(\frac{\delta C}{C}\right)^2}\approx\pm0.3. \qquad (18)$$

The authors are indebted to L. V. Spencer for valuable discussions, and to J. Hubbell for help with the calculations.

7. References

[1] L. V. Spencer and U. Fano, J. Research NBS **46**, 446 (1951) RP2213.
[2] Report of the International Commission on Radiological Units and Measurements, NBS Handbook 62 (1956).
[3] H. Goldstein and J. E. Wilkins, Jr., AEC Report NYO-3075 (1954).
[4] M. J. Berger, J. Appl. Phys. **26**, 1504 (1955).
[5] Table of sine, cosine and exponential integrals, Federal Works Agency (1940).
[6] M. J. Berger and J. A. Doggett, J. Research NBS **56**, 89 (1956) RP2653.

WASHINGTON, May 16, 1957.

Journal of Research of the National Bureau of Standards Vol. 60, No. 2, February 1958 Research Paper 2828

Heat Content of Sodium Borohydride and of Potassium Borohydride from 0° to 400° C

Thomas B. Douglas and Ann W. Harman

The heat content of sodium borohydride, $NaBH_4$, and of potassium borohydride, KBH_4, was measured, relative to that at 0° C, at 50-degree intervals from 0° to 400° C. The so-called "drop" method was used with a precision Bunsen ice calorimeter and a silver-core furnace. Preliminary tests showed that spontaneous decomposition of these compounds is very slow at temperatures up to 400° C. Measurements were made on two samples of each compound, those of sodium borohydride having been obtained from different sources. Smoothed values of the heat-content function, heat capacity, entropy, and the Gibbs free-energy function were derived from the data. These values were increased by 0.5 percent to correct for the presence of an estimated 1 percent of the corresponding *meta*borate in each sample. The heat capacity of sodium borohydride increases monotonically with temperature in the range investigated; that of potassium borohydride passes through a point of inflection, which suggests that there may be a broad second-order transition in the neighborhood of room temperature.

1. Introduction

There has been a wide interest for many years in the unusual properties and possible uses of compounds between boron and hydrogen, and a great many of them have been prepared and studied. More recently, chemical methods have been devised for preparing metallic borohydrides, which contain the monovalent group BH_4^-. The borohydrides of the alkali metals are much more stable than the known hydrides of boron, dissolving in water at room temperature with but slow decomposition, and resisting spontaneous decomposition in the dry state up to temperatures of several hundred degrees C. Since X-ray patterns indicate a crystal lattice of metallic and borohydride ions, it appears that the relative stability of these compounds can be attributed directly to the high coulomb energy characterizing such typical ionic salts.

In recent years a number of investigators have measured some of the fundamental thermodynamic properties of the borohydrides of the alkali metals.[1] The work reported in this paper contributes to this general program. The heat content of the borohydrides of sodium and potassium was measured from 0° C up to temperatures where decomposition begins, and from these values other important thermodynamic properties were derived.

2. Samples

The heat-content measurements were on two samples of $NaBH_4$ and two of KBH_4. Each sample was in the form of fine white crystals, and was used as received without further purification, except for preliminary heating and evacuation as described later. It appears that purification of these compounds, to a high degree (e. g., to a purity of 99.9 weight percent), is difficult with present techniques. This fact may be due to slight solvolysis of the salts when in solution, with subsequent decomposition of the free acid, for it has been reported that increasing the *p*H of the solution increases the stability of the salt.

One of the samples of $NaBH_4$, hereafter designated as No. 1, was obtained from Metal Hydrides Inc., Beverly, Mass., who reported it to have a purity in excess of 99 percent. This sample was received in a glass-stoppered bottle, and was so kept until used. The other sample, designated as No. 2, was obtained from another source. Its suppliers had recrystallized it twice from liquid ammonia. Their subsequent analyses indicated the following percentages of the theoretical: Potassium, 99.9 percent; boron, 99.9 percent; and hydrogen, 99.4 percent. (The hydrogen reported was that obtained by hydrolysis.) However, considering the limitations of reliability of the analytical methods used, they believed that the purity of this sample (No. 2) could not be more precisely stated than as "safely above 99 percent". The sample was received in a sealed glass ampule, which was not opened until very shortly before the sample was used.

Both "samples" of the KBH_4, distinguished subsequently as No. 1 and No. 2, were really specimens of the same sample, but specimens on which heat-content measurements were made 2 months apart. This "stock" sample was obtained from Metal Hydrides Inc., who had found it to contain 0.1 percent by weight of chlorine and 99.6 percent of the theoretical hydrogen (the latter figure resulting from gasometric analysis). On this basis they believed the sample to have a purity of approximately 99.5 percent. The sample was kept in a vacuum desiccator until very shortly before the heat-content measurements were begun.

Assuming that at some stage during their purification these borohydrides were nearly 100-percent pure, contamination by the atmosphere very likely occurred by conversion of some of the borohydride to borates. It appears that whatever borate is thus

[1] References to such work are given later in this paper.

450817—58——3

formed would maintain the 1:1 atomic ratio of alkali metal and boron characterizing the parent borohydride. Such a borate might be a *meta*borate or, before an opportunity for dehydration, more likely an *ortho*borate (such as $KH_2BO_3 \cdot H_2O$). All such borates other than the *meta*borate are known to dehydrate to form the corresponding *meta*borate at the higher temperatures of the present work, and at lower temperatures they would be expected to possess heat capacities which are approximately additive combinations of the heat capacities of the constituent *meta*borate and chemically bound water. For these reasons it seems simpler to interpret the analyses of the samples as though the somewhat impure sample consisted wholly of borohydride, *meta*borate, and water. Letting M represent either Na or K, decomposition by water or oxygen could then be formulated by the following reactions:

$$MBH_4 + 2H_2O = MBO_2 + 4H_2, \quad (1)$$

$$MBH_4 + 2O_2 = MBO_2 + 2H_2O. \quad (2)$$

(In time, the water formed according to eq (2) might react with additional borohydride according to eq (1).)

Several months after the completion of the thermal measurements reported in this paper, specimens of the unused portions of the stock samples were analyzed in the Chemistry Division of the Bureau. The analytical procedures were as follows.

Hydrogen Evolved. A sample of 0.5 to 1.0 g was transferred to a gas-evolution flask and dissolved in 50 ml of water. Twenty milliliters of 1:1 hydrochloric acid was then slowly added dropwise. The hydrogen gas generated was swept by nitrogen through a condenser and an absorber containing Ascarite (sodium hydroxide on asbestos) and anhydrous magnesium perchlorate. The dry hydrogen was then burned in a combustion tube packed with copper oxide heated to 700° C, the water formed being absorbed in a weighed absorption tube containing anhydrone. Each such determination required about 4 hr. The accuracy of the method was tested by using standard melting-point aluminum (NBS standard sample 44d). The hydrogen evolved in four such analyses of aluminum corresponded to 99.80, 99.62, 99.69, and 99.66 percent of aluminum respectively. Spectrographic analysis had shown the aluminum to contain 0.1 percent of impurities, but the content of oxygen, carbon, and nitrogen was not known.

Boron. Either an aliquot portion of the solution of borohydride used in the preceding procedure or a new sample of 0.25 g was used. After the solution had been adjusted in *p*H to the methyl-red endpoint, it was treated with mannitol and then titrated with 0.1N NaOH to the phenolphthalein endpoint. The titration was continued until further addition of mannitol no longer destroyed the pink color.

Alkali Metal, Volumetrically. A 0.25-g sample was dissolved in water, treated with a few drops of methyl-red indicator, and titrated with 0.1N HCl.

Alkali Metal, Gravimetrically. After decomposition of the borohydride with strong acid, the solution was evaporated with sulfuric acid. After evaporation of the boric acid and ignition of the residue, the alkali metal was weighed as sulfate.

The foregoing procedures were tested on potassium borohydride using an extra sample on which no heat-content measurements were made. The results are given in table 1. Each value in the third column was calculated with the assumption that the particular element determined was present only in the form of KBH_4. Of these values, the last three, resulting from the analyses for boron and potassium, agree closely among themselves but are all appreciably higher than the first value, which resulted from the amount of hydrogen evolved. Averaging the last three values and assuming that the sample contained only KBH_4, KBO_2, and H_2O, it is calculated that the weight percentages of these components were respectively 98.8, 0.8, and 0.4.

TABLE 1. *Test of analytical methods on an extra sample of potassium borohydride*

Element determined	No. of determinations	Mean result as weight % KBH_4	Average deviation from mean
Hydrogen (evolution)	3	98.79	0.10
Boron (by titration)	6	99.28	.07
Potassium (by titration)	3	99.36	.09
Potassium (gravimetrically)	4	99.30	.09

The methods for determining hydrogen evolved and boron present were extended to unused portions of the samples on which heat-content measurements had been made, duplicate determinations being made in each case. The mean results, calculated as percentages of borohydride, *meta*borate, and water, are given in table 2. The KBH_4 stock sample analyzed was the source of both heat-content samples No. 1 and No. 2 of this substance, and it will be noted that three sets of results are given for this material. The first set was obtained on a specimen protected from the atmosphere, and the second and third sets were obtained on two specimens which had deliberately been exposed to the laboratory atmosphere for 5 and 20 days respectively, just preceding analysis.

It will immediately be evident from table 2 that these analyses, which were carried out after the heat-content measurements, indicate decidedly less borohydride content than the analyses that preceded the

TABLE 2. *Analyses of borohydride samples after the heat-content measurements*

Stock samples	Borohydride	Metaborate	Water
	Weight %	*Weight %*	*Weight %*
$NaBH_4$, sample No. 1	92.6	5.3	2.1
$NaBH_4$, sample No. 2	98.60	1.18	0.22
KBH_4, unexposed	98.36	1.58	.06
KBH_4, exposed 5 days	98.02	2.17	−.19
KBH_4, exposed 20 days	97.78		

heat-content measurements and which were referred to at the beginning of this section. The slow decomposition of potassium borohydride in contact with moist air also is evident. An attempt is made later (section 4) to estimate the chemical composition of the samples at the times when the heat-content measurements were made, so that appropriate corrections to the observed heat-content values may be applied.

3. Preliminary Tests of Chemical Stability at High Temperatures

It was desirable to extend the heat-content measurements to temperatures as high as possible without incurring sufficient chemical decomposition to invalidate the thermal values. In such cases it is obviously important to know not only the initial purity of the samples but also any significant change in the degree of purity resulting from decomposition during the measurements through exposure of the samples to high temperatures.

Some qualitative information about the borohydrides of sodium and potassium is available in the literature. It has been reported [1],[2] for example, that when potassium borohydride of 98.8-percent purity was heated in a fused silica tube in vacuum, decomposition commenced at about 500° C with the evolution of hydrogen and the simultaneous distillation of potassium. Others have reported that sodium borohydride decomposed only very slowly below its melting point (about 500° C), with formation of free boron and free sodium, but that at the melting point the liquid evolved hydrogen rapidly.

The present authors tested small specimens (each weighing approximately 1 g) of their samples of these two compounds in open containers in a furnace constantly being swept out with pure helium, controlling temperature and time of exposure and observing changes in weight and appearance after each test. Sometimes there were small gains in weight, amounting to a few hundredths of 1 percent, which naturally would mask any small losses in weight that might have occurred simultaneously. The gains in weight that occurred during heating at the higher temperatures were probably due to absorption of traces of oxygen or water vapor from the furnace atmosphere. Sometimes a loss in weight that occurred only on heating to a temperature of several hundred degrees C was followed by a comparable gain in weight (up to 0.1%) during standing overnight in a desiccator. This may be explained if owing to hydrolysis the dried specimens actually contained small amounts of the corresponding metal hydroxides, which are hygroscopic.

The weight changes mentioned above will next be described quantitatively in the case of first, sodium borohydride, then potassium borohydride. Immediately following the discussion of the behavior of each substance in the tests of a small specimen, will be given a description of the preliminary conditioning of the heat-content specimens of that substance, with the weight changes then observed.

The test specimen of sodium borohydride, sample No. 1, lost 0.5 percent of its weight in 35 min at 350° C; in a subsequent 35 min at 400° C the same specimen showed no further significant change in weight, but became somewhat gray. In view of this behavior, the specimens whose heat contents were to be measured were first subjected to preliminary heating to establish approximately constant weight. Sample No. 1 lost 0.1 percent in weight during several hours of drying in vacuum at 80° C, no more during several hours while being similarly treated at 130° C, and an additional 0.2 percent during 30 min of drying at 200° and 50 min at 350° C. Sample No. 2, when first heated for 30 min at 300° C, lost 0.3 percent in weight, but a repetition of this heating produced no further sensible weight change.

The preliminary tests on a small specimen of the stock sample of potassium borohydride, with intermediate cooling and weighing, showed the following consecutive results: The only sensible weight change was a 0.2-percent loss during the initial heating, which was for 40 min at 300° C; there was still no change in appearance of the specimen after 35 min at 350° C; after 50 min at 400° C, some sintering was noted; then 50 min at 450° C led to a dirty-gray appearance; and a subsequent heating for 10 min at 500° C produced somewhat further darkening. The only preliminary treatment of the specimens whose heat contents were to be measured was the heating of each in vacuum at 85° C for several hours, with a weight loss of less than 0.05 percent. During the subsequent heat-content measurements, each specimen gradually underwent further losses in weight totaling about 0.1 percent.

It may be pointed out that these specimens of the two borohydrides initially underwent appreciable weight losses, but no comparable losses in subsequent heatings even at higher temperatures. Barring conceivable catalytic behavior of volatile contaminants initially removed, it would thus seem that the initial loss was not through any sensible, *spontaneous* decomposition of the nominal compound, or else comparable or even more rapid weight losses would have continued to occur. The losses found are assumed to have occurred through the removal of water. Whether this loss of water was more likely by simple evaporation or by chemical reaction with borohydride is discussed in section 4.

4. Correction for Impurity

The immediate aim of the present work is to obtain the best values of the relative heat content of the pure borohydrides of sodium and potassium over the temperature range covered by the thermal measurements. As the precision of these measurements was several times the errors that would be caused by neglecting the presence of impurities in the samples measured, these errors will be estimated and corrected for.

It is convenient to calculate first, the changes in heat content per unit mass of sample as given by the

[2] Figures in brackets indicate the literature references at the end of this paper.

thermal data, and then to estimate the corrections corresponding to replacement of the impurities by an equal mass of the nominal substance. This correction for each impurity is obviously proportional to the weight percentage of the impurity and, approximately, to the difference between the average specific heat (heat capacity per unit mass), of the impurity and that of the nominal substance. The results of the chemical analyses given in section 2, and the interpretation of the mass changes summarized in section 3, necessitate some arbitrariness in deducing the compositions of the samples at the times when their heat contents were measured. Fortunately, however, fairly adequate values are available for the specific heats of the minor components (assumed to be water and $NaBO_2$ or KBO_2, as discussed in section 2).

The specific heats of the crystalline *meta*borates were calculated from equations given by Kelley [2]. These equations,[3] giving the heat capacity C_p in cal mole^{-1} deg K^{-1} at T°K, are:

$$NaBO_2: C_p = 12.9 + 0.0122\ T\ (289°\text{–}1239°\text{K}), \quad (3)$$

$$KBO_2: C_p = 12.6 + 0.0126\ T\ (288°\text{–}1220°\text{K}). \quad (4)$$

Also using the results on the borohydride samples reported in this paper, it can readily be shown that the heat content of the sample would be increased by very nearly 0.5 percent for each 1 percent of *meta*borate, in the sample, that is replaced by the same mass of the corresponding borohydride. This is true for any temperature in the present range 0° to 400° C, and in the case of either the sodium or the potassium compound.

A value for the effective specific heat of chemically-bound water near room temperature was obtained from the calculated losses in heat capacity when a number of salts are dehydrated [2], the mean value found being 10 cal mole^{-1} deg C^{-1}.[4] This value corresponds to a specific heat for such water not far from that of either sodium borohydride or potassium borohydride. Only the potassium compound contained an appreciable amount of water during any of the heat-content measurements, and the amounts present are believed to have been so small (not more than 0.1%) as to make the corrections in heat content for water negligible.

As described in section 3, the samples on which heat-content measurements were made were first heated to dry them. Each of the samples of sodium borohydride thereby decreased in weight by 0.3 percent, and the samples of potassium borohydride by less than 0.05 percent (but by an additional 0.1% when they reached about 200° C during the heat-content measurements). If these losses in weight represent escape of water only, the effects on the heat content of the drying are small and can be easily allowed for. It is conceivable, however, that heating caused the reaction of eq (1) to occur and that the mass loss was due largely to escape of hydrogen, in which case the proper corrections to the heat-content values would be many times as great. However, the second alternative explanation, while it cannot be proved to be entirely false, does not fit the observed facts. It would require that the sample contain, before being heated, about five times as much water as the decrease in mass on heating; also, the large amount of borate formed would lower the specific heat of the sample by 1 percent or more. Excepting the final analyses of sodium borohydride sample No. 1, discussed below, the water contents, roughly deduced from the chemical analyses, approximate these mass losses on heating. Furthermore, as the data in the next section will show, a repetition of heat-content measurements on potassium borohydride sample No. 1 was carried out at 150° and 200° C; these later values were lower than before the loss of 0.1 percent in weight (at 200° to 300° C) by 0.05 to 0.2 percent, amounts which correspond approximately to a simple escape of water vapor.

The analyses of the samples after the heat-content measurements all show less borohydride than the analyses before (section 2), and interpolations may be attempted to give estimates of the compositions of the samples when their heat contents were measured. In this way it may be reasonably assumed that sodium borohydride sample No. 2 and each of the samples of potassium borohydride should be considered as consisting of 99 weight percent of the nominal substance and 1 percent of the corresponding *meta*borate.

A similar interpolation of the analyses on sodium borohydride sample No. 1 would indicate several times as much water as the total weight loss on heating and enough $NaBO_2$ to give heat-content values some 2-percent lower than those of sample No. 2. Actually, sample No. 2 gave the lower heat-content values, but by only 0.25 percent at 100° and 0.15 percent at 200° and 300° C (section 5). It is believed that inferior preservation of sample No. 1 is responsible for the finding of so much impurity in its final analysis, and that it too must have been about 99-percent pure when its heat content was measured.

In accordance with the foregoing conclusions, each heat content of a borohydride sample plus container observed in this work was increased by an amount equal to 0.5 percent of the contribution due to the sample. Any decrease of mass during a measurement was assumed to represent a loss of water, and was treated as though the mass of the specimen had decreased by that amount. But when a mass *increase* occurred, it was assumed to have occurred entirely through conversion, by a trace of water vapor or oxygen gas, of borohydride into *meta*borate by the reaction of eq (1) or eq (2), or both. An additional correction to the measured heat was applied accordingly.

[3] Although these equations are based on old data, at least the equation for $NaBO_2$ gives values in the range 0° to 400° C in approximate agreement with the values additively predicted from more accurate results on other sodium oxysalts and other borates.

[4] Insufficient data were found to justify assigning values at higher temperatures, where the amounts of water left in the borohydride samples were usually negligible anyhow.

5. Measurement of Heat Content

The calorimetric apparatus and "drop" method used have been described in detail in numerous reports and papers from the Bureau, most recently in a paper on the thermal properties of aluminum oxide [3]. Briefly, the method is as follows. The specimen in a suitable container is suspended in a furnace for a sufficient length of time to ensure its reaching the known furnace temperature. It is then dropped into a Bunsen ice calorimeter, which, by absorbing a volume of mercury equivalent to the change in volume due to melting of ice, measures the heat evolved by the sample and container in cooling to 0° C. A similar measurement on the empty container at the same furnace temperature provides correction for the contribution of the container and for the heat lost during the fall into the calorimeter, and enables a computation of the net change in heat content of the specimen alone. Repetition at a sufficient number of furnace temperatures establishes the heat content as a function of temperature.

The temperature of the furnace, adjusted to some desired even value, was measured by an accurately calibrated strain-free platinum-resistance thermometer and was kept constant to ± 0.01 deg C. A silver pipe, 10 in. long and of 1/2-in. wall thickness, together with end silver "guards," reduced the temperature gradients to negligible amounts, thereby permitting the sample to assume the same temperature as that measured. That the time of the sample in the furnace was adequate was established by determining the relaxation time in a special drop run after a time in the furnace deliberately too short to give thermal equilibrium. The adequacy of the times used was tested also by varying the times in the furnace in each set of duplicate measurements so as to detect any systematic time-dependence, which did not appear. The furnace core, calorimeter, and specimen container were filled with pure helium, which flowed through during the measurements to minimize not only the times required for reaching thermal equilibrium but also the oxidation of specimen and container. A cylindrical vessel constructed of the alloy 80 Ni–20 Cr, closed approximately but not gas-tight by a screw lid of nickel, served to contain the specimen.[5] The inside surface of the container had been thoroughly cleaned of oxide to prevent oxidation of the borohydride specimens. The container was evacuated and filled with helium just before each introduction into the furnace, but with air after each run in order to place the weight on a known and reproducible buoyancy basis.[6]

The corrected individual measurements of the heat content of the empty container are recorded in absolute joules in table 3. In terms of absolute amount of heat, the agreement of the duplicate results at each furnace temperature is typical of that usually obtainable with this apparatus in the absence of a material undergoing chemical or physical change with time. According to table 3, the deviation from the mean of two duplicates averaged 0.4 j, with a maximum of 1.0 j. It may be noted that these variations seem to be independent of furnace temperature.

The results of the individual measurements on container with sample are given, in chronological order for each of the four samples, in table 4 for sodium borohydride and in table 5 for potassium borohydride. The third column of each table indicates the change in the mass of specimen plus container as compared with the mass before the heat-content measurements were begun. These changes were due almost entirely to changes in the mass of the specimen itself, as discussed in section 4. The values in the

TABLE 3. *Individual heat-content measurements on the empty container*

Furnace temperature	Measured heat	Furnace temperature	Measured heat	Furnace temperature	Measured heat
°C	*abs j*	°C	*abs j*	°C	*abs j*
50	252.0	250	1,331.3	450	2,491.5
	253.6		1,330.5		2,489.5
100	514.3	300	1,614.0	500	2,789.4
	513.8		1,614.3		2,789.0
150	780.7	350	1,902.2		
	780.7		1,902.4		
200	1,053.4	400	2,192.6		
	1,054.5		2,193.4		

TABLE 4. *Individual heat-content measurements on sodium borohydride + container*

Furnace temperature, t	Time in furnace	Mass in excess of original	Corrected measured heat, sample + container	Relative heat content of $NaBH_4$, $H_t - H_0$°C		
				Individual run	Mean observed for set	Observed minus calculated, eq (5)
Sample No. 1 (2.5715 g)[a]						
°C	*min*	*mg*	*abs j*	*abs j g*$^{-1}$	*abs j g*$^{-1}$	*abs j g*$^{-1}$
350	35	−0.8	4,229.2	904.9	904.4	−0.4
	45	−.7	4,226.5	903.8		
50	40	+.5	546.2	114.1	113.9	−.3
	35	+.6	545.1	113.7		
100	30	+.7	1,115.1	233.7	233.8	.0
	40	+.9	1,115.8	234.0		
150	45	+1.3	1,704.7	359.3	359.4	+.8
	30	+1.4	1,705.0	359.5		
200	30	+1.8	2,311.6	489.0	488.7	+.4
	40	+2.0	2,309.6	488.3		
250	30	+3.0	2,933.9	623.4	623.2	+.6
	40	+3.5	2,933.1	623.1		
300	30	+3.7	3,573.2	761.8	761.6	+.1
	40	+4.0	3,572.0	761.4		
400	30	+6.1	4,903.9	1,054.2	1,053.0	+.5
	40	+7.5	4,896.1	1,051.2		
	30	+12.0	4,902.5	1,053.6		
Sample No. 2 (3.4104 g)[b]						
300	30	+0.4	4,207.6	760.4	760.4	−1.0
	40	+.8	4,207.6	760.4		
100	30	+.8	1,309.5	233.2	233.3	−0.6
	40	+1.0	1,309.8	233.3		
200	30	+1.3	2,718.1	488.0	488.0	−.2
	40	+1.6	2,718.5	488.1		

[a] Sample No. 1 was obtained from Metal Hydrides, Inc.
[b] Sample No. 2 was obtained from an independent source.

[5] There was no reason other than convenience for choosing this particular container; preliminary tests had shown that it was not attacked by the specimens.
[6] All weights were corrected to vacuum.

TABLE 5. *Individual heat-content measurements on potassium borohydride+container*

Furnace temperature, t	Time in furnace	Mass in excess of original	Corrected measured heat, sample +container	Relative heat content of KBH_4, $H_t-H_0°_C$		
				Individual run	Mean observed for set	Observed minus calculated, eq (6)
Sample No. 1 (3.4862 g)[a]						
°C	*min*	*mg*	*abs j*	*abs j g*$^{-1}$	*abs j g*$^{-1}$	*abs j g*$^{-1}$
50	35	+0.1	564.3	89.3	89.1	−0.2
	35	+.1	563.0	88.9		
100	30	.0	1,149.4	182.1	182.0	+.2
	40	−.1	1,148.6	181.9		
150	30	−.1	1,743.3	275.9	275.8	+.6
	40	−.6	1,742.9	275.8		
200	30	−1.6	2,342.0	369.1	369.0	−.2
	40	−2.4	2,340.8	368.8		
250	30	−2.7	2,948.9	463.7	463.8	.0
	35	−2.8	2,949.7	463.9		
300	30	−1.3	3,577.4	(562.6)[b]	559.9	+.2
	40	+0.3	3,568.4	560.1		
	35	+.1	3,567.0	559.7		
150	30	+.1	1,741.7	275.4	275.3	.0
	40	+.4	1,740.5	275.1		
200	30	+.7	2,340.7	368.8	368.8	−.4
	40	+.7	2,340.5	368.7		
350	30	+.5	4,198.5	658.1	658.0	+.1
	40	+.1	4,197.9	657.9		
400	30	+.2	4,845.1	760.1	760.0	+.3
	35	.0	4,844.4	759.9		
Sample No. 2 (3.3794 g)[a]						
100	40	+0.2	1,127.5	181.5	181.5	−0.2
	30	.0	1,127.3	181.4		
400	40	−4.2	4,759.4	759.4	759.3	−.4
	45	−3.7	4,758.4	759.1		
100	30	−2.8	1,127.4	181.5	181.4	−.3
	40	−2.2	1,127.0	181.4		

[a] Samples 1 and 2 were actually specimens of the same sample, obtained from Metal Hydrides, Inc.
[b] Discarded because of poor precision.

fourth column have been corrected to the basis of the fixed mass of pure compound given in the heading. Each value in the fifth column was obtained by subtracting from the corresponding "gross" value in the fourth column the mean value for the empty container (table 3) and then dividing by the mass of sample. The "calculated" values of heat content referred to in the last column of tables 4 and 5 are the final smoothed values derived as described in section 6.

For some temperatures, two mean values of net heat content are listed in the sixth column of table 5. If both these values were exactly correct, they would naturally be the same. Their small disagreement was discussed in section 4. Potassium borohydride sample No. 2, though really a specimen of the same stock sample as sample No. 1 but measured 2 months later, gave mean values of heat content lower than those of sample No. 1 by 0.3 percent at 100° and 0.1 percent at 400° C. The consistent decrease with time of values for potassium borohydride indicates that, to at least the extent of these rather small discrepancies, the corrections for changing degree of purity (incorporated in the values of table 5) are not completely adequate.

6. Thermodynamic Functions, 298.15° to 700° K

The observed values of heat content for each compound were smoothed by using them to derive the coefficients of an empirical equation giving the relative heat content as a function of temperature. For each substance equal weight was given to the average of the mean values for each furnace temperature given in the sixth column of table 4 or 5.[7] For each substance, a form of equation was so chosen that the deviations between calculated and mean observed values (shown in the last column of table 4 or 5) are comparable in magnitude to the differences between the individual values from duplicate runs at the same temperature.[8] With the heat content at $t°$ C in excess of that at 0° C expressed in absolute joules per gram, the equations obtained for the crystalline salts from 0° to 400° C are as follows.

$NaBH_4$:

$$H_t-H_{0°C}=2.4384t+8.083(10^{-4})t^2 -133.0\log_{10}[(t+273.15)/273.15]. \quad (5)$$

KBH_4:

$$H_t-H_{0°C}=4.0898t-2.9030(10^{-3})t^2 +2.641(10^{-6})t^3-1{,}482.7\log_{10}[(t+273.15)/273.15]. \quad (6)$$

Equations (5) and (6) were then converted to the form most commonly used in chemical thermodynamics by expressing the heat content relative to that at 0° K, in calories per mole, with the temperature in deg K.[9] From the resulting equations the common thermodynamic functions (at the standard thermodynamic pressure of 1 atm) were derived using the following relations.

$$(H°-H°_0)/T=(H°+H°_{298.15})/T+(H°_{298.15}-H°_0)/T, \quad (7)$$

$$C°_p=d(H°-H°_0)/dT, \quad (8)$$

$$S°=S°_{298.15}+\int_{298.15}^{T}(C°_p/T)dT, \quad (9)$$

$$-(F°-H°_0)/T=S°-(H°-H°_0)/T, \quad (10)$$

where C_p is heat capacity at constant pressure, S is entropy, F is Gibbs free energy, and the subscript "0" refers to 0° K. Equation (10) permits the cal-

[7] Except that the two mean values given in table 5 for sample No. 2 at 100° C were each given half weight.
[8] The logarithmic terms and those in t and t^2 were introduced because they have been found to account closely for the relative heat content at these temperatures of a number of crystalline solids devoid of apparent transitions [3]. In the case of potassium borohydride, an equation containing also a term in t^4 was first derived. However, the resulting equation gave values almost identical with those of eq (6).
[9] Taking one defined calorie=4.1840 abs j, 0° C=273.15° K, and the molecular weights of $NaBH_4$ and KBH_4 as 37.843 and 53.952, respectively [4].

culation of the free energy of formation of the compound at various temperatures when its heat of formation and its absolute entropy at some one temperature are both known, provided that the corresponding thermodynamic functions of the free elements also have been evaluated. The heat of formation of sodium borohydride has been measured [5], but no corresponding value for the potassium compound was found in the literature.

Values for the constants in eq (7) and (9) were selected from the work of other investigators. Although the low-temperature heat capacity of sodium borohydride had been measured earlier [6], the work of Johnston and Hallett [7] appears to be more comprehensive and more accurate, leading to the values of $(H^\circ_{298.15}-H^\circ_0)$ and $S^\circ_{298.15}$ adopted here, 3,889.5 and 24.26 respectively.[10] In the case of potassium borohydride, the values adopted for the same constants, 3,948.8 and 25.48 respectively, were obtained in preliminary measurements at the Bureau [8].

The thermodynamic functions derived in the foregoing manner are as follows (in cal mole^{-1} deg K^{-1} at T°K and for the temperature range 298° to 700°K).[11]

$NaBH_4$:

$$(H^\circ-H^\circ_0)/T=18.0607+7.3108(10^{-3})T-1{,}202.94(1/T)\log_{10}T+831.4/T, \quad (11)$$

$$C^\circ_p=18.061+0.014622T-522/T, \quad (12)$$

$$S^\circ=41.586\log_{10}T+0.014622T+522/T-84.754, \quad (13)$$

$$-(F^\circ-H^\circ_0)/T=41.586\log_{10}T+1{,}202.9(1/T)\log_{10}T+7.311(10^{-3})T-309/T-102.815. \quad (14)$$

KBH_4:

$$(H^\circ-H^\circ_0)/T=80.8100-0.0653403T+3.4055(10^{-5})T^2-19{,}119.18(1/T)\log_{10}T+32{,}070.2/T, \quad (15)$$

$$C^\circ_p=80.810-0.130681T+1.0217(10^{-4})T^2-8{,}303/T, \quad (16)$$

$$S^\circ=186.072\log_{10}T-0.130681T+5.108(10^{-5})T^2+8{,}303/T-428.371, \quad (17)$$

$$-(F^\circ-H^\circ_0)/T=186.072\log_{10}T+19{,}119.2(1/T)\log_{10}T-0.065340T+1.703(10^{-5})T^2-23{,}767/T-509.181. \quad (18)$$

[10] These values are based on a molecular weight of 37.843.

[11] Though the heat content was actually measured relative to 273°K, its temperature derivative has increased uncertainty near the end of the range of measurement and it therefore seems better to limit the derived thermodynamic functions to temperatures of 298°K and above.

Values of the thermodynamic functions calculated for even temperatures from eq (11) to (18) are given in tables 6 and 7.

TABLE 6. *Thermodynamic functions of sodium borohydride* [a]

Temperature	$H^\circ-H^\circ_0/T$	C°_p	S°	$-(F^\circ-H^\circ_0)/T$
°K	cal deg^{-1} mole^{-1}	cal deg^{-1} mole^{-1}	cal deg^{-1} mole^{-1}	cal deg^{-1} mole^{-1}
298.15	13.045[b]	20.67	24.26[b]	11.21
300	13.093	20.71	24.39	11.29
320	13.581	21.11	25.74	12.15
340	14.035	21.50	27.03	12.99
360	14.460	21.87	28.27	13.81
380	14.860	22.24	29.46	14.60
400	15.238	22.60	30.61	15.37
420	15.597	22.96	31.72	16.12
440	15.940	23.31	32.80	16.86
460	16.268	23.65	33.84	17.57
480	16.582	23.99	34.85	18.27
500	16.885	24.33	35.84	18.95
520	17.178	24.66	36.80	19.62
540	17.461	24.99	37.74	20.28
560	17.736	25.32	38.65	20.92
580	18.003	25.64	39.55	21.54
600	18.263	25.96	40.42	22.16
620	18.516	26.28	41.28	22.76
640	18.764	26.60	42.12	23.35
660	19.007	26.92	42.94	23.93
680	19.244	27.24	43.75	24.51
700	19.477	27.55	44.54	25.07

[a] Molecular weight = 37.843.
[b] Taken from reference [7].

TABLE 7. *Thermodynamic functions of potassium borohydride* [a]

Temperature	$H^\circ-H^\circ_0/T$	C°_p	S°	$-(F^\circ-H^\circ_0)/T$
°K	cal deg^{-1} mole^{-1}	cal deg^{-1} mole^{-1}	cal deg^{-1} mole^{-1}	cal deg^{-1} mole^{-1}
298.15	13.244[b]	23.08	25.48[b]	12.23
300	13.305	23.12	25.62	12.32
320	13.931	23.51	27.13	13.20
340	14.503	23.77	28.56	14.06
360	15.023	23.94	29.92	14.90
380	15.495	24.05	31.22	15.73
400	15.925	24.13	32.46	16.53
420	16.317	24.18	33.64	17.32
440	16.675	24.22	34.76	18.09
460	17.004	24.27	35.84	18.84
480	17.308	24.33	36.87	19.57
500	17.590	24.41	37.87	20.28
520	17.854	24.52	38.83	20.97
540	18.103	24.66	39.75	21.65
560	18.340	24.84	40.66	22.32
580	18.568	25.07	41.53	22.96
600	18.789	25.34	42.39	23.60
620	19.006	25.67	43.22	24.22
640	19.220	26.05	44.04	24.82
660	19.433	26.49	44.85	25.42
680	19.648	26.98	45.65	26.00
700	19.865	27.54	46.44	26.57

[a] Molecular weight = 53.952.
[b] Taken from reference [8].

7. Discussion of Results

Although the thermal measurements reported in this paper are of relative heat content, it is more informative to examine the resulting values of heat capacity. These are shown for the two compounds in figure 1. The curves represent the smooth values calculated from eq (12) and (16). The points may be considered the unsmoothed values, as each one represents the difference between the mean values of heat content for two adjacent furnace temperatures as given in the sixth column of table 4 or 5.[12]

[12] The points so computed were corrected for the curvature of the smooth curves, but the largest such correction amounted to only 0.2 percent of the heat capacity.

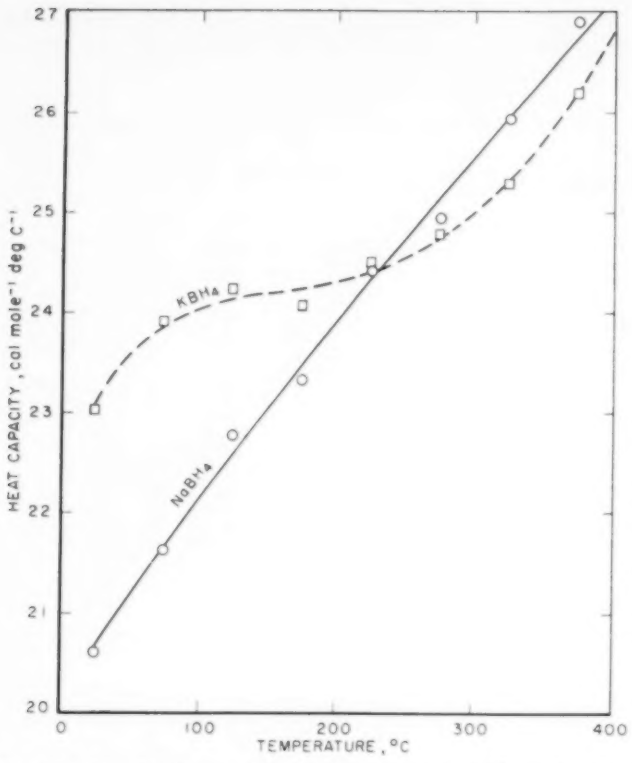

FIGURE 1. *Heat capacity of sodium borohydride and potassium borohydride, as determined by the drop method.*

○, $NaBH_4$, mean observed; □, KBH_4, mean observed; —, $NaBH_4$, smoothed; — —, KBH_4, smoothed.

It will be noted that in the temperature range investigated, the heat capacity of sodium borohydride increases with temperature in the usual manner observed for many crystalline solids. On the other hand, the heat-capacity-temperature curve of potassium borohydride shows a distinct point of inflection, which suggests the existence of a broad second-order transition of some sort in the neighborhood of room temperature.

The authors' smoothed values of heat capacity may be compared with the results of other investigators. The present measurements on sodium borohydride overlap those of Johnston and Hallett [7] from 277° to 301° K. The agreement in mean heat capacity over this temperature range is almost perfect, but their value at 298° K is about 0.25-percent higher. The less precise values for sodium borohydride of Boodman, Stegeman, and Mason [6] are somewhat lower in this temperature range than those of Johnston and Hallett. Davis, Mason, and Stegeman [5] obtained a value of 0.55 $\pm$0.01 cal g^{-1} deg C^{-1} for the mean heat capacity between 273° and 298° K; this is 2-percent higher than the authors' corresponding value. In the case of potassium borohydride, Furukawa et al. [8], who use an adiabatic calorimeter to make the preliminary measurements from low temperatures to 370° K referred to in section 6, obtained somewhat higher values of heat capacity than the authors. In the range from 298° to 370° K the discrepancy averaged 0.3 percent and reached a maximum of 0.5 percent.[13]

The authors believe that their corrected and smoothed values of the heat capacity of these two compounds are reliable to within 1 percent. The thermal measurements were made using a method and apparatus that appears to give consistently much greater accuracy than this when the substance measured is pure, stable, and physically reproducible. It is therefore likely that in the present case the uncertainty in the exact chemical compositions of the samples contributed the major uncertainty in the heat capacity, and, as indicated in section 4, by approximately the same percentage for each of the two compounds over the whole range from 0° to 400° C. If this is true, approximately the same percentage error for each compound resulted in the parts of the entropy and heat-content function which are in excess of the respective values at 298° K.

This work was supported by the Bureau of Aeronautics, U. S. Department of the Navy. The authors thank R. A. Paulson, of the National Bureau of Standards, for the chemical analyses of the samples following the heat-content measurements.

8. References

[1] M. D. Banus, R. W. Bragdon, and A. A. Hinckley, J. Am. Chem. Soc. **76**, 3848 (1954).
[2] K. K. Kelley, Contributions to the data on theoretical metallurgy, X. High-temperature heat-content, heat-capacity, and entropy data for inorganic compounds, U. S. Bureau of Mines Bulletin 476, pp. 210, 211 (U. S. Government Printing Office, Washington, D. C., 1949).
[3] G. T. Furukawa, T. B. Douglas, R. E. McCoskey, and D. C. Ginnings, J. Research NBS **57**, 67 (1956) RP2694.
[4] E. Wichers, J. Am. Chem. Soc. **76**, 2033 (1954).
[5] W. D. Davis, L. S. Mason, and G. Stegeman, J. Am. Chem. Soc. **71**, 2775 (1949).
[6] D. Boodman, G. Stegeman, and L. Mason, Thermal properties of some hydrides, Univ. of Pittsburgh, ONR Contract No. N6ori 43, T. O. I. Technical Report (Oct. 10, 1949).
[7] H. L. Johnston and N. C. Hallett, J. Am. Chem. Soc. **75**, 1467 (1953).
[8] G. T. Furukawa (private communication).

[13] As can be seen from figure 1, the authors could have chosen a smooth heat-capacity function for KBH_4 which passes through the observed points below 200° C. Such a function would have corresponded to a slightly sharper transition peak in this temperature region and at the same time would have agreed substantially better with the preliminary adiabatic-calorimeter values referred to. However, unless the latter values are explicitly given considerable weight, the observations reported in this paper are really not sufficiently precise nor at enough different temperatures to justify this more detailed formulation.

WASHINGTON, March 27, 1957.

Journal of Research of the National Bureau of Standards Vol. 60 No. 2, February 1958 Research Paper 2829

Infrared Spectra of Crystalline Polyphenyls

James E. Stewart [1] and Max Hellmann

Infrared absorption spectra of sixteen selected polyphenyls ranging from biphenyl to *m*-octaphenyl are presented for the 5- to 38-micron region. The observed vibration bands are discussed in terms of a pseudo-symmetry approximation in which the individual rings are assumed to vibrate separately. Indications of interactions between rings are seen in the C–H out-of-plane bending vibrations of ortho- and metasubstituted rings. Evidence is given for the existence of two rotational isomers of *m*-quatraphenyl with a free energy difference of about 250 calories per mole.

1. Introduction

Studies of the vibrational spectra of large molecules have been mostly restricted to empirical correlations of bands with the presence of specific functional groups. Recent publications, however, give evidence of progress in the spectral analysis of large molecules such as polyethylene [1],[2] substituted polyethylenes [2], and infinite chains of $HgNH_2)^+$ ions [3]. These substances have the property of possessing translational symmetry and symmetric repeating units, thus reducing the secular equations to a good approximation, from order infinity to some manageable finite order. The homologous series of polyphenyls, C_6H_5-$(C_6H_4)_n$-C_6H_5, have symmetric repeating units, but except for the para-polyphenyls, they have no translational symmetry. However, empirical spectra-structure correlations and analogies with benzene and the substituted benzenes [4] have provided information on the nature of the bands found in the spectra of aromatic compounds and, furthermore, have shown that many of these vibrations are virtually independent of the nature of the substituent but do depend only on its position.

In view of these considerations it seems reasonable to attempt to treat the vibrations of polyphenyls in terms of the symmetry of the individual substituted phenyl units. This is equivalent to replacing the substituents on a given aromatic ring with identical point masses. A pseudosymmetry can then be assigned to the resulting structure and the vibrations of the ring classified under the appropriate symmetry species in the usual way. This paper is a report on an investigation into the feasibility of assigning in this way the infrared absorption bands of a series of polyphenyls containing from 2 to 8 mono- and disubstituted aromatic rings. These compounds have the following advantages: The ring-to-substituent force constants are probably nearly the same in all the compounds; the masses of the substituents are quite large (at least 77 atomic mass units) so the number of phenyl units between a given ring and the last ring in the molecule is not likely to greatly affect its vibrations; and, confusion from overlapping bands of nonphenyl substituents is avoided.

Randle and Whiffen [5] (referred to hereinafter as RW) have analyzed infrared and Raman data from the literature for a large number of substituted single ring aromatic compounds using the pseudosymmetry approximation and have arrived at some very satisfactory assignments. They have also calculated some out-of-plane vibration frequencies for aromatic molecules using the force constants of benzene. More recently, Shimanouchi, Kakiuti, and Gamo [6] have also reported calculations made in this way on single ring compounds.

The polyphenyls were studied in the solid phase, rather than in solution, because it was desired to observe, if possible, the contributions of the individual units of a polyphenyl chain to the characteristic absorption bands. In liquids, the variations in environment tend to broaden absorption bands until the finer structure is lost. On the other hand, the analysis of crystal phase spectra is often complicated by the occurrence of lattice vibrations and the strengthening of combination vibrations and splitting of bands by intermolecular vibrational interactions.

2. Experimental Details

Infrared spectra of 16 polyphenyls are shown in figures 1 through 8. The frequencies of some of the bands and their assignments are given in table 1. A Perkin-Elmer model 21 spectrophotometer was used for the measurements. The instrument was equipped with a sodium chloride prism for use in the 5- to 15-μ region and a cesium bromide prism for the 15- to 38-μ region. Reststrahlen filter plates of lithium fluoride and calcium fluoride were used to control stray radiation in the 15- to 30-μ and 30- to 38-μ regions, respectively. Stray radiation did not exceed 2 percent.

Samples were prepared in the form of alkali halide pellets using the die and procedure reported earlier [7]. Potassium iodide was found to be most satisfactory in reducing scattered energy losses, but even so, scatter losses at shorter wavelengths were sometimes excessive. No attempt was made to compensate for scatter or reflection losses. A satisfactory spectrum of biphenyl in pellet form was not obtained in the 5- to 15-μ region. The spectrum shown is of a specimen of biphenyl melted and recrystallized between sodium chloride windows separated with a

[1] Present address: Beckman Instruments, Inc., Fullerton, Calif.
[2] Figures in brackets indicate the literature references at the end of this paper.

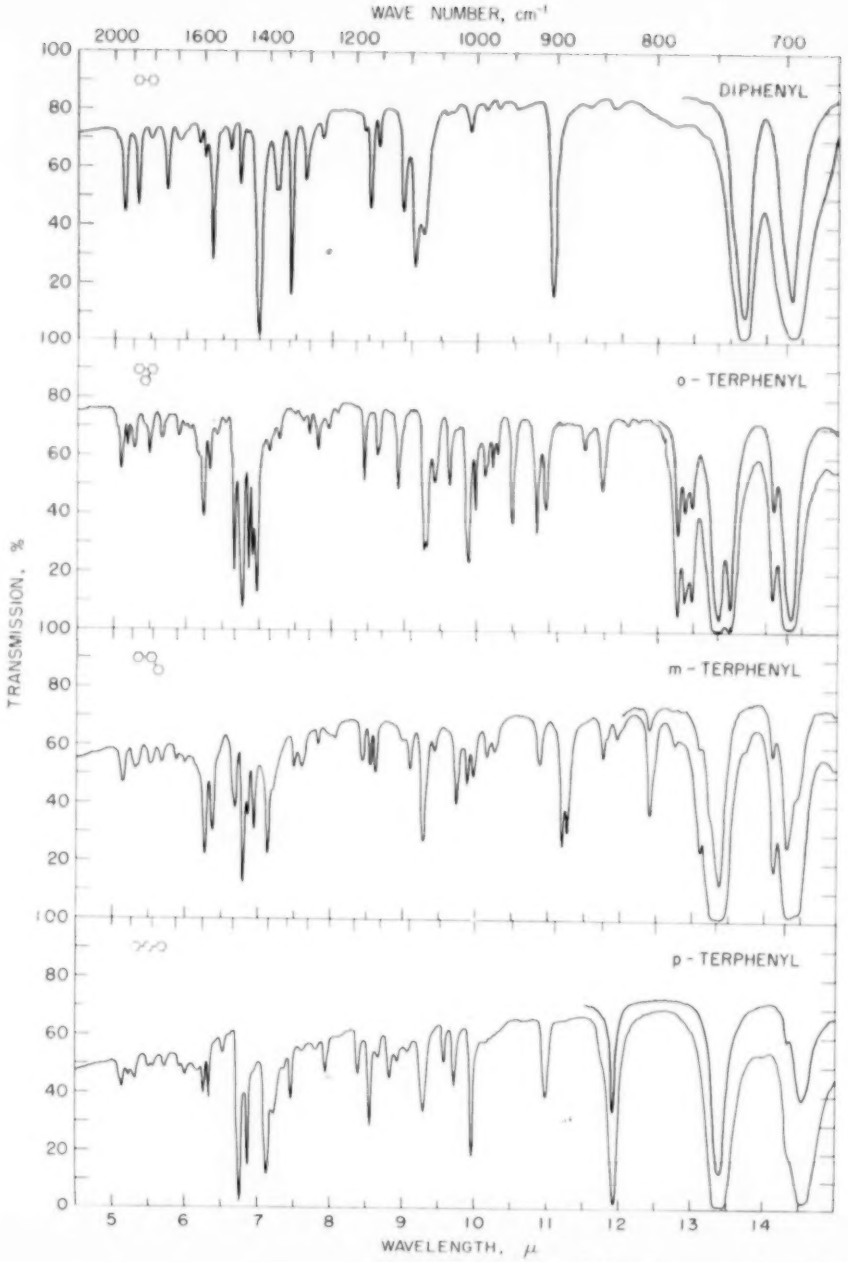

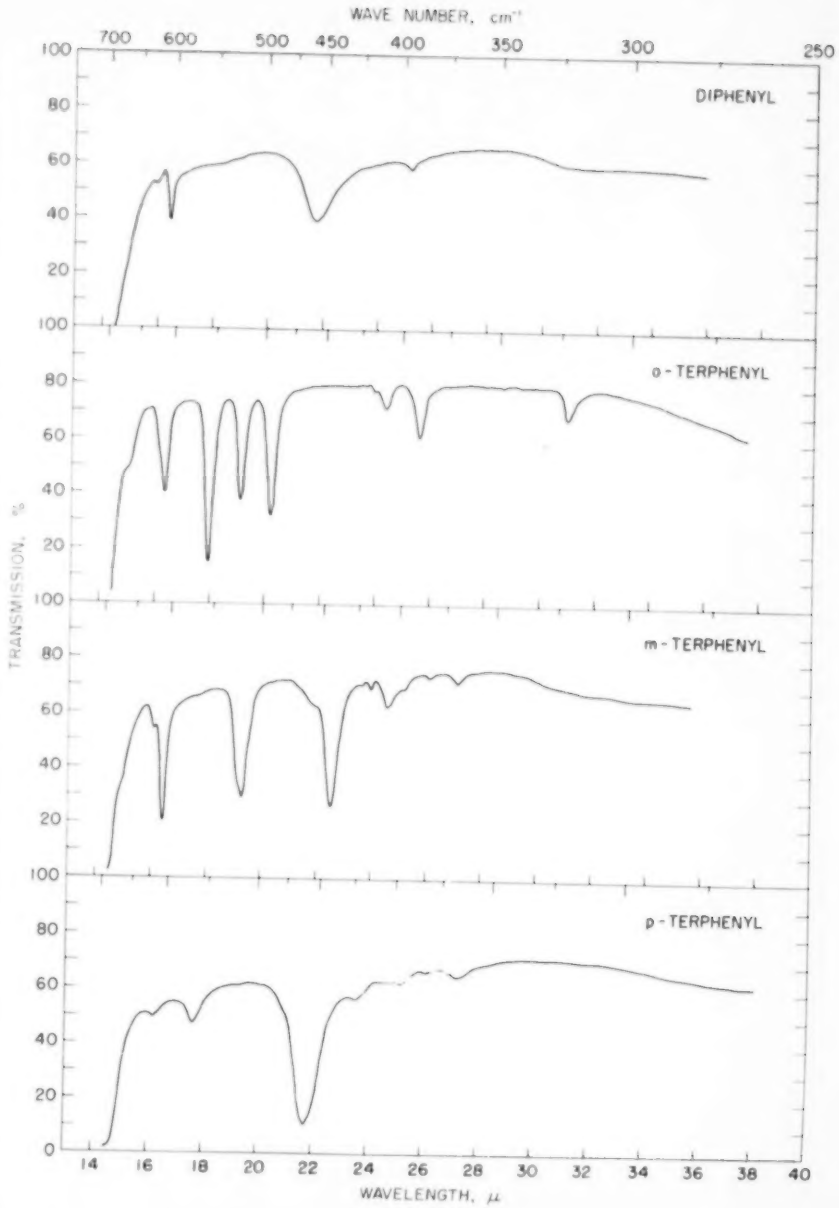
WAVE NUMBER, cm⁻¹
700 600 500 450 400 350 300 250
DIPHENYL
o - TERPHENYL
m - TERPHENYL
p - TERPHENYL
TRANSMISSION, %
WAVELENGTH, μ
14 16 18 20 22 24 26 28 30 32 34 36 38 40

FIGURES 1 and 2. *Infrared spectra of: Diphenyl; o-terphenyl; m-terphenyl; and p-terphenyl.*

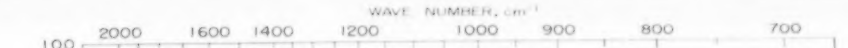

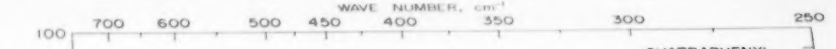

WAVELENGTH, μ

FIGURES 1 and 2. *Infrared spectra of: Diphenyl; o-terphenyl; m-terphenyl; and p-terphenyl.*

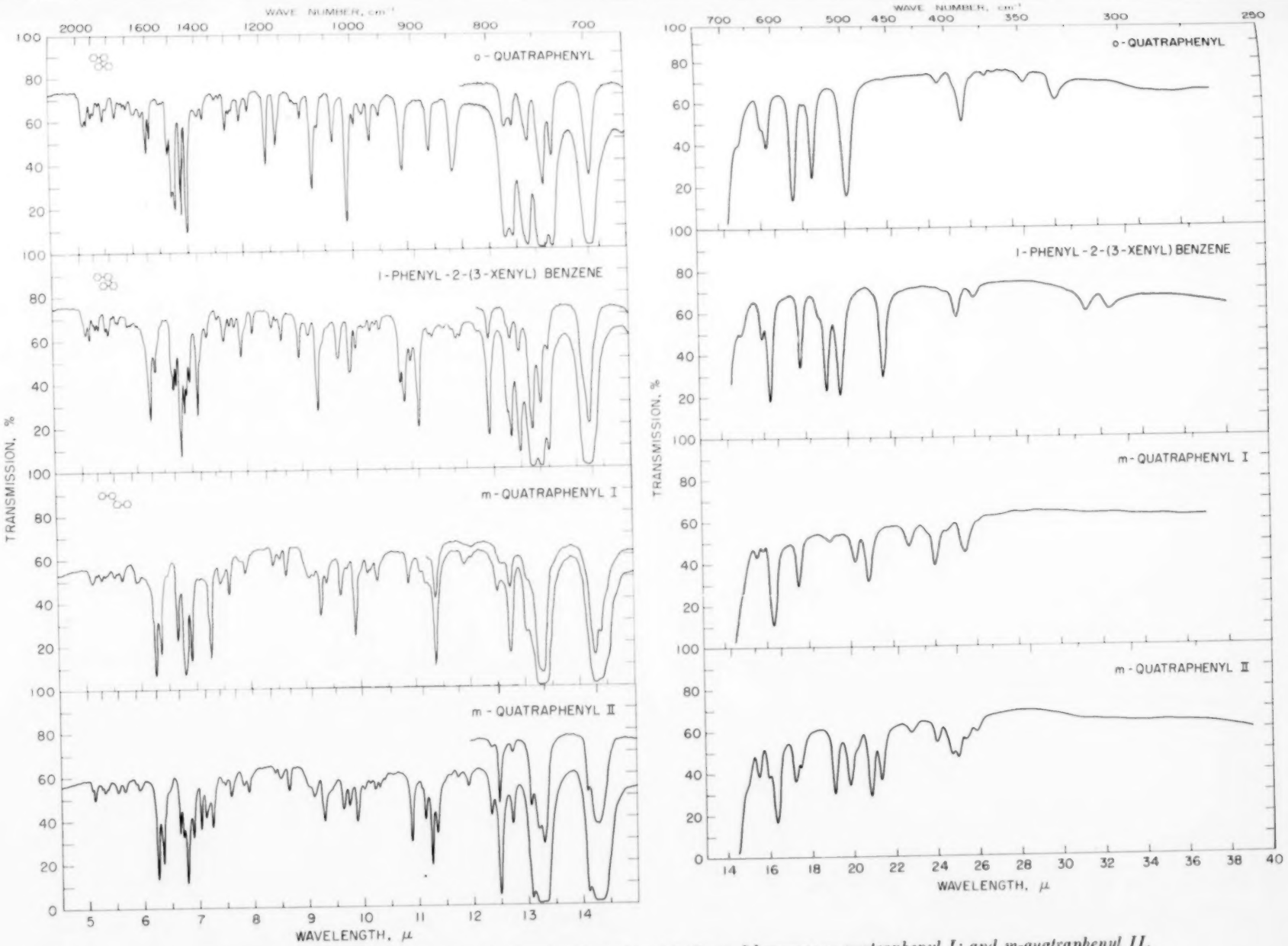
WAVE NUMBER, cm⁻¹
2000 1600 1400 1200 1000 900 800 700
o - QUATRAPHENYL
1-PHENYL-2-(3-XENYL) BENZENE
m-QUATRAPHENYL I
m - QUATRAPHENYL II
TRANSMISSION, %
WAVELENGTH, μ
5 6 7 8 9 10 11 12 13 14
WAVE NUMBER, cm⁻¹
700 600 500 450 400 350 300 250
o-QUATRAPHENYL
1-PHENYL-2-(3-XENYL) BENZENE
m-QUATRAPHENYL I
m-QUATRAPHENYL II
14 16 18 20 22 24 26 28 30 32 34 36 38 40
WAVELENGTH, μ

FIGURES 3 and 4. *Infrared spectra of: o-Quatraphenyl; 1-phenyl-2-(3-xenyl)benzene; m-quatraphenyl I; and m-quatraphenyl II.*

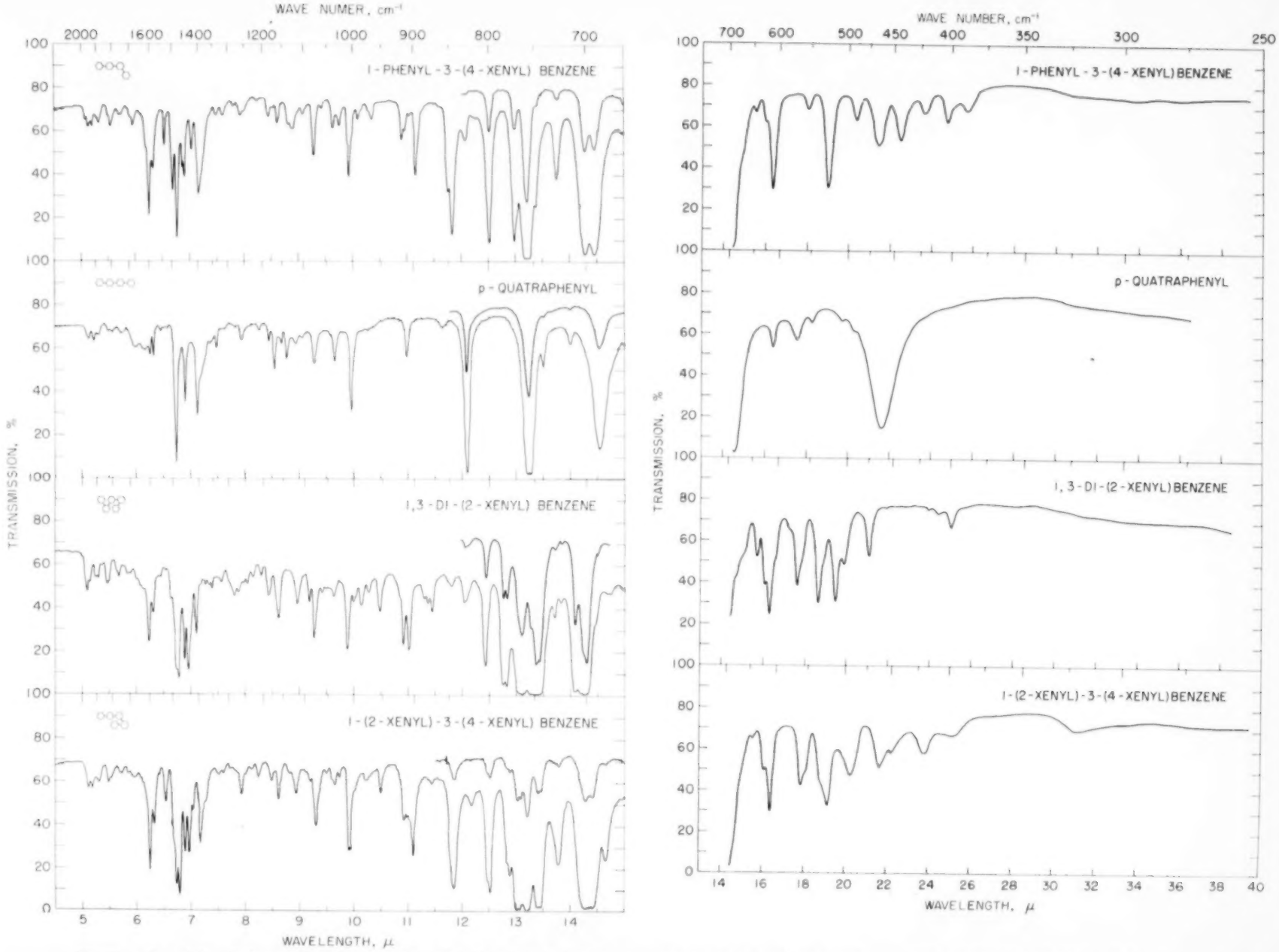

FIGURES 5 and 6. *Infrared spectra of: 1-Phenyl-3-(4-xenyl) benzene; p-quatraphenyl; 1,3-di-(2-xenyl) benzene; and 1-(2-xenyl)-3-(4-xenyl) benzene.*

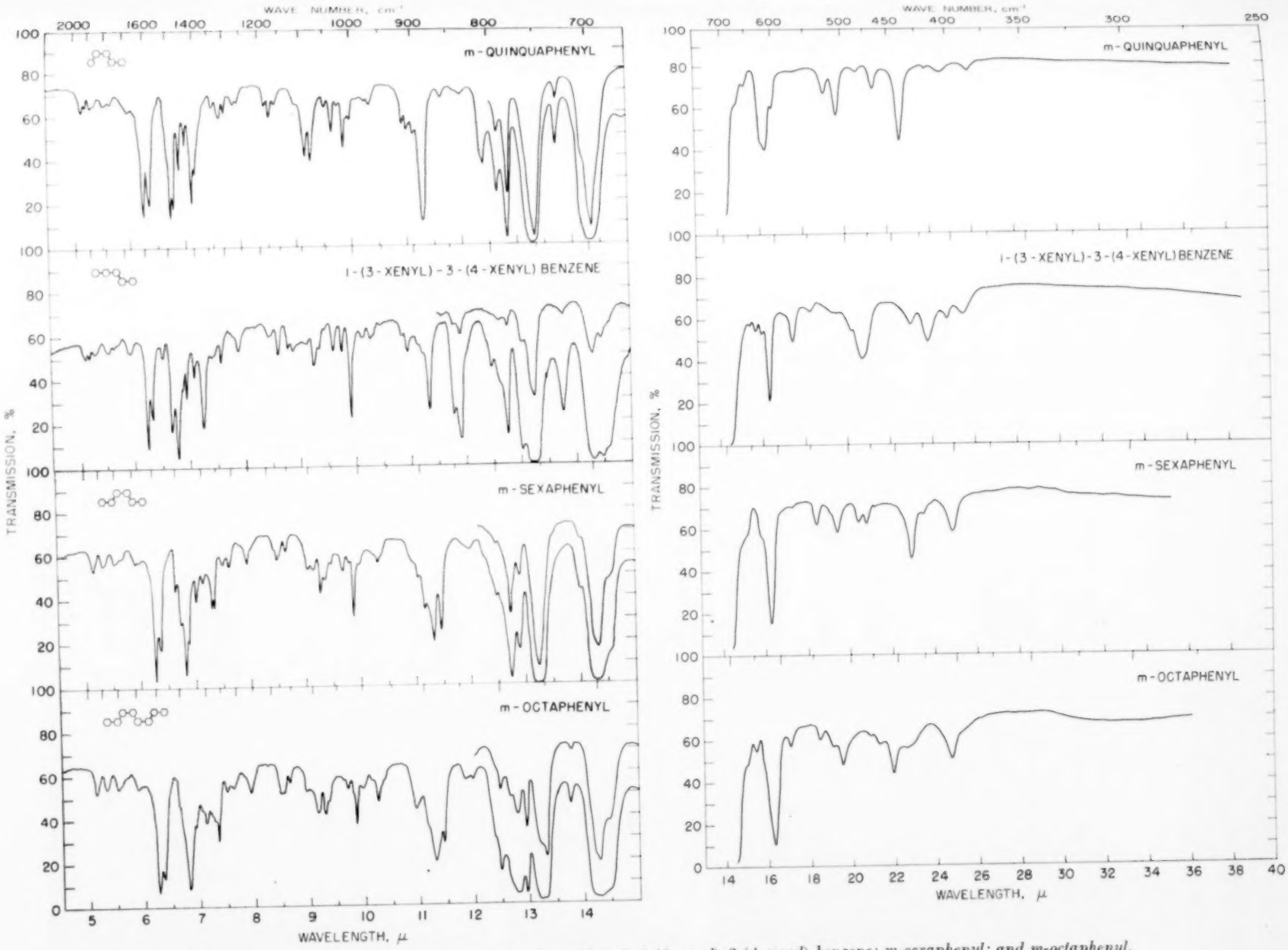

FIGURES 7 and 8. *Infrared spectra of: m-Quinquaphenyl; 1-(3-xenyl)-3-(4-xenyl) benzene; m-sexaphenyl; and m-octaphenyl.*

TABLE 1. *Frequencies and assignments of some bands in the infrared spectra of polyphenyls*

M, o, m, p refer to mono-, ortho-, meta-, and parasubstituted rings. ∥H, ∥C, ⊥H, and ⊥C refer to vibrations which are primarily in-plane CH, in-plane CCC, out-of-plane CH, and out-of-plane CCC bending motions. The letters in parentheses are the symmetry species designations. These abbreviations are used: v, very; s, strong; m, medium; w, weak; sh, shoulder.

Biphenyl

cm^{-1}			cm^{-1}		
397	vw	M(A_2)⊥C	970	vvw	M(A_2), M(B_2)⊥H
469	m	M(B_2)⊥C	987	vvw	
609	m	M(B_1)∥C	1,006	m	M(A_1)∥C
626	vw	M(A_1)∥C	1,042	m	M(A_1)∥H
696	vs	M(B_2)⊥C	1,078	m	M(B_1)∥H
730	vs	M(B_2)⊥H	1,092	m	
835	vw	M(A_2)⊥H	1,112	w	M(B_1)∥H ?
903	m	M(B_2)⊥H	1,168	m	M(B_1)∥H
			1,182	w	M(A_1)∥H

o-Terphenyl

391	m	o(A_2), M(A_2)⊥C	852	m	o(A_2)⊥H
410	w		870	w	
495	m		912	s	o(A_2)⊥H
524	s	o	922	s	o(B_2)⊥H
557	m		953	s	M(B_2)⊥H
612	m	M(B_1), o(B_1)∥C	1,000	m	M(A_1), o(B_1)∥C
619	sh ?	M(A_1)∥C	1,010	s	
697	vs	M(B_2)⊥C	1,038	m	M(A_1)∥H
709	s	o(A_2)⊥C	1,060	m	o(A_1)∥H
741	vs	M(B_2)⊥H	1,073	s	M(B_1)∥H
749	vs		1,077	s	
770	s	o(B_2)⊥H	1,120	m	o(B_1)∥H
776	s		1,157	m	M(B_1), o(A_1)∥H
782	s		1,182	m	o(B_1)∥H

m-Terphenyl

408	w	m(A_2), M(A_2)⊥C	880	m	m(B_2)⊥H
444	s	m	893	m	
455	sh	M(B_2)⊥C	918	w	M(B_2), m(A_2)⊥H
519	s	m	974	w	m(B_2)⊥H
610	s	M(B_1), m(B_1)∥C	1,003	w	M(A_1), m(A_1)∥C
622	w	M(A_1)∥C	1,011	w	
692	sh	M(B_2), m(B_2)⊥C	1,027	m	m(B_1), M(A_1)∥H
698	vs		1,080	m	m(A_1), M(B_1)∥H
708	m		1,160	w	M(B_1)∥H
748	vs	M(B_2)⊥H	1,170	w	m(B_1)∥H
806	m	m(B_2)⊥H	1,185	w	M(A_1), m(B_1)∥H

p-Terphenyl

397	w	p(A_u), M(A_2)⊥C	1,003	s	p(B_{2u}), M(A_1)∥C
460	s	p(B_{1u}), M(B_2)⊥C	1,028	w	p(B_{2u})∥H
618	w	M(B_1)∥C	1,043	w	M(A_1)∥H
688	vs	p(B_{1g}), M(B_2)⊥C	1,075	m	M(B_1)∥H
698	vs		1,083	w	
746	vs	M(B_2)⊥H	1,132	w	p(B_{1u})∥H
838	vs	p(B_{1u})⊥H	1,168	m	p(A_g), M(B_1)∥H
850	sh	p(B_{2g})⊥H	1,190	w	p(B_{1g})∥H
911	m	M(B_2), p(A_u or B_{1g})⊥H			

o-Quatraphenyl

390	m	o(A_2), M(A_2)⊥C	773	vs	o(B_2)⊥H
409	w		781	vs	
498	s		876	m	o(A_2)⊥H
541	s	o	916	m	o(B_2), M(B_2)⊥H
569	s		968	w	o(A_2)⊥H
613	m	M(B_1), o(B_1)∥C	1,010	s	o(B_1)∥C
			1,035	m	M(A_1)∥H
622	sh	M(A_1)∥C	1,066	w	o(A_1)∥H
698	vs	M(B_2), o(A_2)⊥C	1,078	m	M(B_1)∥H
733	vs	M(B_2)⊥H	1,103	w	o(B_1)∥H
741	vs		1,159	m	o(A_1)∥H
757	vs		1,185	m	o(B_1)∥H

TABLE 1. *Frequencies and assignments of some bands in the infrared spectra of polyphenyls*—Continued

1-Phenyl-2-(3-xenyl) benzene

cm^{-1}			cm^{-1}		
384	w	M(A_2), o(A_2), m(A_2)⊥C	804	s	m(B_2)⊥H
397	w		878	w	o(A_2)⊥H
403	vw		897	s	m(B_2)⊥H
461	s	m, M(B_2)	908	w	M(B_2)⊥H
509	s	o	918	m	m(A_2)⊥H
			925	m	o(B_2)⊥H
525	s	o, m	959	w	m(B_2)⊥H
563	s	o, m	975	w	o(A_2)⊥H
613	s	o, m, M(B_1)	1,001	w	M(A_1), o(B_1), m(A_1)∥C
626	w	M(A_1)∥C	1,011	m	
669	w	m(A_1)∥C	1,013	m	
			1,034	m	o(A_1), m(B_1), M(A_1)∥H
702	vs	M(B_2), o(A_2)?⊥C			
740	w	M(B_2)⊥H	1,076	s	M(B_1)∥H
748	vs		1,094	w	m(A_1)∥H
757	vs		1,116	m	o(B_1)∥H
770	s	o(B_2)⊥H	1,170	w	M(B_1), o(A_1), m(B_1)∥H
783	w		1,181	w	o(B_1), m(B_1)∥H

m-Quatraphenyl I

393	m	m(A_2), M(A_2)⊥C	751	vs	M(B_2)⊥H
406	w		767	vs	
417	m		784	s	m(B_2)⊥H
458	m	m, M(B_2)	801	m	
			880	s	m(B_2)⊥H
525	w	m	919	w	m(A_2), M(B_2)?⊥H
571	m	m	969	w	m(B_2)⊥H
612	s	m(B_1), M(B_1)∥C	1,010	m	m(A_1), M(A_1)∥C
631	w	M(A_1)∥C	1,037	m	m(B_1), M(A_1)∥H
			1,066	w	m(A_1), M(B_1)∥H
642	w	m(A_1)∥C	1,078	m	
690	sh	M(B_2), m(B_2)⊥C	1,156	w	M(B_1)∥H
695	vs		1,172	w	m(B_1)∥H
700	vs		1,189	w	m(B_1)∥H

m-Quatraphenyl II

386	w	M(A_2, m(A_2)⊥C	799	s	m(B_2)⊥H
394	w		810	m	
400	m		888	s	m(B_2)⊥H
404	w		898	m	
417	w		920	s	m(A_2), M(B_2)⊥H
439	w	m, M(B_2)⊥C	971	w	m(B_2)⊥H
469	m		978	w	
504	m	m	1,012	m	m(A_1), M(A_1)∥C
523	m		1,026	w	m(B_1)∥H
571	w	m	1,038	w	M(A_1)∥H
579	m		1,076	m	m(A_1)∥H
611	m	m(B_1), M(B_1)∥C	1,099	w	M(B_1)∥H
625	w	M(A_1)∥C	1,105	w	
645	w	m(A_1)∥C	1,157	w	M(B_1)∥H
699	vs	M(B_2), m(B_2)⊥C	1,179	w	m(B_1)∥H
701	vs		1,192	w	m(B_1), M(A_1)∥H
708	vs				
752	vs	M(B_2)⊥H			
756	vs				
765	vs				

1-Phenyl-3-(4-xenyl) benzene

399	w	M(A_2), m(A_2), p(A_u)⊥C	799	s	m(B_2)⊥H
403	m		845	s	p(B_{1u})⊥H
443	m	m	851	m	p(B_{2g})⊥H
465	m	p(B_{1u}), M(B_2)⊥C	896	m	m(B_2)⊥H
525	s	m	918	w	m(A_2), p(A_u; B_{1g}), M(B_2)⊥H
553	w	m			
611	s	m(B_1), M(B_1)∥C	966	w	m(B_2)⊥H
623	w	M(A_1)∥C	1,007	m	M(A_1), m(A_1), p(B_{2u})∥C
642	w	m(A_1)∥C			
691	vs	M(B_2), m(B_2)⊥C	1,026	w	m(B_1), p(B_{2u})∥H
			1,038	w	M(A_1)∥H
700	vs				
748	vw	M(B_2)⊥H	1,077	m	m(A_1), M(B_1)∥H
757	vs		1,136	w	p(B_{1u})∥H
770	s		1,161	w	m(B_1), p(A_g), M(B_1)∥H
			1,183	w	m(B_1), p(B_{1g}), ∥H

TABLE 1. *Frequencies and assignments of some bands in the infrared spectra of polyphenyls*—Continued

p-Quatraphenyl

cm^{-1}			cm^{-1}		
394	vw	M (A_2), p(A_u) ⊥C	910	m	p(A_u or B_{1g}), M (B_2) ⊥H
473	s	p(B_{1u}), M (B_2) ⊥C			
610	w	M (B_1) ∥C	1,003	s	p(B_{2u}), M (A_1) ∥C
688	vs	p(B_{1g}), M (B_2) ⊥C	1,035	m	M (A_1), p(B_{2u}) ∥H
760	vs	M (B_2) ⊥H	1,077	m	M (B_1) ∥H
826	vs	p(B_{1u}) ⊥H	1,139	m	p(B_{3u}) ∥H
859	w	p(B_{2g}) ⊥H	1,168	m	p(A_g), M (B_1) ∥H
			1,183	w	p(B_{1g}) ∥H

1,3-Di-(2-xenyl) benzene

399	w	o(A_2), m(A_2), M (A_2) ⊥C	805	s	m(B_2) ⊥H
409	w		875	w	o(A_2) ⊥H
473	m	m	881	w	m(B_2) ⊥H
502	m	o	887	w	
513	s	m	908	s	M (B_2) ⊥H
536	s	o	917	s	m(A_2), o(B_2) ⊥H
562	sh	m	955	m	o(A_2) ⊥H
567	m	o	974	w	m(B_2) ⊥H
612	s	M (B_1), m(B_1), o(B_1) ∥C	1,001	w	o(B_1), M (A_1), m(A_1) ∥C
			1,013	s	
621	w	M (A_1) ∥C	1,040	w	o(A_1), M (A_1) ∥H
636	w	m(A_1) ∥C	1,063	w	m(B_1) ∥H
699	vs	M (B_2) ⊥	1,079	s	M (B_1) ∥H
710	vs	o(A_2) ⊥C	1,090	w	m(A_1) ∥H
745	vs	M (B_2) ⊥H	1,117	w	o(B_1) ∥H
748	vs		1,161	m	o(A_1), m(B_1), M (B_1) ∥H
754	sh	M (B_2) ⊥H			
765	vs		1,188	w	o(B_1), m(B_1) ∥H
780	s	o(B_2) ⊥H			
784	s				

1-(2-Xenyl)-3-(4-xenyl) benzene

396	w	M (A_2), o(A_2), m(A_2), p(A_u) ⊥C	798	s	m(B_2) ⊥H
420	w		801	sh	
451	w	m	821	w	M (A_2) ⊥H ?
462	m	p(B_{1u}) ⊥C	844	s	p(B_{1u}) ⊥H
494	m	o	875	w	o(A_2) ⊥H
523	s	m	901	s	m(B_2), M (B_2) ⊥H
532	sh	o	907	w	
556	sh	m	910	w	
561	m	o	915	m	
610	s	m(B_1), M (B_1) ∥C	953	w	o(A_2) ⊥H
622	w	M (A_1), ∥C	978	w	m(B_2) ⊥H
644	w	m(A_1) ∥C	1,007	s	o(B_1), m(A_1), p(B_{2u}), M (A_1) ∥C
683	s	o(A_2), M (B_2), m(B_2), p(B_{1g}) ⊥C	1,010	s	
693	vs		1,028	w	m(B_1), p(B_{2u}) ∥H
701	vs		1,036	w	o(A_1), M (A_1) ∥H
746	vs	M (B_2) ⊥H	1,075	m	m(A_1), M (B_1) ∥H
757	vs		1,120	w	o(B_1), p(B_{3u}) ∥H
767	vs	o(B_2) ⊥H	1,161	w	o(A_1), m(B_1), p(A_g), M (B_1) ∥H
775	s				
778	sh		1,179	w	o(B_1), m(B_1), p(B_{1g}) ∥H

m-Quinquaphenyl

394	w	m(A_2), M (A_2) ⊥C	886	s	M (B_2) ⊥H
406	w		898	w	
418	vw		907	w	
441	s	m	914	w	m(A_2), M (B_2) ⊥H
466	w	M (B_2) ⊥C	967	w	m(B_2) ⊥H
			1,002	w	m(A_1), M (A_1) ∥C
508	m	m	1,013	m	
568	vw	m	1,024	m	m(B_1) ∥H
614	s	m(B_1), M (B_1) ∥C	1,035	m	
621	sh	M (A_1) ∥C	1,048	w	M (A_1) ∥H
651	vw	m(A_1) ∥C	1,078	m	m(A_1) ∥H
			1,090	m	
693	vs	m(B_2), M (B_2) ⊥C	1,159	w	M (B_1) ∥H
724	vs	M (B_2)	1,172	w	m(B_1) ∥H
780	vs	M (B_2) ⊥H	1,183	w	m(B_1) ∥H
791	s				
807	m				
810	m				

TABLE 1. *Frequencies and assignments of some bands in the infrared spectra of polyphenyls*—Continued

1-(3-xenyl)-3-(4-xenyl) benzene

cm^{-1}			cm^{-1}		
392	w	p(4u), m(A_2), M (A_2) ⊥C	782	s	m(B_2) ⊥H
403	m		801	m	
419	m		838	s	p(B_{1u}), p(B_{2g})? ⊥H
434	w	m	848	s	
482	s	p(B_1=) ⊥C	882	s	m(B_2) ⊥H
			913	w	M (B_2), m(A_2), p(A_u, B_{1g}) ⊥H
515	vw	m			
572	m	m	972	w	m(B_2) ⊥H
611	s	M (B_1), m(B_1) ∥C	1,008	s	m(B_2), p(B_{2u}), M (A_1) ∥C
622	w	M (A_1) ∥C			
636	w	m(A_1) ∥C	1,014	w	p(B_{2u}) ∥H
			1,042	w	m(B_1), M (A_1) ∥H
645	w	m(A_1) ∥C	1,081	w	m(A_1), M (B_1) ∥H
691	vs	M (B_2), m(B_2), p(B_{3g}) ⊥C	1,138	w	p(B_{3u}) ∥H
698	vs		1,161	w	m(B_1), p(A_g), M (B_1) ∥H
755	vs	M (B_2) ⊥H			
767	s		1,185	w	m(B_1), p(B_{1g}) ∥H

m-Sexaphenyl

402	m	M (A_2), m(A_2) ⊥C	873	s	m(B_2) ⊥H
436	m	m	883	s	
480	w	M (B_2) ⊥C	897	m	
514	w	m	907	w	
577	vw	m	913	w sh	m(A_2), M (B_2) ⊥H
613	s	M (B_1), m(B_1) ∥C	970	w	m(B_2) ⊥H
629	w sh	M (A_1) ∥C	1,013	m	M (A_1), m(A_1) ∥C
698	vw	M (A_1) ∥C	1,034	w	M (A_1) ∥H
699	w		1,058	w	m(B_1) ∥H
698	vs	M (B_2), m(B_2) ⊥C	1,070	w	m(A_1) ∥H
			1,079	m	
714	w				
755	vs	M (B_2) ⊥H	1,094	w	M (B_1) ∥H
776	s	m(B_2) ⊥H	1,158	w	m(B_1), M (B_1) ∥H
786	vs		1,180	w	m(B_1) ∥H
803	w				
816	w				

m-Octaphenyl

406	m	M (A_2), m(A_2) ⊥C	875	s	m(B_2) ⊥H
456	m	m	887	s	
468	w	M (B_2) ⊥C	897	sh	
512	m	m	914	m	
568	vw?	m	922	vw sh	m(A_2) ⊥H
614	s	m(B_1), M (B_1) ∥C	975	w	m(B_2) ⊥H
647	w	m(A_1) ∥C	1,015	m	M (A_1), m(A_1) ∥C
692	vs	M (B_2), m(B_2) ⊥C	1,031	w	m(B_1), M (A_1) ∥H
701	vs		1,070	wsh	M (B_1) ∥H
751	vs	M (B_2) ⊥H	1,076	m	m(A_1) ∥H
758	vs		1,093	m	
772	vs		1,157	w	M (B_1) ∥H
728	vs		1,174	w	m(B_1) ∥H
791	s sh	m(B_2) ⊥H	1,181	w	
802	s				
810	w sh				

0.001-in. spacer and with no spacer for the thin layer. For spectra in the rocksalt region, 2 mg and 0.25 mg of sample were suspended in 100 mg of potassium iodide; the lower concentration was necessary to resolve the strong bands in the 13- to 15-μ region. For the cesium bromide region 5 mg of sample in 150 mg of potassium iodide was required in order to give observable spectra. The mineral oil mull technique is not satisfactory for the observation of spectra of crystalline polyphenyls because of the solubility of these materials in paraffins. The spectrum of biphenyl in mineral oil, for example, resembles that of a carbon tetrachloride solution.

Two obviously different spectra are presented for *m*-quatraphenyl. The samples, obtained from different sources, were evidently of different crystal structure. Spectra of liquid films of the two samples

were identical, as were spectra of crystalline films deposited on rocksalt windows by cooling the melted material. After making due allowances for the effect of orientation [8] on the band intensities, it seems that the spectra of the crystalline films most nearly resemble the pellet spectrum of *m*-quatraphenyl-II. A specimen of *m*-quatraphenyl was melted in vacuum and recrystallized. The spectrum of the resulting material was that of *m*-quatraphenyl-II. When the same substance was dissolved in benzene and recrystallized by slow evaporation, a spectrum of *m*-quatraphenyl-I was obtained. The spectrum of *m*-quatraphenyl-II shown in figures 3 and 4 evidently contains some *m*-quatraphenyl-I. In some preparations the bands at 784 and 880 cm^{-1}, for example, were greatly weakened. The possibility that rotational isomerism might be responsible for the two forms was investigated by studying the effect of temperature on the spectrum of a melted film. A cell was constructed for use at temperatures as high as 250° C. Spectra were observed between 2 and 15μ with a Beckman IR-4 spectrophotometer equipped with sodium chloride prisms. The results of this study are discussed in section 4.

The polyphenyls measured were obtained from different sources. Biphenyl, and *o*-, *m*-, and *p*-terphenyl were Eastman chemicals which had been purified by recrystallization. The higher *m*-polyphenyls, viz, quatraphenyl-I, quinquaphenyl, hexaphenyl, and octaphenyl were prepared in this laboratory by R. L. Alexander, Jr. [9]. The samples of *o*- and *p*-quatraphenyl were purchased from the Organic Specialties Co., and the sample marked *m*-quatraphenyl-II was bought from the Mathieson Co. The remaining five compounds (quatra- and quinquaphenyls) were obtained from the laboratory of Prof. G. F. Woods at the University of Maryland. Their preparation and properties have been reported in the literature [10,11,12].

The spectrum of *p*-quatraphenyl contains weak bands at 740 and 714 cm^{-1} not observed in the spectrum given by Cannon and Sutherland [13] although the spectra seem to agree in other respects. These bands are presumably contributed by impurities.

3. Discussion

Monosubstituted and ortho- and metadisubstituted rings have pseudosymmetry C_{2v}, while parasubstituted rings have pseudosymmetry V_h. The symmetry species of the vibrations of the substituted rings correlate with those of benzene as shown in table 2. Vibrations that are forbidden to appear in the infrared spectra under the selection rules appropriate for a given symmetry group are shown in parentheses. They are actually quite likely to appear in the spectra, though probably with reduced intensity. The vibrations listed in table 2 and discussed in the following paragraphs are arranged on the basis of an approximate description, e. g., C—H stretching, solely for convenience. It is recognized that more than one symmetry coordinate is involved in most normal vibrations. It should also be noted that the stretching and bending of carbon-to-substituent bonds in the substituted aromatics correlate with stretching and bending of carbon-to-hydrogen bonds in benzene, requiring adjustments in the counting of vibrations.

TABLE 2. *Correlation of symmetry species of substituted rings*[a]

	Out-of-plane C—C bending			In-plane C—C bending		
para (V_h)	(B_{1g})	(A_u)	B_{1u}	(A_g)	(B_{1g})	B_{2u}
meta (C_{2v})	B_2	(A_2)	B_2	A_1	B_1	A_1
ortho (C_{2v})	(A_2)	(A_2)	B_2	A_1	B_1	B_1
mono (C_{2v})	B_2	(A_2)	B_2	A_1	B_1	A_1
benzene (D_{6h})	B_{2g}	(E_{2u})		(E_{2g})		(B_{1u})
Out-of-plane C—H bending						
(B_{1g}) S	(B_{2g})	(B_{1g})	B_{1u}	(A_u)		B_{1u} S
B_2 S	(A_2)	B_2	B_2	(A_2) S		B_2
(A_2) S	(A_2)	B_2	B_2	(A_2)		B_2 S
B_2 S	(A_2)	B_2	B_2	(A_2)		B_2
(B_{2g})	(E_{1g})		A_{2u}	(E_{2u})		
In-plane C—H bending						
(B_{1g})	(A_g)	(B_{1g}) S	B_{1u}	B_{2u}		B_{2u} S
B_1	A_1 S	B_1	B_1	A_1		B_1 S
B_1	A_1 S	B_1	A_1	A_1		B_1 S
B_1	A_1	B_1	B_1	A_1		B_1 S
(A_{2g})	(E_{2g})		(B_{2u})	E_{1u}		
C—C stretching						
(A_g)	(A_g)	(B_{1g})	B_{1u}	B_{2u}		B_{2u}
A_1	A_1	B_1	B_1	A_1		B_1
A_1	A_1	B_1	A_1	A_1		B_1
A_1	A_1	B_1	B_1	A_1		B_1
(A_{1g})	(E_{2g})		(B_{2u})	E_{1u}		
C—H stretching						
(A_g) S	(A_g)	(B_{1g})	B_{2u}	B_{2u} S		B_{1u}
A_1 S	A_1	B_1	A_1	A_1		B_1 S
A_1 S	A_1	B_1	B_1	A_1		B_1 S
A_1 S	A_1	B_1	A_1	A_1		B_1
(A_{1g})	(E_{2g})		(B_{1u})	E_{1u}		

[a] Species in parentheses are infrared inactive under strict selection rules. S designates vibrations involving carbon-to-substituent bonds, rather than carbon-to-hydrogen bonds.

3.1. C—C Stretching Vibrations

Characteristic aromatic ring stretching vibrations are found near 1,600 and 1,450 to 1,500 cm^{-1}. Vibrations of ortho-, meta-, and monosubstituted rings that correlate with the degenerate E_{2g} Raman line of benzene at 1,595 cm^{-1} are infrared active, but the corresponding vibrations of V_h parasubstituted rings are inactive. All of the polyphenyls have absorptions near 1,600 cm^{-1} which are resolved into at least two components. Following RW, the high-frequency component probably contains the A_1 absorptions, and the low-frequency component the B_1 absorptions of the mono-, ortho-, and meta-substituted rings. The 1,600 cm^{-1} bands are quite weak in *p*-terphenyl and even weaker in *p*-quatraphenyl, as would be expected with a reduction in the mono- to pararing ratio. However, there seems to be no noticeable weakening of the 1,600 cm^{-1} bands in the other polyphenyls which contain parasubstituted rings. All of the polyphenyl vibrations that are correlated with the E_{1u} band of benzene at

1,485 cm^{-1} are infrared active, and the spectra of all of the polyphenyls have a complex series of bands in this region. RW have assigned the higher frequency absorptions near 1,500 cm^{-1} to the A_1 modes in mono-, ortho-, and metasubstituted rings and the B_{2g} mode in parasubstituted rings; and they assigned the lower frequency absorptions near 1,450 cm^{-1} to the B_1 modes in mono-, ortho-, and metasubstituted rings and the B_{3u} mode in parasubstituted rings. Those polyphenyls that contain meta- and parasubstituted rings have bands near 1,400 cm^{-1} which are missing or weak in compounds containing a high proportion of orthosubstituted rings and in biphenyl. These bands are probably C—C stretching modes shifted from the 1,450 to 1,500-cm^{-1} region, possibly because of the influence of neighboring rings. These bands are discussed further in section 3.6.

The C—C vibrations correlated with the A_{1g} Raman line of benzene at 992 cm^{-1} are sensitive to substituents and have not been assigned. Vibrations corresponding to the uncertain B_{2u} benzene vibration have been placed at 1,324 and 1,315 cm^{-1} (both weak) in mono- and orthosubstituted ring compounds by RW. Weak absorptions are observed near there in the infrared spectra of the polyphenyls.

3.2. In-Plane Ring Bending Vibrations

The doubly degenerate E_{2g} ring bending vibration of benzene is found at 605 cm^{-1} in the Raman spectrum. The A_1 and B_1 pair of vibrations in mono-, ortho-, and metasubstituted rings which correlate with the E_{2g} benzene mode should be active in the infrared, but the corresponding A_g and B_{1g} modes of parasubstituted rings should be inactive under V_h selection rules. All of the polyphenyls studied have a band at 614 ± 4 cm^{-1}. This band, which is fairly strong, except in the case of *p*-terphenyl and *p*-quatraphenyl, is assigned to the B_1 modes of mono-, ortho-, and metasubstituted rings. RW place the corresponding B_{1g} mode of parasubstituted rings at 699 ± 6 cm^{-1} in the region obscured by strong absorption of the monosubstituted rings. All but three of the polyphenyls absorb weakly at 625 ± 6 cm^{-1}. These bands are assigned to the A_1 mode of monosubstituted rings placed at 620 ± 4 (618 ± 5 cm^{-1} in the Raman effect) by RW. In addition, all but two of the compounds containing metasubstituted rings have bands at 647 ± 11 cm^{-1} which we assign to the A_1 mode of metasubstituted rings.

The B_{1u} ring deformation of benzene has been calculated by Lord and Andrews [14] to lie at 1,008 cm^{-1}. RW assign bands at $1{,}001 \pm 4$ and 999 ± 5 cm^{-1} to the corresponding A_1 modes of mono- and metasubstituted rings, respectively. All of the polyphenyls have bands of medium intensity near 1,000 cm^{-1} which probably represent these modes as well as the corresponding B_1 modes in ortho- and B_{2u} modes in parasubstituted rings.

3.3. In-Plane C—H Bending Vibrations

The in-plane C—H bending vibrations of benzene lie in the fairly narrow region from about 1,030 to 1,200 cm^{-1}. Of these, a band is observed at 1,037 cm^{-1} in the infrared and another at 1,178 cm^{-1} in the Raman spectrum, while the remaining two inactive modes have been calculated [14] to lie at 1,190 and 1,145 cm^{-1}. After removing the carbon-to-substituent bond bending modes there remain 1 A_1 and 3 B_1; 2 A_1 and 2 B_1; 1 A_1 and 3 B_1; and 1 B_{3u}, 1 B_{2u}, 1 B_{1g}, and 1 A_g transitions in the mono-, ortho-, meta-, and parasubstituted rings, respectively. Only the B_{2u} and B_{3u} transitions are infrared active in parasubstituted rings under V_h selection rules.

RW have observed that numerous bands in the 1,000- to 1,200-cm^{-1} region are relatively invariant from molecule to molecule of a given isomeric type. They assign $1{,}029 \pm 5$, $1{,}031 \pm 5$, $1{,}045 \pm 7$, and $1{,}018 \pm 10$ cm^{-1} to A_1 mono, A_1 ortho, B_1 meta, and B_{2u} paravibrations; $1{,}072 \pm 7$, $1{,}126 \pm 12$, $1{,}081 \pm 10$, and $1{,}125 \pm 10$ cm^{-1} to B_1 mono, B_1 ortho, A_1 meta, and B_{3u} paravibrations; and $1{,}156 \pm 5$, $1{,}159 \pm 7$, $1{,}165 \pm 6$, and $1{,}179 \pm 11$ cm^{-1} to B_1 mono, A_1 ortho, B_1 meta, and A_g paravibrations, respectively. These three groups of bands are readily associated with bands found near 1,040, 1,080, and 1,160 cm^{-1}, respectively, in all of the polyphenyl spectra. RW further assign a band at $1{,}177 \pm 6$ cm^{-1} to an A_1 mode of monosubstituted benzenes. Bands found near 1,190 cm^{-1} in the polyphenyl spectra very likely correspond to this A_1 monomode, and also to the B_1 ortho, B_1 meta, and the forbidden B_{1g} paravibrations as well.

The regions of absorption, as given by RW, are seen to depend somewhat on isomeric substitution, and lead to some complexity in the polyphenyl bands. For example, the spectrum of *p*-terphenyl has a pair of bands with peaks at 1,043 and 1,028 cm^{-1}, which can be assigned to the A_1 mono and B_{2u} paravibrations, respectively. These separations are more than the amount expected from RW's tables, perhaps because of interactions of the Fermi type.

3.4. Out-of-Plane C—H Bending Vibrations

These are the vibrations used most frequently for the qualitative analysis of substituted aromatic compounds. RW give the following regions of absorption for the strong bands: Mono B_2 751 ± 15; ortho B_2 751 ± 7; meta B_2 782 ± 9, and B_2 876 ± 10; and para B_{1u} 817 ± 13 cm^{-1}. These values do not hold for strongly electrophylic substituents such as fluorine and nitro groups. In the spectra of polyphenyls the metabands are found at 795 ± 13 and 894 ± 21 cm^{-1} and the paraband at 854 ± 6 cm^{-1}. These values are somewhat higher than those given by RW. The orthobands are also found at higher frequencies, 776 ± 9 cm^{-1}, rendering them distinct, or nearly so, from the monobands at 766 ± 22 cm^{-1}.

The weaker C—H out-of-plane bending vibrations are given by RW as follow: Mono B_2 908 ± 10, B_2 and A_2, 962 ± 6, and 982 ± 6, A_2 837 ± 10; ortho A_2 865 ± 14 and 977 ± 9, B_2 934 ± 11; meta A_2 904 ± 13, B_2 964 ± 10; and para B_{2g} 840 (in the Raman effect), A_u or B_{3g} 961 ± 12 cm^{-1}. All of the polyphenyls have one or more weak-to-medium bands near 850 cm^{-1} which are easily mistaken for the

characteristic B_{1u} para-absorption. It is likely that these bands are contributed by vibrations involving the connecting links (see section 3.6).

A more careful study of the strong characteristic C—H bands reveals some curious progressions. The metabands are seen to be resolved into components with increasing complexity in compounds containing larger numbers of such rings. In those cases where only one metasubstituted ring is present the strongest peak in the 894 cm^{-1} region is generally found at a somewhat higher frequency than when more than one metaring is present. In the 795-cm^{-1} region (see fig. 9) the strongest peak shifts regularly to lower frequencies as the number of metarings increases, while an increasingly complex set of weaker peaks develops on the high-frequency side of the major peak. This complex set of weaker peaks develops on the high-frequency side of the major peak. This complex structure is less resolved in the spectra of some of the polyphenyls in the solution phase, but it is still recognizable, thus eliminating the possibility that lattice vibrations or intermolecular vibrational interactions are involved. A plausible explanation is that the C—H bending vibrations of different metasubstituted rings in the same molecule are interacting. This idea can be developed further through the use of quantum mechanical perturbation theory, which shows that if all interaction terms are set equal to zero except those between nearest neighbors, which are assumed to be identical, the degeneracy of the vibrations is removed and the levels are split symmetrically. The inclusion of next-nearest neighbor interactions results in a regular change in the separation of adjacent components with the spacing of the bands becoming compressed at one side and expanded at the other.

The magnitude of the interaction force constant must be about 0.2 of the value of the diagonal terms in order to explain the magnitude of the observed splitting. The relative intensities of the components of the bands were determined from the elements of the dipole moment transition matrices after first determining the correct sums of the product functions for each value of the perturbation energy. The theory predicts that the component of lowest frequency will be the strongest, with the intensities of the higher frequency components decreasing more or less regularly in agreement with the observed spectra, provided that λ, the interaction force constant, is taken to be negative. The physical significance of a negative value is that it is easier to distort the hydrogens on a ring out of their normal plane if the hydrogens on the neighboring ring are already out of their plane. It is interesting to observe that Kakiuti and Shimanouchi [6] calculate negative values for the out-of-plane interaction force constants of neighboring hydrogens on the same ring, and that the magnitude of the interaction constant is about 0.18 that of the C—H out-of-plane bending force constant.

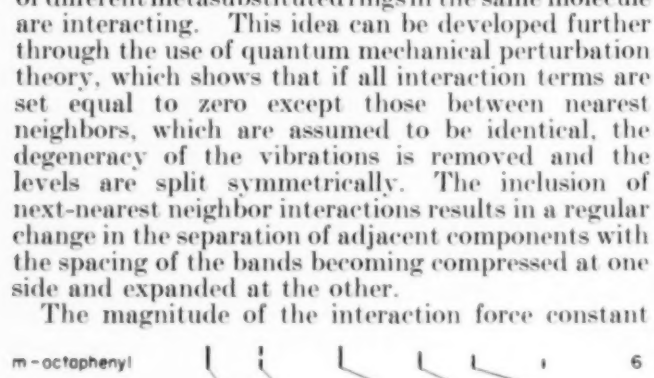

FIGURE 9. *Bands in 800-cm^{-1} region for compounds containing metasubstituted rings.*

Numbers at right indicate number of metasubstituted rings in the molecule. *m*-Heptaphenyl was not available for study, but predicted bands are included in the figure. The line predicted for *m*-octaphenyl at 780 cm^{-1}, was not observed, perhaps because of insufficient resolution.

Orr [15] has recently explained the broadening of the out-of-plane bending bands (960 cm^{-1}) of the olefinic hydrogens in orthosubstituted *trans*stilbenes on the basis of damping accompanying the transfer of vibrational energy to a motion involving the substituent groups which are quite close to the olefinic hydrogens. This situation differs from that encountered in the case of the metasubstituted polyphenyls because in the stilbenes energy is transferred between vibrational states of considerably different energy. However, Orr's process is very likely involved in the case where neighboring rings are substituted in different ways.

The bands characteristic of orthosubstitution near 776 cm^{-1} and the 766-cm^{-1} band of monosubstituted rings in molecules containing orthosubstituted rings are also split into complex structures, but not in so systematic a fashion as that displayed by the metaring compounds. This is probably the result of interactions between the out-of-plane C—H vibrations of ortho- and monosubstituted rings, as well as interactions between orthosubstituted rings. The number of peaks resolved in the 760- to 780-cm^{-1} band seems excessive. For example, *o*-terphenyl has five peaks resolved, but contain only three rings. This is possibly a consequence of the occurrence of more than one molecule per unit cell. *o*-Terphenyl has four molecules in each unit cell [16]. The spectrum of *o*-terphenyl in solution in carbon disulfide does not display such pronounced splitting, for only three components are resolved. *o*-Quatraphenyl in carbon disulfide solution, on the other hand, has five components in the 740- to 790-cm^{-1} region, just as in the solid phase.

No splitting is observed in the out-of-plane C—H bending vibrations of the parasubstituted rings, but the band is found at a somewhat lower frequency in *p*-quatraphenyl (826 cm^{-1}), which contains two parasubstituted rings, than in those molecules (843 ± 5 cm^{-1}) containing only one parasubstituted ring.

3.5. Out-of-Plane Ring Bending Vibrations

The frequency of the B_{2g} out-of-plane ring bending mode of benzene has been calculated [6] to be 698 cm^{-1}. RW have placed the corresponding B_2 modes of mono- and metasubstituted rings at 697 ± 11 and 690 ± 15 cm^{-1}, respectively. These bands are quite intense in the infrared spectra and are used with the nearby C—H bands in the qualitative analysis of substituted aromatic compounds. RW place the infrared forbidden B_{3g} vibration of parasubstituted rings at 699 ± 6 cm^{-1} where weak bands are sometimes observed in the infrared spectra. The corresponding orthoband is of species A_2 and is also forbidden in the infrared.

The 404 cm^{-1} E_{2u} benzene vibration is doubly degenerate. Its A_2 component in monosubstituted rings, and its A_u component in parasubstituted rings, are observed in the Raman effect at 406 ± 10 and 404 ± 10 cm^{-1} according to RW, and sometimes occur as weak absorptions in the infrared. All of the polyphenyls absorb weakly near 400 cm^{-1}, which suggests that the A_2 components of this vibration in ortho- and metasubstituted rings also absorb here. The B_2 component corresponding to the E_u benzene vibration is reported by RW to lie in the 450- to 500-cm^{-1} region and to be sensitive to the nature of the substituent. The polyphenyls have bands in this region which permit some general assignments, but until Raman data are available for these compounds the situation cannot be described as satisfactorily as for the 11- to 14-μ region. Biphenyl has a band at 460 cm^{-1}, and the parasubstituted compounds have single strong bands at 471 ± 11 cm^{-1}, which are readily assigned to the B_2 mono- and B_{1u} paravibrations. The orthosubstituted compounds have a pattern of three bands at 503 ± 10, 532 ± 10, and 564 ± 7 cm^{-1}, while the metasubstituted compounds also have a pattern of bands in this region at 454 ± 20, 514 ± 12, and sometimes 563 ± 10 cm^{-1}. Other bands usually occur also. In table 1 these bands are merely assigned to ortho- or metasubstituted rings.

3.6. Connecting Link Vibrations and Unassigned Bands

Each of the ring-connecting bonds contributes 1 stretching, 1 torsion, 2 in-plane bending, and 2 out-of-plane bending internal coordinates to the normal vibrations. If these internal coordinates acted independently, without simultaneous vibration of the other internal coordinates, their vibrational frequencies would probably be well below the region of observation available in this study. However, other internal coordinates are almost certainly involved and might in fact, predominate. Without actually performing a normal coordinate determination it is not possible to guess where these vibrations are to be found.

There is little doubt that the para- and metasubstituted ring systems are planar, or nearly so, while the orthosubstituted ring systems are nonplanar because of steric hindrance. Hence the ring-connecting bonds in orthosubstituted systems must have less double bond character than in the other structures. If the vibrations loosely described as connecting-bond stretching actually involve large contributions from motions of the ring bonds, it would be reasonable for the frequencies to be not much lower than those of the "normal" ring vibrations, and they might indeed account for the bands observed near 1,400 cm^{-1} in the meta- and parasubstituted polyphenyls. The loss of double bond character in the ring-connecting bonds of the orthosubstituted systems would then explain the absence of these bands in the spectra of the orthosubstituted compounds.

Five of the polyphenyls have bands of medium intensity at 727 ± 2 cm^{-1}. A sixth compound has a pair of weak bands at 722 and 728 cm^{-1} and another compound has a weak shoulder at 714 cm^{-1}. All of these compounds contain at least 1 metasubstituted ring, all but 1 contain 5 or more rings, and all but 1 have at least 1 metasubstituted ring which is not adjacent to a monosubstituted ring. The correlation of these bands with vibrations involving connecting links to metasubstituted rings seems reasonable.

There are other bands in the infrared spectra of the polyphenyls which are possibly associated with the ring-connecting bonds. Among these are the bands at 846 ± 13 cm^{-1} mentioned previously, and the multitude of absorptions observed in the cesium bromide region, particularly those correlated with ortho- and with metasubstituted rings.

4. Rotational Isomerism in *m*-Quatraphenyl

The connecting bond between phenyl rings in polyphenyl molecules is stabilized by about 7 kcal/mole [17] of resonance energy. This is sufficient double-bond character to insure planarity except in such molecules as *o*-terphenyl [16] where the steric repulsion is too great. On the other hand, a barrier of this magnitude is not too high to permit hindered rotation and the rapid establishment of equilibrium if more than one stable configuration exists. The structure of *m*-quatraphenyl has not been determined, but it is reasonable to assume that the planar *trans*form is the most stable one in view of the known planarity of biphenyl, *p*-terphenyl, and *p*-quatraphenyl. The planar *cis*form is very likely also a stable configuration with somewhat greater free energy than the *trans*form because of the closer proximity of the hydrogen atoms.

The intensities of all bands of liquid *m*-quatraphenyl were found to decrease reversibly as the temperature was increased, partly as a result of thermal expansion, but some bands decreased more rapidly than others. Several bands were sufficiently well resolved to permit intensity measurements. The results, shown in figure 10, are readily interpreted [18] as evidence for the existence of rotational isomers having a free energy difference of about 250 cal/mole. A crude calculation of the additional electrostatic repulsion energy in the *cis*configuration yields a value of this order of magnitude. Included in figure 10 are data for two pairs of bands which behave similarly as the temperature is changed. The nearly zero slope ($E < 20$ cal/mole) for these pairs is evidence that possible perturbing influ-

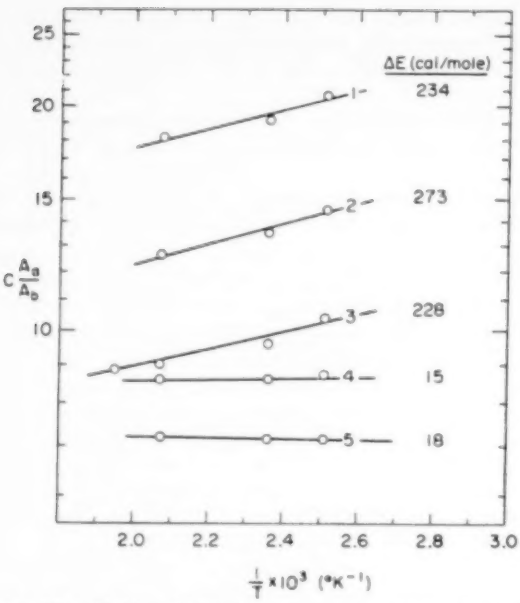

FIGURE 10. *Ratios of absorbancies for several band pairs in the infrared spectrum of m-quatraphenyl as a function of temperature.*

The free-energy differences are calculated from the slopes. C is an arbitrary constant, selected for each curve for convenience in plotting. Band pairs used are: 1, 1,013 and 1,075 cm^{-1}; 2, 1,094 and 1,075 cm^{-1}; 3, 1,170 and 1,158 cm^{-1}; 4, 1,170 and 1,094 cm^{-1}; 5, 1,013 and 1,026 cm^{-1}.

ences, such as radiation from the hot cell, are not important.

The absorptions used in this determination are in a spectral region where bands are fairly insensitive to structural changes and where contributions from mono- and metasubstituted rings overlap. This tends to reduce the sensitivity of the spectrum to changes in isomer equilibrium and could lead to a low value for the isomeric energy difference. This circumstance also renders useless one of the standard tests for the existence of isomeric forms, namely the disappearance of a set of bands upon crystallization. Consequently, this experiment failed to demonstrate whether different isomeric forms are involved in the two different crystalline samples of *m*-quatraphenyl.

Recent discoveries of the temperature sensitivity of absorption band intensities in cyclohexanone [19] and some substituted phenols [20] seem to raise questions about the validity of determining isomeric energy differences from the temperature behavior of band intensities. A completely satisfactory explanation of this behavior has not yet been given, although Liddel and Becker [21] attribute the variation of O—H bands with temperature to alcohol-solvent interactions resembling very weak hydrogen bonds. Meanwhile, the existence of rotational isomers in liquid *m*-quatraphenyl can be considered probably established.

5. Conclusion

In general, the assignments given by RW for substituted benzenes provide a satisfactory basis for the discussion of the infrared spectra of the polyphenyls. The assignments have been extended somewhat to include some additional vibrations, including some that are peculiar to polyphenyl compounds. The splitting observed in some of the out-of-plane bending vibration bands indicates that the individual rings of polyphenyls do not vibrate as independent units, at least as far as the out-of-plane modes are concerned. Indeed, the fine structure observed in the C—H out-of-plane deformation vibration bands of metasubstituted rings near 790 cm^{-1} can be explained on the basis of interaction between a ring and its nearest neighbors. On the other hand, pronounced splitting of this sort is not observed in the case of the in-plane vibrations and many of the other out-of-plane vibrations.

It is concluded that the in-plane vibrations of polyphenyl molecules can be treated as though they they arise in individual uncoupled rings, and that the out-of-plane vibrations can also be treated in this way for classification purposes, but due allowance must be made for interactions between rings when more detailed assignments are to be made. In either case, vibrations involving the ring-connecting bonds must, of course, be treated separately.

6. References

[1] S. Krimm, C. Y. Liang, and G. B. B. M. Sutherland, J. Chem. Phys. **25,** 549 (1956).
[2] C. Y. Liang and S. Krimm, J. Chem. Phys. **25,** 563 (1956).
[3] San-Ichiro Mizushima, I. Nakagawa, and D. M. Sweeny, J. Chem. Phys. **25,** 1006 (1956).
[4] L. J. Bellamy, The infrared spectra of complex molecules (John Wiley & Sons, Inc., New York, N. Y., 1954).
[5] R. R. Randle and D. H. Whiffen, Molecular spectroscopy, Report of a Conference of the Hydrocarbon Research Group (The Institute of Petroleum, Oct. 1954).
[6] T. Shimanouchi, Y. Kakiuti, and I. Gamo, J. Chem. Phys. **25,** 1245 (1956); Y. Kakiuti and T. Shimanouchi, J. Chem. Phys. **25,** 1252 (1956).
[7] J. E. Stewart, J. Research NBS **54,** 41 (1955) RP2563; J. Chem. Phys. **26,** 248 (1957).
[8] J. E. Stewart, J. Chem. Phys. **23,** 986 (1955).
[9] R. L. Alexander, Jr., J. Org. Chem. **21,** 1464 (1956).
[10] G. F. Woods and I. W. Tucker, J. Am. Chem. Soc. **70,** 3340 (1948).
[11] G. F. Woods and F. T. Reed, J. Am. Chem. Soc. **71,** 1348 (1949).
[12] G. F. Woods, A. L. Van Artsdale, and F. T. Reed, J. Am. Chem. Soc. **72,** 3221 (1950).
[13] C. G. Cannon and G. B. B. M. Sutherland, Spectrochim. Acta **4,** 373 (1951).
[14] R. C. Lord and D. H. Andrews, J. Phys. Chem. **41,** 149 (1937).
[15] S. F. D. Orr, Spectrochim. Acta **8,** 218 (1956).
[16] J. D. H. Donnay and W. Nowachi, Crystal data, Memoir 60 (Geological Society of America, New York, N. Y., 1954).
[17] L. Pauling, The nature of the chemical bond, p. 217 (Cornell University Press, Ithaca, N. Y., 1948).
[18] San-Ichiro Mizushima, Structures of molecules and internal rotation (Academic Press, New York, N. Y., 1954).
[19] E. J. Slowinski, Jr., and G. C. Claver, J. Opt. Soc. Am. **45,** 396 (1955).
[20] R. H. Hughes, R. J. Martin, and N. D. Coggeshall, J. Chem. Phys. **24,** 489 (1956).
[21] U. Liddel and E. D. Becker, J. Chem. Phys. **25,** 173 (1956).

WASHINGTON, August 29, 1957.

Journal of Research of the National Bureau of Standards Vol. 60, No. 2, February 1958 Research Paper 2830

On the Application of Steam-Driven Water Jets for Propulsion Purposes*

J. M. Burgers[1] and A. Ghaffari[2]

Calculations have been made concerning the momentum that can be given to a jet of water by mixing it with a jet of high-speed steam. Apart from an application of the equations of momentum and enthalpy, this raises questions concerning the speed of condensation and the acceleration of the water.

1. Introduction

Basic equations for the change of temperature and of momentum to be expected when jets of steam and water are mixed have been given by Chiarulli and Dressler [1].[3]

The present authors extended these calculations to a case where momentum must be communicated to a jet of water by mixing it with a jet of high-speed steam in such a way that complete condensation of the steam will take place. It was thought that *condensation under constant pressure* would have certain advantages. On the one hand there is a much smaller loss of useful momentum, while on the other hand the thermodynamic aspect of the condensation becomes simpler. It was also thought that there would be less chance for the appearance of shocks. In order to obtain condensation under constant pressure, the chamber in which the condensation takes place must have a sectional area decreasing in the direction of the flow (as is applied in the injector for steam locomotives), according to some law that must be determined.

It was thought useful to have a concrete example in mind with definite numerical values. It was assumed therefore that the pressure in the mixing chamber should be kept equal to 0.8 atm.

The water is supposed to enter into the mixing chamber in the axial direction, with a velocity $u'=10$m/sec and a temperature of $T'=20°$ C. The enthalpy of the water then is $H'=20.1$ kcal/kg, the density $\rho'=998$ kg/m^3.

Data have been taken from W. Koch and K. Schmidt, VDI-Wasserdampftafeln (Springer-Verlag, 1952); since these data are presented in technical units, we must make use to a certain extent of the system in which the kilogram is taken as the unit of weight or force. We shall write kg* in this case, and reserve the notation kg when it refers to mass.

The steam used as a driving force is supposed to be obtained from a boiler where the temperature is about 165° C and the pressure 7.5 atm (saturation pressure for this temperature). After coming from the boiler the steam is superheated to $T_0=360°$ C, the pressure remaining $p_0=7.5$ atm. The steam then has an enthalpy $H_0=759.4$ kcal/kg. It will be assumed that the expansion of the steam from 7.5 atm to 0.8 atm occurs without friction losses and without change of entropy. If losses and entropy change cannot be avoided, we suppose that they are compensated for by a suitable increase of T_0 and p_0, so that we shall still have the same data for the expanded state as are given below. After expansion the steam will then have the following properties:

pressure $p''=0.8$ atm$=8{,}000$ kg*/m^2
temperature $T''=99.0°$ C
density $\rho''=0.462$ kg/m^3
enthalpy $H''=639.4$ kcal/kg
velocity $u''=1{,}003$ m/sec.

It is assumed that also the velocity u'' of the steam is directed axially.

The entrance area of the mixing chamber will be denoted by A; of this the part $A\,s$ is taken in by the water jet, and the part $A\,(1-s)$ by the steam jet.

We write A_m for the sectional area of the mixing chamber at the point where complete condensation has been reached; u_m for the speed of the water when all is condensed; ρ_m for the density of this water, for which we shall use a mean value $\rho_m=985$ kg/m^3; further T_m for its temperature, H_m for its enthalpy. We note that the mechanical equivalent of heat in technical units is $J=427$ kg*m per kcal; and that g=acceleration of gravity$=9.8$ m/sec^2.

2. Basic Equations for the Mixing Process

The following equations hold for the mixing process:

Equation of continuity:

$$As\rho'u'+A\,(1-s)\,\rho''\,u''=A_m\,\rho_m\,u_m. \qquad (1)$$

When numbers are inserted, we solve for $(A_m/A)\,u_m$ and obtain:

$$(A_m/A)\,u_m=0.47+9.56\,s, \qquad (2)$$

Equation of momentum:

$$As\rho'u'^2+A\,(1-s)\,\rho''\,u''^2=A_m\,\rho_m\,u_m^2. \qquad (3)$$

*The preparation of this paper was supported by the Office of Naval Research, U. S. Navy.

[1] Guest worker, National Bureau of Standards, from American University; and University of Maryland.

[2] National Bureau of Standards, and on leave from Teheran University.

[3] Figures in brackets indicate the literature references at the end of this paper.

Inserting numerical values we find:

$$(A_m/A)\ u_m^2 = 472 - 372\ s. \qquad (4)$$

Equation of enthalpy:

$$As\rho' u'(H' + u'^2/2gJ) + A(1-s)\rho'' u''(H'' + u''^2/2gJ)$$

$$= A_m\ \rho_m\ u_m\ (H_m + u_m^2/2gJ). \qquad (5)$$

Inserting numerical values we arrive at:

$$(A_m/A)\ u_m\ (H_m + u_m^2/2gJ) = 258 - 156\ s. \qquad (6)$$

From eqs (4) and (2) we can obtain u_m; from (6) and (2) we obtain $H_m + u_m^2/2gJ$ and then H_m itself; from the latter quantity the temperature of the water can be found. It is also possible to find (A_m/A).

The condensed water has the speed u_m and the pressure $p_m = p' = 8{,}000$ kg*/m². When it is to be used for propulsion, it may have to be driven out against a higher pressure p_e. In such a case it will be appropriate after the mixing to make the water flow through an expanding duct, in which the velocity decreases from the value u_m to a value u_e, adjusted so that the pressure will increase from p_m to p_e. In what follows we have assumed: $P_e = 2.0$ atm = 20,000 kg*/m². We then find:

$$u_e^2 = u_m^2 - 239\ (\text{m/sec})^2. \qquad (7)$$

Formulas for other values of p_e can easily be derived.

The equations can be worked out for various values of s. After some trials it was found that $s = 0.5$ gave a convenient case. Larger values of s (meaning that more water is admitted in the mixing chamber in comparison with the steam) make the exit speed rather low; smaller values of s (meaning that more steam is used in comparison with the water) make the final temperature higher and may lead to incomplete condensation. With $s = 0.5$ the following results are obtained:

$$u_m = 54.5 \text{ m/sec}$$
$$u_e = 52.3 \text{ m/sec}$$
$$H_m = 52.9 \text{ kcal/kg}$$
$$T_m = 52.9° \text{ C}$$
$$A_m/A = 0.096.$$

To the temperature T_m corresponds a saturation pressure of 1,450 kg*/m². Since the pressure in the mixing chamber is 8,000 kg*/m², it was thought that there would be no danger for incomplete condensation provided the time for condensation is not made too short (see section 4).

3. Momentum and Efficiency of the Issuing Jet

The total mass flow of water in the issuing jet is:

$$A_m\ \rho_m\ u_m \text{ kg/sec} = A_m\ \gamma_m\ u_m/g \text{ technical units of mass per second.} \qquad (8)$$

Here γ_m is used to represent the specific weight of the water, which, when expressed in kg*/m³, is given by the same number 985 as for its density in kg/m³.

When the jet is applied to drive an underwater object with a speed of V m/sec, the usual arrangement will be that the water is taken out of the surroundings, where it had the speed V relative to the object, while it is reissued as a jet with the speed u_e relative to this object. Hence the thrust to be obtained is given by:

$$\text{thrust} = (A_m\ \gamma_m\ u_m/g)\ (u_e - V) \text{ kg*}. \qquad (9)$$

The useful work done in unit of time is:

$$\text{power} = (A_m\ \gamma_m\ u_m/g)\ (u_e - V)\ V \text{ kg*m/sec}. \qquad (10)$$

It may be possible to choose V so that this expression has a maximal value; this occurs when $V = \frac{1}{2}\ u_e$. We then find:

$$\text{thrust} = \tfrac{1}{2}\ (A_m\ \gamma_m\ u_m/g)\ u_e \text{ kg*} \qquad (9a)$$

$$\text{power} = \tfrac{1}{4}\ (A_m\ \gamma_m\ u_m/g)\ u_e^2 \text{ kg*m/sec}. \qquad (10a)$$

Inserting numerical values with $s = 0.5$, we arrive at:

$$\text{thrust} = \text{approx } 13{,}800\ A \text{ kg*} \qquad (9b)$$

$$\text{power} = \text{approx } 360{,}000\ A \text{ kg*m/sec}. \qquad (10b)$$

In these formulas A is expressed in m^2. When the entrance area of the mixing chamber is taken as 100 cm² = 0.01 m², the values become:

$$\text{thrust} = \text{approx } 138 \text{ kg*} \qquad (9c)$$

$$\text{power} = \text{approx } 3{,}600 \text{ kg*m/sec}. \qquad (10c)$$

In order to obtain a rough idea concerning the efficiency of the arrangement, we will consider only the energy used for the steam production. We have assumed that the water needed for this purpose is taken from the surroundings, at the temperature of 20° C, so that the enthalpy is 20.1 kcal/kg. It follows that per kg water to be turned into steam, the enthalpy difference $H_0 - H' = 759.4 - 20.1 = 739.3$ kcal is needed. Since the mass of the steam needed per second is given by $A\ (1-s)\ \rho''\ u'' = A\ (1-s) \times 463$ kg/sec, the energy required per second is:

$$A\ (1-s) \times 463 \times 739.3 \times 427 \text{ kg*m/sec}.$$

With $s = 0.5$ this becomes: $A \times 0.73 \times 10^8$ kg*m/sec, and for $A = 0.01$ m² the energy required (at least) is 730,000 kg*m/sec. This would give a maximal efficiency of

$$3{,}600/730{,}000 = 0.0049.$$

The low value of the efficiency should not be used as a measure for the merits or demerits of the system, since its merit is in the simplicity of operation.

4. Speed of Condensation

For complete condensation not only a sufficient difference must be maintained between the pressure in the mixing chamber and the saturation pressure at the temperature after the condensation, but there is involved also a question of time.

It is desirable that the condensation should require not too much time, since otherwise a mixing chamber of considerable dimensions will be needed in view of the velocity of the water which rises from $u'=10$ m/sec to $u_m=54.5$ m/sec. In order to have a definite case it was thought that each element of volume of the water should stay not longer than 0.1 sec in the mixing chamber. The problem is whether complete condensation will be possible under this condition. Because we have condensation of steam in the presence of water, the question of obtaining a sufficient number of condensation nuclei does not present itself, but the important matter is to have a sufficient surface area of the water in order to make rapid condensation possible.

The speed of condensation depends on two factors: (a) Whether the difference between the pressure in the steam and the saturation pressure at the water surface will accelerate the steam sufficiently rapidly in order that it can reach the water surface within the time limit set above; and (b) whether the heat liberated by the condensation can flow off towards the interior of the water sufficiently rapidly. The latter problem depends on heat conduction and a simple estimate gave the impression that this was the really important question.

In treating the problem of heat conduction into the interior a mathematical difficulty presents itself in consequence of the circumstance that the condensation adds water to the already existing surface, so that the surface where condensation occurs displaces itself with time. For the case of a plane surface a treatment will be given (a) based on the ordinary solution of the one-dimensional heat equation, in which this displacement is neglected; and (b) on a solution in which the displacement is taken into account according to a method indicated by I. I. Kolodner [2].

The equation for the heat conduction in one dimension is,

$$\frac{\partial T}{\partial t}=\kappa\frac{\partial^2 T}{\partial y^2}, \tag{11}$$

where y is the distance measured from the surface of the water inwards. Here $\kappa=\lambda/\rho C$, where λ is the thermal conductivity of the water; ρ is the density and C is the specific heat. For λ we can take (approximately) 1.4×10^{-3} cal sec^{-1} cm^{-1} °C^{-1}; in c-g-s units $\rho=1$ and $C=1$, so that κ has the value 1.4×10^{-3} cm^2 sec^{-1}.

When the initial temperature of the water is T'(=20° C) and the surface on which the steam condenses acquires a temperature T_s (=93° C, the saturation temperature for the pressure of 0.8 atm), the appropriate solution of the equation is,

$$T=T'+a\left(1-\operatorname{erf}\frac{y}{2\sqrt{\kappa t}}\right). \tag{12}$$

When we *neglect the displacement of the surface*, we must have $T=T_s$ for $y=0$, which gives,

$$a=T_s-T'=73°\text{C}. \tag{13}$$

The heat flow to the interior then becomes (per cm^2 and per sec)

$$q=-\lambda\left(\frac{\partial T}{\partial y}\right)_0=\rho C(T_s-T')\sqrt{\frac{\kappa}{\pi t}}. \tag{14}$$

The heat flowing to the interior in the time t is,

$$q_t=\frac{2}{\sqrt{\pi}}\rho C\,(T_s-T')\sqrt{\kappa t}\cong3.08\sqrt{t}\text{ cal/cm}^2. \tag{15}$$

Taking $t=0.1$ sec we find,

$$q_t=0.975\text{ cal/cm}^2. \tag{15a}$$

The amount of heat to be taken up by the water is found as follows: There enters into the mixing chamber per second, $A(1-s)\ \rho''u''$ kg steam.[4]

This steam is condensed into water with a temperature of at most 53° C (for $s=0.5$). We take as mean temperature of the water: $(20°+53°)/2=36°.5$. The steam has the enthalpy $H''=639.4$ kcal/kg. The heat to be taken up by the water entering into the mixing chamber is given by the loss in enthalpy plus kinetic energy of the steam on condensation. Since the enthalpy plus kinetic energy of a given mass of steam remains the same as its value in the boiler, say 759.4 kcal/kg, and since the kinetic energy of the water is 0.1 kcal/kg, the rate at which heat is taken up by the water is

$$A(1-s)\rho''u''\ (759.4-36.5-0.1)$$
$$=A\times0.5\times0.462\times1{,}003\times722.8$$
$$\cong1.675\times10^8\ A\text{ kcal/sec}=1.675\times10^8\ A\text{ cal/sec}.$$

If we divide this by q we find that per second a surface of

$$1.675\times10^8\times A/0.975\times1.72\times10^8\ A\text{ cm}^2$$

must be available.

There enters the mass of water,

$$A\ s\ \rho'\ u'\text{ kg/sec}=5{,}000\ A\text{ kg/sec}=5\times10^6\ A\ g/\text{sec},$$

which has the volume 5×10^6

A cm^3/sec ($\rho'=1{,}000$ kg/m^3 and $u'=10$ m/sec).

It thus follows that per cm^3 of water we must have a surface area of

$$1.72\times10^8/5\times10^6=34.4\text{ cm}^2/\text{cm}^3.$$

When the water is dispersed into drops of radius R, the ratio of area to volume is $3/R$. Hence we require drops of a radius not larger than 0.104 cm, that is, drops of a diameter of about 2 mm.

[4] In this formulas A is expressed as m^3. However, this does not effect the results since A finally drops out.

When *the displacement of the surface must be taken into account*, we assume (following Kolodner [2]) that the surface at time t finds itself at a position,

$$X=2b\sqrt{\kappa t}. \tag{16}$$

We now must have $T=T_s$ for $y=-X=-2b\sqrt{\kappa t}$. Instead of (13) this gives,

$$T_s-T'=a(1+\text{erf } b). \tag{17}$$

A second condition relating a and b is found by considering the balance between the heat liberated by the condensation and the heat flowing to the interior; it can be written,

$$q=-\lambda\left(\frac{\partial T}{\partial y}\right)_{y=-X}=\rho L\frac{dX}{dt}=\rho LC\sqrt{\frac{\kappa}{t}}, \tag{18}$$

where $L=H''-36.5=603$ kcal/kg$=603$ cal/g.

With (12) and (16) we obtain

$$\frac{\lambda a}{\sqrt{\pi\kappa t}}\exp(-b^2)=\rho Lb\sqrt{\frac{\kappa}{t}}$$

The time factor drops out, and with $\lambda=\rho C\kappa$ we find,

$$a=\sqrt{\pi}be^{b^2}\frac{L}{C}. \tag{19}$$

Substituting this into (17) we arrive at

$$be^{b^2}(1+\text{erf } b)=\frac{C(T_s-T')}{L\sqrt{\pi}}. \tag{20}$$

Now with the data used above

$$C(T_s-T')/L\sqrt{\pi}=0.068;$$

thus

$$b=0.064, \text{ and } a=68.8^\circ \text{ C}.$$

From (18) we now obtain

$$q_t=2\rho LC\sqrt{\kappa t}\cong 2.90\sqrt{t} \text{ cal/cm}^2.$$

Again taking $t=0.1$ we find

$$q_t=0.916 \text{ cal/cm}^2,$$

instead of 0.975 cal/cm^2 as given by (15a).

It appears from these calculations that the effect of the condensation of water upon the surface makes the heat flow to the interior somewhat smaller, although the difference remains below 10 percent.

Since it is necessary to disperse the water into fine drops in order to guarantee a sufficient condensation area, the calculations must be repeated for a spherical surface. This has been done only for the case where the displacement of the surface is neglected, in view of the mathematical difficulties involved in a more complete calculation. In this case it appears that with spherical drops the heat flow to the interior is smaller than with a plane surface. Probably the effect of the condensation upon the surface will again give a further reduction by at most 10 percent.

Although the calculations cannot easily be made precise, they make it possible to obtain an estimate for the total surface area needed for the water entering into the mixing chamber per second, in order to allow the condensation of all the steam entering in the same period, when it is assumed that each water droplet will stay in the mixing chamber not over 0.1 sec. Fine dispersion of the water is necessary, in such a way that the drop size should be of about 2 mm in diameter. When this cannot be obtained, much more time must be allowed for the condensation.

5. Equations of Motion for the Water Droplets

Provisional equations have been developed for the motion of the water droplets in the mixing chamber, in order to find their speed as a function of the distance traversed. This is needed for the determination of the cross-sectional area which the mixing chamber must have at various distances from its entrance.

For this purpose it is assumed that the water has already been dispersed into fine drops and it is supposed that condensation takes place on these drops, so that no new drops are formed.

The speed of the water drops will be denoted by u'; this speed increases with time, and we can also consider u' to be a function of the coordinate x measured along the axis of the mixing chamber. We then can write for the drops, $dx=u'\,dt$, and express their acceleration as, $du'/dt=u'\,(du'/dx)$.

The speed of the steam will be denoted by u''. Also this speed can be a function of x.

We assume that the mixture of steam and water retains a constant pressure, and that the steam retains a constant temperature T''. The density of the steam, ρ'', will then be constant. The temperature of the water droplets, on the other hand, increases in consequence of the condensation of steam upon them. The density of the water drops ρ' will be considered as constant.

We shall write A_x for the sectional area of the mixing chamber at the position x. Let the number of water drops per unit volume at x be n; the number of drops crossing a section of the chamber per second is then given by,

$$N=A_x n u'. \tag{21}$$

As mentioned it is supposed that no new drops are formed; when the state of motion is stationary the quantity N must be a constant (independent of t and x).

The volume of a drop will be written, $w=4\pi R^3/3$.

The mass of steam condensing on a single drop in unit time will be denoted by M, which may be a function of x. We then have,

$$\rho' dw/dt=M. \tag{22}$$

The speed of the drops increases in consequence of the momentum gained from the condensing steam. This momentum is given by $M\,u''$ per second. It is possible that there is also a frictional force f acting on the drops in surplus of the direct gain of momentum (it may be, however, that a closer analysis of the phenomenon of condensation will lead to the result that $f=0$, since the steam in the neighborhood of the drop will flow towards the drop, so that there will be no appreciable shearing effect at the surface of the drop).

Keeping both the direct transfer of momentum $M\,u''$ and the frictional force f in the equations, we obtain for a single drop,

$$\rho'\,d(wu')/dt=M\,u''+f, \tag{23}$$

from which, with the aid of (22),

$$\rho'\,w\,du'/dt=M\,(u''-u')+f. \tag{24}$$

To form the conservation equations for the mixture of steam and drops we observe that the part of any section A_x taken in by water is given by $A_x nw$, while the part taken in by steam is $A_x(1-nw)$. Complete condensation will have occurred when nw has become equal to unity.

The equation of continuity takes the form,

$$A_x nw\rho'u'+A_x(1-nw)\rho''u''=\text{constant}=K_1. \tag{25}$$

The equation of momentum becomes (since the pressure is constant),

$$A_x nw\rho'u'^2+A_x(1-nw)\rho''u''^2=\text{constant}=K_2. \tag{26}$$

The equation of enthalpy transport can be added to these equations; it can be used to find the temperature of the drops. We shall omit it here.

From eqs (25) and (16) we deduce,

$$A_x nw\rho'u'(u''-u')=K_1u''-K_2. \tag{27}$$

With the aid of (21) this can be written,

$$N\rho'w(u''-u')=K_1u''-K_2.$$

Differentiation with respect to the time gives,

$$N\rho'(u''-u')(dw/dt)+N\rho'w(du''/dt)-N\rho'w(du'/dt)=K_1(du''/dt),$$

from which,

$$(K_1-N\rho'w)(du''/dt)=-Nf. \tag{28}$$

It follows that the speed of the steam u'' changes only if there is an extra frictional force f.

Equations (25), (26), and (21) can be used to express A_x and n as functions of the other variables,

$$A_x=\frac{(\rho'u'-\rho''u'')K_2-(\rho'u'^2-\rho''u''^2)K_1}{\rho'\rho''u'u''(u''-u')}, \tag{29}$$

$$n=\frac{N\rho'\rho''u''(u''-u')}{(\rho'u'-\rho''u'')K_2-(\rho'u'^2-\rho''u''^2)K_1}$$

$$=\frac{(K_1u''-K_2)\rho''u''}{w[(\rho'u'-\rho''u'')K_2-(\rho'u'^2-\rho''u''^2)K_1]} \tag{30}$$

The central problem is situated in the following three equations,

$$dw/dt=M/\rho'$$

$$du'/dt=[M(u''-u')+f]/\rho'w$$

$$du''/dt=-f/(K_1/N-\rho'w).$$

If we attempt to neglect f, the last equation gives $u''=$constant. We then obtain from the other two equations,

$$dw/du'=w/(u''-u'),$$

the integral of which is,

$$w(u''-u')=\text{constant}.$$

If we know the volume of the individual water drops at the entrance of the mixing chamber ($x=0$), and if we make a scale for u' (we know that u' increases from the value 10 m/sec to the value 54.5 m/sec with $s=0.5$) we can find the course of w as a function of u'.

Equation (30) then gives the corresponding value of n. When $nw=1$, the process is completed. Finally eq (29) would give the cross-sectional area A_x as a function of u'.

What remains is to find the relation between u' and x. This is determined by the equation

$$du'/dx=(du'/dt)/u'=M(u''-u')/\rho'u'w,$$

where du'/dt is obtained from (23) with $f=0$. In order to integrate this equation it is necessary to know M, and this must follow the analysis of the condensation process.

6. References

[1] P. Chiarulli and R. F. Dressler, Condensation interfaces in two-phase flows, J. Appl. Phys. **28,** 990 (1957).

[2] I. I. Kolodner, Free boundary problem for the heat equation with application to problems of change of phase, Comm. Pure Appl. Math. **IX,** 1 (1956).

Washington, September 11, 1957.

Journal of Research of the National Bureau of Standards Vol. 60, No. 2, February 1958 Research Paper 2831

Mass Spectra and Relative Sensitivities of Some Polyphenyls

Paul Bradt and Fred L. Mohler

Mass spectra have been measured by evaporating polyphenyls from a tube furnace into the ionization chamber of a 60° mass spectrometer operated at constant ion accelerating voltage. Mass spectra of pure tetraphenyl, hexaphenyl, and octaphenyl are reported. A synthetic mixture of terphenyl, tetraphenyl, pentaphenyl, hexaphenyl, and octaphenyl in known proportions was evaporated as the temperature was increased step by step from 125° to 290° C and time integrals of the five molecule ion currents were recorded over the time required to completely evaporate the sample. The relative sensitivity increases rapidly with increasing molecular weight.

1. Introduction

The Mass Spectrometry Section has published several papers on detection and analysis of heavy molecules evaporated from a vacuum-tube furnace directly into the ionization chamber of a mass spectrometer [1, 2, 3, 4].[1] Mixtures of heavy molecules have been studied by recording the spectra as the temperature is increased step by step. This affords the advantage that the mixture is fractionated in the process of evaporation and the complexity of the mass spectra is reduced. However, the results are qualitative as the abundance of the ions from a given compound will depend both on the amount of the compound in the sample and on the temperature of evaporation. A quantitative measure of the relative abundance of the compounds requires a time integral of the ion current over the time required to completely evaporate the compound from the sample.

At the Bureau there has been interest in the analysis of mixtures of polyphenyls formed when biphenyl is irradiated by neutrons and gamma rays in a high flux reactor. As a basis for analysis of these mixtures, R. L. Alexander of the Engine Fuel Section has supplied us with *m*-terphenyl, *m*-tetraphenyl, *m*-pentaphenyl, *m*-hexaphenyl, and *m*-octaphenyl. He also supplied us with a mixture containing the five polyphenyls in known proportions.

2. Experimental Procedure

Mass spectra were measured with a 60° mass spectrometer of 6-in. radius of curvature and the spectrum was scanned by varying the magnetic field with a constant electric field of 1,100 v. The repeller electrode of the ionization chamber was a fine wire gauze that allowed free entry of the vapor from a tube furnace. The synthetic sample was in a copper tube which extended to within about 5 mm of the gauze and this was in a 6-mm Pyrex tube which fitted into the entrance port of the ionization chamber. A thermocouple attached to the copper tube recorded the temperature of the sample.

The ionization chamber block attained a temperature of about 190° C from heat from the cathode and the sample tube reached a temperature of 131° without external heating. Heating the sample tube in turn raised the temperature of the ionization chamber by an amount that was not measured but results indicated that there was no condensation of material in the ionization chamber with the sample at 290° C. In other experiments the sample holder was further from the ionization chamber and the initial temperature was less than 131° C.

3. Results

Table 1 lists some of the larger peaks in the mass spectra of *m*-tetraphenyl, *m*-hexaphenyl, and *m*-octaphenyl. A striking feature of the spectra is that

TABLE 1. *Mass spectra of tetraphenyl, hexaphenyl, and octaphenyl*

m/e	Tetraphenyl	Hexaphenyl	Octaphenyl
	°C	°C	°C
	126	168	265
77	1.0	1.0	.....
91	0.3	0.7	0.2
128	1.2	.64	.19
152	.....	2.5	.11
306++	*14.8*	1.3	.....
165	1.1	1.4	.4
178	0.8	0.6	.4
189	1.4	.9	.3
202	3.0	.....	.....
215	1.15	1.6	.2
226	5.3	.....	.....
228	5.4	.....	.7
458++	.....	20.7	.....
239	0.9	1.1	.2
252	1.2	1.3	.4
265	0.9	1.3	.5
276	3.0	2.2	.5
289	6.3	4.4	1.1
302	4.6	.....	.....
610++	.....	.....	*23*
306	*100*	3.5	.....
320	.....	1.1	0.22
350	.....	0.9	.3
365	.....	2.3	.4
380	.....	1.2	.5
441	.....	2.3	.4
458	.....	*100*	.4
517	.....	.....	.3
532	.....	.....	.2
579	.....	.....	.3
593	.....	.....	.7
610	.....	.....	*100*

[1] Figures in brackets indicate the literature references at the end of this paper.

all fragment ion peaks are small and get progressively smaller as the molecular weight increases. Fragmentation involving breaking bonds between phenyl rings is negligible and most of the fragment ions involve breaking one of the rings. Spectra of terphenyl and pentaphenyl have been recorded with a 180° mass spectrometer with a heated reservoir and inlet manifold [5]. All the spectra show that the molecule ion peaks can be used without any correction for interference to analyze a mixture of polyphenyls.

The synthetic mixture contained 23.4-mole percent terphenyl, 21.6-percent tetraphenyl, 17.6-percent pentaphenyl, 22.7-percent hexaphenyl, and 14.7-percent octaphenyl. A drop of molten material estimated to be about half a cubic millimeter was placed in the sample holder. This sample was completely evaporated into the ionization chamber over a period of 27 hr and the time integrals of the molecule ion currents were recorded. Only the molecule ion peaks were recorded and only two molecules contributed measurably to the spectrum at any one time. Readings on two peaks could be repeated within about 5 min. The temperature of the sample was increased by small steps to maintain an easily measured rate of change.

Figure 1 is a plot of the ion currents for the five molecule ions (designated ϕ_3, ϕ_4, ϕ_5, ϕ_6, and ϕ_8) as a function of time. Upward inflections of the curves mark the times when the temperature was increased. The mass spectrometer filament was turned on at 2:20 P. M. and at 3 P. M. the terpehnyl and tetraphenyl ion currents began to rapidly rise to sharp maxima. Heating of the tube furnace began at 7:30 P. M. and over a period of 6 hr the spectrum showed predominantly pentaphenyl with temperatures ranging from 162° to 174° C. The hexaphenyl evaporated from 187° to 214° C and the octaphenyl was predominant from 250° to 287° C. There was no visible residue left in the sample holder.

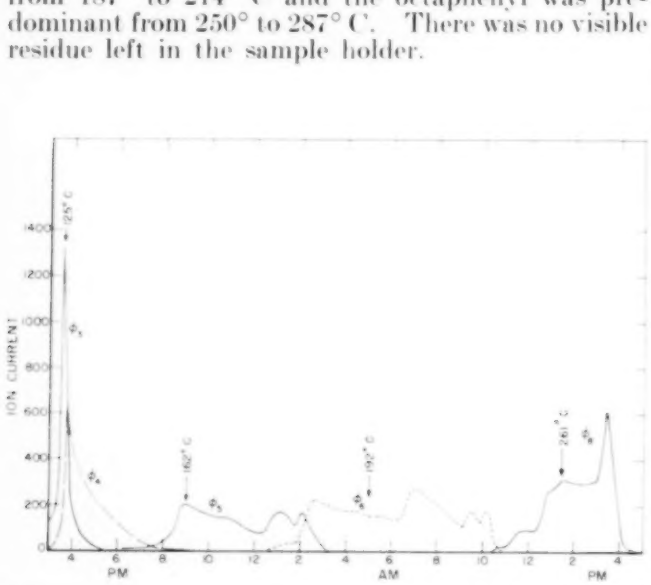

FIGURE 1. *Ion currents from a mixture of five polyphenyl molecules as a function of time.*

ϕ_3, ϕ_4 etc., designate the molecule ions. The temperature of evaporation at various times is also indicated.

The rate of evaporation of the terphenyl was so rapid that there is some doubt as to the accuracy of the time integral. For the other compounds the rate of evaporation stayed within a measurable range. Table 2 gives the results. Column 3 gives the time integrals in units of current in arbitrary scale divisions and time in minutes. Column 4 gives the composition of the synthetic mixture in mole percent and column 5 is proportional to the time integrals of column 3 divided by the mole percent abundance of the compound of column 4.

TABLE 2. *Relative sensitivity of polyphenyl molecule ions*

Molecule	m/e	Integral of ion current	Mole percent	Relative sensitivity	Isotope correct	Monoisotopic sensitivity
Terphenyl	230	3.08×10^{4}	23.4	1.0	1.22	1.0
Tetraphenyl	306	4.91	21.6	1.74	1.31	1.87
Pentaphenyl	382	5.97	17.6	2.58	1.41	2.98
Hexaphenyl	458	9.83	22.7	3.27	1.50	4.02
Octaphenyl	610	7.95	14.7	4.09	1.72	5.76

The results show that the sensitivity increases rapidly with increasing molecular weight. The experiment was not designed to give sensitivity in absolute units. The long series of observations was made by one observer and the experiment was not repeated because of the exceptional physical effort involved. Figure 1 indicates that the time schedule of increasing the temperature could be improved.

4. Discussion

There are extensive data in the API Catalog of mass spectral data on heavy hydrocarbons obtained with 180° Consolidated mass spectrometers using a heated reservoir and inlet system held at a temperature sufficient to vaporize the sample completely. Data commonly include sensitivity of the maximum peak of the compound relative to the molecule ion of *n*-hexadecane. These data are not comparable with data obtained in this work and indeed it is difficult to intercompare the published spectra when there are large differences in the molecular weights of the base peaks. This is because the Consolidated mass spectrometer records the spectrum at a constant magnetic field and a variable ion accelerating voltage, and there is a decrease in sensitivity with increasing molecular weight. In this research the ion accelerating voltage was held at a constant value.

The polyphenyls afford an excellent opportunity to study the variation in sensitivity with molecular weight, as the molecule ions are by far the largest peaks and other characteristics of the spectra are similar in all the molecules. Unfortunately some limitations in the experimental data limit the theoretical significance of the results. On theoretical grounds, with chemically similar molecules of this type, one would expect the total ionization at constant pressure to be nearly proportional to the molecular weight [6,7].

The total ion current cannot be accurately evaluated. The sum of all the measured peaks in tetraphenyl was 1.67 times the molecule ion peak, in hexaphenyl the ratio was 1.76 and in octaphenyl 1.38. These are lower limits as many little peaks were omitted and the sum of these is not negligible. In spectra obtained with a Consolidated mass spectrometer and heated inlet system the sum of the measured peaks in terphenyl, tetraphenyl, and hexaphenyl was about 2 relative to the molecule ion peak. In pentaphenyl the sum was 1.6 but the data are incomplete. Part of the difference between measurements with the two instruments comes from mass discrimination in the Consolidated mass spectrometer. It is concluded that the ratio of the molecule ion current to the total ion current remains roughly the same with the possible exception of octaphenyl.

There is a large isotope correction in these heavy molecules for molecules containing C^{13} and D. For terphenyl the abundance of $C^{12}_{18}H^{1}_{14}$ is 0.816 times the monoisotopic abundance of $C_{18}H_{14}$ and for octaphenyl, $C_{48}H_{34}$, the factor is 0.582. The reciprocal of this fraction is the correction factor to be applied to the $C^{12}_{n}H^{1}_{m}$ peak to give the monoisotopic abundance. The 6th and 7th columns of table 2 give the correction factor and the monoisotopic relative sensitivity.

The resolving power of the mass spectrometer is about 1/300 and is insufficient to resolve unit mass for the hexaphenyl and octaphenyl ions. For octaphenyl the peaks at 610 and 611 will be completely unresolved and there can be a large error in evaluating the abundance of 610. For hexaphenyl the error is much less.

It is noted above that theory indicates that the effective collision area for ionization of polyphenyls will be proportional to the molecular weight. The relative sensitivity increases much more rapidly than this. Thus the ratio of the monoisotopic sensitivity of octaphenyl to that of terphenyl is 5.76 while the molecular weight ratio is 2.66. The experimental ratio is considered to be more reliable for tetraphenyl and octaphenyl. Here the sensitivity ratio is 3.1 and the molecular weight ratio is 2. The experimental uncertainties cannot account for this large increase in sensitivity with molecular weight.

These preliminary results are published because the experimental work has been interrupted and there is no immediate prospect of getting more accurate data. Results are of some interest as they afford the only experimental data on the sensitivity of mass spectrometers of this type for heavy molecules. The change in sensitivity with molecular weight is in marked contrast to data obtained with instruments operating at constant magnetic field. The API Catalog of mass spectral data gives sensitivities for some fused ring aromatics [8] and in these spectra also the molecule ion is the only large peak. For isomers of $C_{16}H_{10}$ (mass 202) the sensitivity is 56 times that for the molecule ion of hexadecane; for $C_{18}H_{12}$ isomers (mass 228) sensitivity ratios range from 23 to 12; for $C_{20}H_{12}$ (mass 252) the ratio is 26, and for $C_{22}H_{14}$ the ratio is 19. The sensitivity per micron shows the same unsystematic variation.

5. References

[1] Paul Bradt, V. H. Dibeler, and F. L. Mohler, J. Research NBS **50,** 201 (1953) RP2410.

[2] Paul Bradt and F. L. Mohler, Anal. Chem. **27,** 875 (1955).

[3] Paul Bradt and F. L. Mohler, J. Research NBS **55,** 323 (1955) RP2637.

[4] Paul Bradt, F. L. Mohler, and V. H. Dibeler, J. Research NBS **57,** 223 (1956) RP2713.

[5] Preston P. Morris, Jr. (unpublished research).

[6] J. W. Otvos and D. P. Stevenson, J. Am. Chem. Soc. **78,** 546 (1956).

[7] F. W. Lampe, J. L. Franklin, and F. H. Field, J. Am. Chem. Soc. **79,** 6129 (1957).

[8] API Catalog of Mass Spectral Data; Serial Numbers 958, 959, 1017, 1018, 1019, 1020, 1022, and 1237.

Washington, July 31, 1957.

Journal of Research of the National Bureau of Standards Vol. 60, No. 2, February 1958 Research Paper 2832

Infrared Spectra of Thermally Degraded Poly(Vinyl Chloride) *

Robert R. Stromberg, Sidney Straus, and Bernard G. Achhammer

The changes in chemical structure occuring in poly(vinyl chloride) as a result of heating in a vacuum in the range 100° to 400° C were studied using infrared spectrophotometry. The principal changes occurring in the residue during pyrolysis in a vacuum were the formation of unsaturated structures and a change from an aliphatic spectrum to one showing aromatic absorption. The data are used to support a previously proposed mechanism of decomposition for poly(vinyl chloride).

1. Introduction

The kinetics of the thermal decomposition of poly(vinyl chloride) in a vacuum have been previously reported [1].[1] Under pyrolytic conditions, poly(vinyl chloride) decomposes predominantely into hydrogen chloride and a colored solid residue. The color of the residue has been attributed to a polyene structure existing after the dehydrochlorination [2]. The role of oxygen in the decomposition mechanism has not yet been resolved although hydroperoxide mechanisms have been proposed [3].

Recently group theory has been applied to the interpretation of the infrared spectra of poly(vinyl chloride) and the spectrum has been analyzed in a comprehensive manner [4]. The head-to-tail arrangement of the monomer units [5], and the alternate arrangements of the chlorine atoms in the plane of the carbon chain [6], with the conclusion that the crystallographic repeating unit consists of two monomer units, were further verified by the work of Krimm and Liang [4]. Polarized spectra were used by Krimm and Liang to make band assignments. Other, more limited analyses of the infrared spectra of poly(vinyl chloride) have also been reported [7, 8]. The branching of poly(vinyl chloride) has been measured [9] by determining the methyl group concentration of the reduced polymer. The application of infrared spectrophotometry to the explanation of the degradation process occurring in poly(vinyl chloride) has, however, not been extensively reported in the literature. Campbell and Rauscher [3] utilized changes in the infrared spectra of poly(vinyl chloride) in a study of the base-accelerated degradation of this polymer. Others [10, 11] limited their studies to changes in only one portion of the spectrum.

This paper describes the results of an investigation in which infrared spectrophotometry was used to study changes in chemical structure occurring in the solid residue during pyrolysis of poly(vinyl chloride) in vacuum.

2. Experimental Procedure

Three poly(vinyl chloride) polymers were studied. They were prepared from vinyl chloride monomer as follows:

Polymer	Preparation
PVC—γ	Initiator—γ radiation from 0.3 Curie Co–60 source
PVC—bp	Initiator—0.1 mole percent of benzoyl peroxide; 40° C
PVC—azo	Initiator—0.02 mole percent of 2,2′ azobis (isobutyronitrile); 40° C

All the polymer samples were powdered by grinding under liquid nitrogen. The white powders were sieved through a 325 mesh screen to a particle size less than 44 microns in diameter.

Specimens of these polymers were pyrolyzed in a vacuum for 30 min at temperatures up to 400° C after outgassing at 110° C for approximately 1 hour. At temperatures above 180° C volatile products were evolved. The color of the residue changed to light brown at the lower pyrolysis temperatures and to dark brown at the more elevated temperatures.

After the exposure to pyrolytic conditions was completed, the degraded powder samples were removed and prepared for infrared analysis. Untreated poly(vinyl chloride) is soluble in only a few solvents, which include cyclohexanone, tetrahydrofuran, dimethyl formamide and to a limited extent, ketones. Some of the degraded material had an even more limited solubility. Cyclohexanone and tetrahydrofuran tend to form hydroperoxides, which decompose easily and may initiate decomposition of the polymer. If these solvents are retained in the polymer film, they also can lead to erroneous conclusions about the structure of the polymer. This is especially true when hydroperoxide breaks down to give carbonyl and hydroxyl groups. Therefore, the solid phase pellet method was used to prepare the material for infrared analysis. Potassium bromide (Harshaw Chemical Co.) was used for the suspending medium

*Presented at the 8th Annual Pittsburgh Conference of Analytical Chemistry and Applied Spectroscopy, March 1957.

[1] Figures in brackets indicate the literature references at the end of this paper.

because it has a refractive index, n_D of 1.56 which approximates that of untreated poly(vinyl chloride) (1.55). The polymer and the potassium bromide in the ratio of 1 to 50 were mixed in a dry box and the pellets were prepared in the manner described previously [12]. Although the ratio by weight of polymer to potassium bromide was the same for all samples, there was an increase in the molar ratio of degraded polymer to potassium bromide as a result of the loss of hydrogen chloride.

A Perkin-Elmer Model 21 double-beam infrared spectrophotometer with a sodium chloride prism was used for measurements in the 5000 to 670 cm^{-1} region. For increased resolution a Perkin-Elmer Model 12–B instrument with a lithium fluoride prism was used for measurements in the 3000 to 2600cm^{-1} region.

3. Infrared Spectra and Discussion

3.1. Untreated Polymers

The infrared spectra of the three poly(vinyl chloride) polymers studied are shown in figure 1. These patterns were obtained by placing a potassium bromide pellet containing the untreated poly(vinyl chloride) in the sample beam and a blank potassium bromide pellet in the reference beam. A commercial polymer, Geon 101 [2], was studied with a lithium fluoride prism in the region of 3000 to 2820 cm^{-1}. This spectrum is given in figure 2.

The assignments of the principle absorption bands of the basic polymer are given in table 1. Krimm and Liang [4] reported absorptions in the region of 3000 cm^{-1} that varied slightly from those given in table 1 and figure 2. It is possible that this small difference is a result of the nature and perhaps scatter of the pellet specimen. Krimm and Liang

[2] B. F. Goodrich Chemical Co.

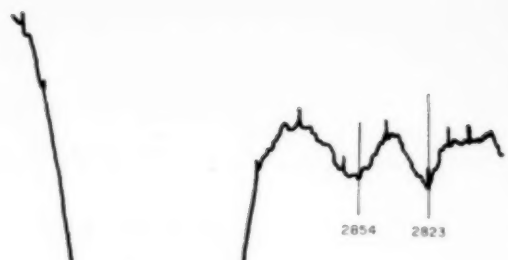

FIGURE 2. *Portion of infrared spectrum of Geon-101 PVC using lithium fluoride prism.*

TABLE 1. *Assignments of absorption bands for untreated poly(vinyl chloride)*

Frequency	Assignment	References
cm^{-1}		
680	C—Cl stretch	3,4
833	chain stretch	4
963	chain stretch	4
1095	perpendicular chain stretch	4
1120	parallel chain stretch	4
1200	CH wag, out of phase	4
1250	CH bend, in phase	4
1330	CH bend, out of phase	4
1352	CH_2 wag, in phase	4
1427	CH_2 bend, in phase	3,4
2823	CH stretch, in phase	4
2854	CH_2 stretch, symmetrical, in phase	4,13
2919	CH_2 stretch, asymmetrical, in phase	4,13
2977	CH stretch, out of phase, on neighboring CHCl groups	4

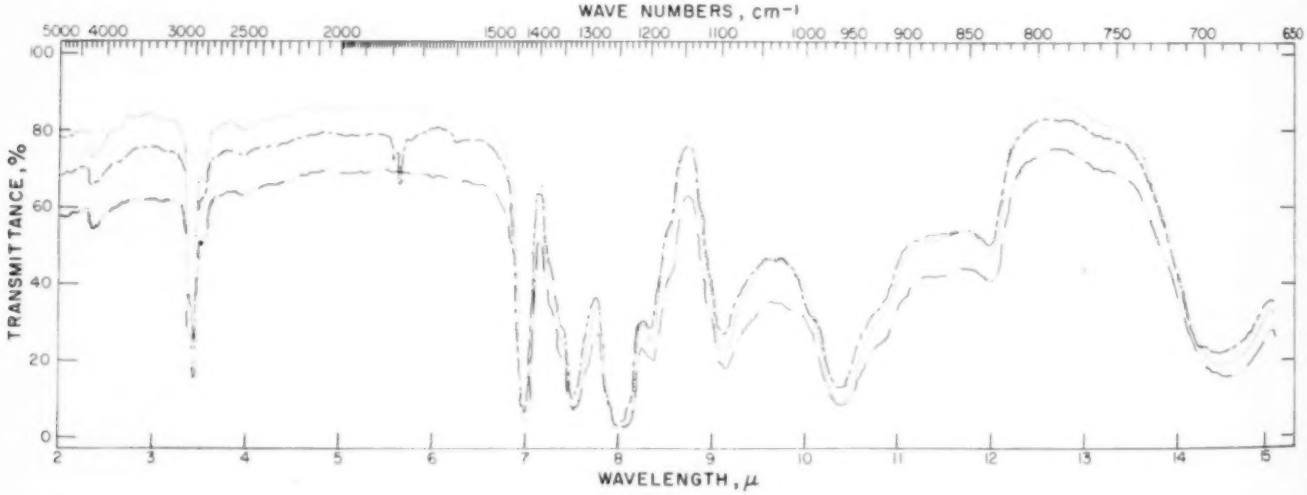

FIGURE 1. *Infrared spectra of the poly(vinyl chloride) polymers studied.*
PVC–γ
PVC–bp
PVC–azo

obtained their spectra from a film and the spectrum shown in figure 2 was obtained from a pellet.

A weak absorption band at 1590 cm^{-1} is observed in the spectrum of the PVC–γ sample. This is assigned to a carbon—carbon double bond stretching vibration [13]. The double bond structure is formed as a result of some dehydrochlorination [1] of the polymer while exposed to the γ-radiation.

The curve obtained from the PVC-bp sample exhibits several absorption bands not observed in the other polymers. The bands at 1795 cm^{-1} and 1773 cm^{-1} are assigned to the carbonyl vibration of the catalyst, benzoyl peroxide [13]. The band at 1733 cm^{-1} is probably from the carbonyl stretching vibration of an aldehyde or ketone [13], formed from interaction of the catalyst with vinyl chloride. Benzoyl peroxide shows an absorption [13] near 1000 cm^{-1} and the band at 990 cm^{-1} is probably from unreacted catalyst.

3.2. Spectra of Poly(Vinyl Chloride) After Pyrolysis

Figure 3 shows the spectra of PVC-bp residue after pyrolysis for 30 min in a vacuum at several temperatures. The spectra are progressively altered as a result of increasing the pyrolysis temperature. There is considerable radiation scatter for the pellets of the samples pyrolyzed at higher temperatures where the refractive index of the more highly degraded colored specimens did not match that of the potassium bromide. The samples were pretreated by heating at 110° C in a vacuum for approximately 1 hour. The only changes observed in the spectrum of the material after this treatment was the disappearance of the peroxide bands at 1795 and 1773 cm^{-1}, indicating removal of the unreacted catalyst by this pretreatment. At temperatures up through 250° C, the infrared pattern, although somewhat altered, is easily identified as that of poly(vinyl chloride). At temperatures of the order of 300° C and higher, there is a marked over-all departure from the spectrum of poly(vinyl chloride). It was shown in a previous study [1] that at approximately 300° C practically all of the chloride atoms have been removed from the polymer as HCl without any apparent appreciable breakdown of the polymer chain. This removal of the highly electronegative halogen from the chain could cause frequency shifts in some absorption bands as well as other spectral changes resulting from the new structural configurations. Substantial breakdown of the polymer chain occurs at 400° C [1].

In the region of the carbon—hydrogen stretching absorption, 3000 cm^{-1}, a new band is formed at 3030 cm^{-1} that may be associated with the carbon—hydrogen stretching vibration from an unsaturated carbon—carbon linkage [13]. The intensity of this band increases with increasing temperatures of pyrolysis. Nonconjugated carbon—carbon double bonds are suggested by the absorption at 1670 cm^{-1} [13]. The absorption band at 1610 cm^{-1} is assigned to the carbon—carbon double bond stretching vibration for conjugated bonds, either aromatic or aliphatic or both [13].

The shoulder at 1590 cm^{-1} is assigned to the carbon—carbon double bond vibration of an aromatic ring [13]. A resonance splitting of the absorption bands with the appearance of one band near 1600 cm^{-1} and one near 1500 cm^{-1} occurs when there are three unsaturated carbon—carbon vibrations in a ring [13]. The bands at 1610 and 1500 cm^{-1} are therefore assigned, at least in part, to an aromatic structure. The broad absorption bands at 880, 820, 750, and 700 cm^{-1} are present in the spectra of asphalts, heavy petroleum oil fractions, coal, etc., [14] and indicate the presence of aromatic structures, with the latter two indicating carbon—hydrogen out-of-plane deformations of monosubstituted aromatic groups [13]. The absence of aromatic structural bands in the untreated poly(vinyl chloride) and

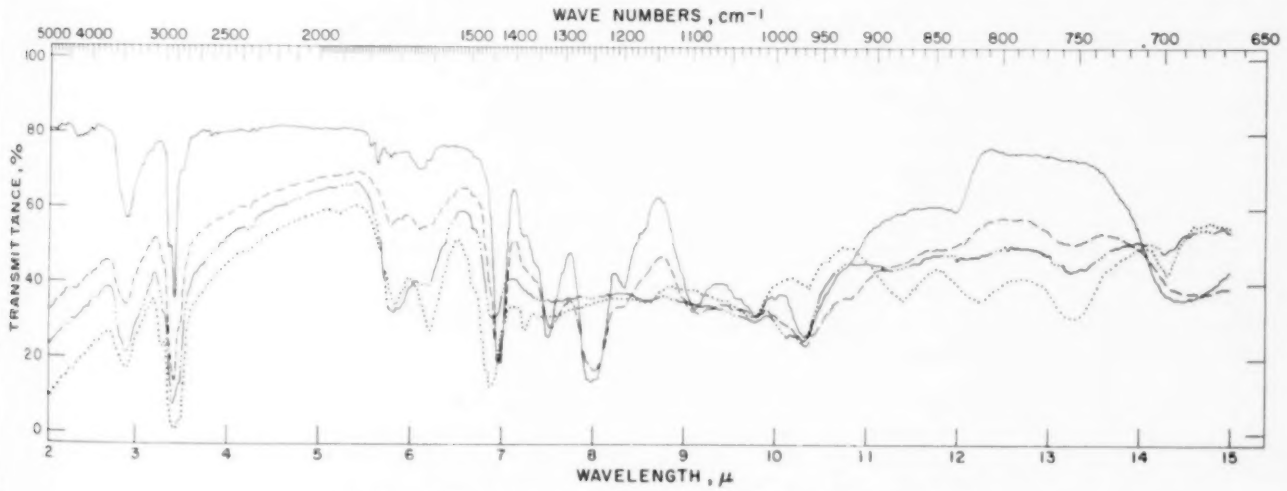

FIGURE 3. *Infrared spectra of PVC–bp after 30 minutes' pyrolysis.*
—— Untreated
— — — 255° C
— · · · — · · · — 300° C
· · · · · · · · · · 400° C

their appearance and increase in intensity as a result of higher degradative temperatures can be readily observed.

The absorption at 1720 cm^{-1} indicates the presence of carbonyl vibrations. This band did not appear to any appreciable extent when the pyrolyzed material was stored under an inert atmosphere. As this spectral change does not occur at room temperature in untreated polymer, it appears that the double bonds in the degraded polymer are subject to attack by atmospheric oxygen, forming such oxygenated structures.

The shifting of the carbon—hydrogen vibration of CH_2 [3] from 1430 cm^{-1} in the spectrum of untreated polymer to 1455 cm^{-1} for the more highly decomposed samples may be a result of a loss of the chlorine atoms or an increase in the CH_3 concentration [13]. The band at 1380 cm^{-1} in the most highly degraded material may be assigned to the carbon—hydrogen deformation frequency for the aliphatic C—CH_3 bond [13].

The removal of the band at 690 cm^{-1}, assigned to the C—Cl stretching vibration [3, 4], from the spectrum of the sample pyrolyzed at 300° C correlates with mass spectrometer and weight loss measurements [1] which showed that almost all the chlorine atoms were removed from the polymer at this temperature.

The infrared spectra of the PVC–γ polymer after pyrolysis at several temperatures are shown in figure 4. The changes in the spectra as a result of increasing the pyrolysis temperature are similar to those observed for the PVC-bp material. The spectrum of the specimen degraded at 250° C can be readily identified as poly(vinyl chloride). Increasing the temperature to 275° C gives a spectrum, from 1400 to 650 cm^{-1} that is different from the spectrum of poly(vinyl chloride). This is probably caused by the almost complete removal of chlorine atoms as shown by the absence of a band at 690 cm^{-1}. The presence of the conjugated aromatic structure is revealed in the spectra of the specimens pyrolyzed at 342° and 400° C by the bands at 880, 820, 750, 700 cm^{-1} and the shoulder at 1490 cm^{-1}. There is also absorption caused by aromatic structure in the spectrum of the specimen pyrolyzed at 275° C.

The spectra of the pyrolyzed PVC—azo sample is shown in figure 5. The same general observations made with the PVC—bp and PVC—γ polymers also apply to this material. However, this sample is observed to have undergone more degradation at a given temperature than the other two polymers did. For example, no C—Cl stretching band at 690 cm^{-1} remains in the specimen pyrolyzed at 253° C, while this band is relatively intense for the PVC—bp polymer, pyrolyzed at the same temperature. This is in agreement with the faster rate of decomposition, as measured by rate of weight loss for this material as previously reported [1]. This faster rate was attributed to unreacted catalyst remaining in the sample.

The pyrolysis of poly(vinyl chloride) produces volatile products and a solid residue. At 400° C some of these products are volatile at the temperature of pyrolysis but not at room temperature. This portion is a brown, waxlike material at room temperature. The spectrum of this wax is similar to that of the more highly degraded specimens observed earlier and probably consists of fragments of the dehydrochlorinated polymer. The C—Cl band at 690 cm^{-1} is absent, accounting for a flat spectrum observed at the lower wave numbers. A broad carbonyl band at 1730 cm^{-1} is probably the result of the oxidation of double bond structures following the pyrolysis. The CH vibration [3] in CH_2 is shifted from 1430 cm^{-1} in the original material to 1470 cm^{-1}. A band at 1380 cm^{-1}, assigned to the C—H deformation for the aliphatic C—CH_3 bond [13], is present in this spectrum as well as in the spectrum of the residue of the material pyrolyzed at 400° C. Although there are weak bands at 700,

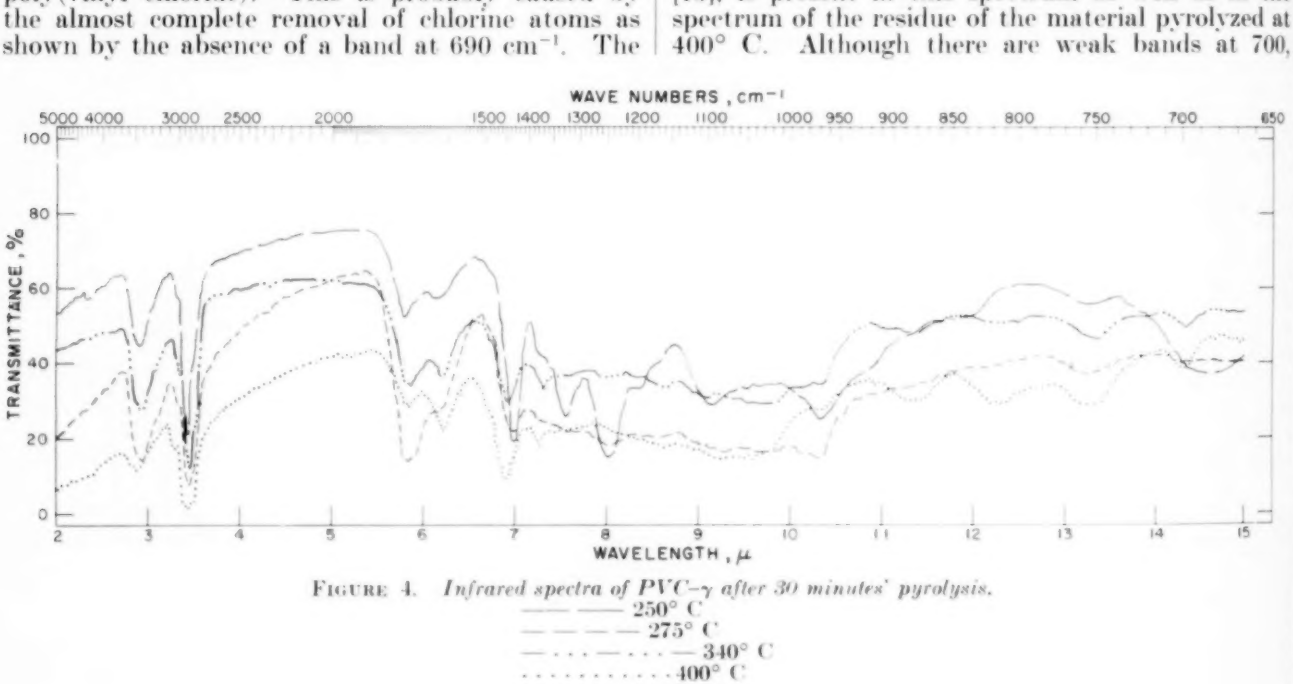

FIGURE 4. *Infrared spectra of PVC–γ after 30 minutes' pyrolysis.*
—— —— 250° C
— — — — 275° C
— · · — · · — 340° C
· · · · · · · · · · 400° C

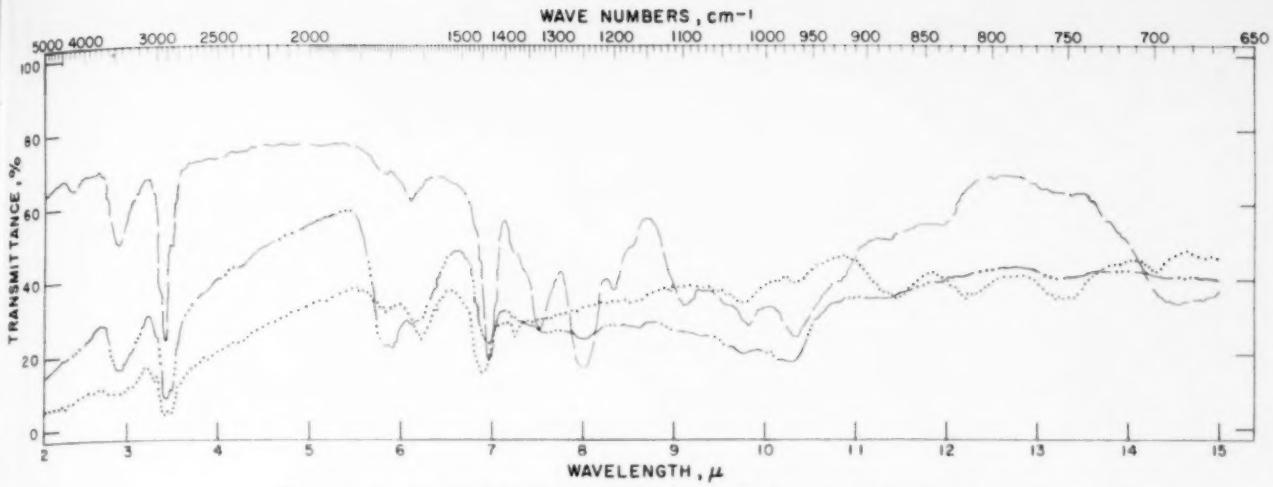

FIGURE 5. *Infrared spectra of PVC–azo after 30 minutes' pyrolysis.*
— — — — — 220° C
— · — · — · — 255° C
· · · · · · · · · 400° C

720, and 755 cm^{-1}, the relatively intense bands assigned to aromatic structures in the spectrum of the residue of the material pyrolyzed at 400° C are absent from this spectrum. The differences between the spectrum of the residue and the spectrum of the waxlike material are attributed to the different molecular weights of these portions.

4. Conclusions

Specimens pyrolyzed in a vacuum at temperatures up to 400° C yielded some spectra that were decidedly different from the original material and which varied from each other depending upon the temperature. The volatile products obtained from the poly(vinyl chloride) polymers at temperatures up to 300° C consisted primarily of HCl and a few mole percent of benzene [1]. At 400° C, the volatile products produced from the dehydrochlorinated polymer consisted, in addition, of larger quantities of benzene and various hydrocarbons. The principal alterations in the infrared spectra of these degraded specimens were loss of chlorine atoms, with complete removal at temperatures near 300° C, establishment of double bond character, both aliphatic and aromatic, and a possible increase in CH_3 concentration. A variety of carbonyl structures is formed when the degraded material is allowed to stand exposed to the air for several days at room temperature. Within the limits of this technique the spectral changes are independent of polymerization initiators used.

The mechanism of the decomposition appears to be a removal of chlorline as HCl in such a manner as to form a conjugated polyene structure, even when only small quantities of chlorine have been removed. No infrared evidence was found for hydroperoxides. It appears reasonable, therefore, that oxygen does not play a direct role in the dehydrochlorination process of the systems studied here, but adds to the double bond structure, producing the oxygenated structures observed. This action may further degrade the polymer by reducing the size of the chain. The infrared technique was, however, insensitive to measurement of chain length, although the apparent rise in methyl group concentration is an indication of an increased number of chain ends.

The formation of aromatic structures in the spectra of the degraded aliphatic poly(vinyl chloride) correlates with the presence of benzene in the volatile products of such decomposition reactions [1]. This indicates that an aliphatic conjugated structure is present at chain ends. This structure can occur as a result of dehydrochlorination at the original ends, either by initiation or termination, or by sission of an internal portion of a dehydrochlorinated chain. The dehydrochlorination reaction that has been previously proposed [1] would allow a free radical at the end of a polyene group in either instance. As a result of kinetic motion, various cyclic configurations are formed. Because of resonance considerations, benzene is the most stable structure, and as a result of this stabilization, the carbon—carbon bond alpha to the benzene ring is weakened and breaks, evolving benzene as a product. The more complete removal of chlorine at the higher temperatures, together with the increased opportunity for chain cleavage at these elevated temperatures, yields a more aromatic structure. Moreover, the material that is volatile at the temperature of pyrolysis but not at room temperature apparently consists of short aliphatic segments of the residue.

The authors express appreciation to the following members of the National Bureau of Standards: James E. Stewart for his suggestions regarding some of the interpretations and for obtaining some of the spectra, and Mary R. Harvey and Mary K. Wharton for preparing some of the spectra.

5. References

[1] R. R. Stromberg, S. Straus, and B. G. Achhammer, Thermal decomposition of poly(vinyl chloride) in a vacuum (presented at the 139th meeting of the American Chemical Society, Atlantic City, N. J., Sept. 1956).

[2] C. S. Marvel, Synthetic polymers of organic chemistry, an advanced treatise, vol. I, p. 754, edited by Gilman (John Wiley & Sons, Inc., New York, N. Y., 1943).

[3] J. E. Campbell and W. H. Rauscher, J. Polymer Sci. **18,** 461 (1955).

[4] S. Krimm and C. Y. Liang, J. Polymer Sci. **22,** 95 (1956).

[5] C. S. Marvel, J. H. Sample, and M. F. Ray, J. Am. Chem. Soc. **61,** 324 (1939).

[6] C. S. Fulla, Chem. Revs. **26,** 143 (1940).

[7] H. W. Thompson and P. Torkington, Proc. Roy. Soc. (London) [A] **184,** 21 (1945).

[8] H. W. Thompson and P. Torkington, Trans. Faraday Soc. **41,** 246 (1945).

[9] J. D. Cotman, Jr., Ann. N. Y. Acad. Sci. **57,** 417 (1953).

[10] A. L. Scarbrough, W. L. Kellner, and P. W. Rizzo, Modern Plastics **29,** 111 (1952); Polymer degradation mechanisms, p. 95, NBS Circ. 525 (1953).

[11] V. W. Fox, J. G. Hendricks, and H. J. Ratti, Ind. Eng. Chem. **41,** 1774 (1949).

[12] M. R. Harvey, J. E. Stewart, and B. G. Achhammer, J. Research NBS **56,** 225 (1955) RP2670.

[13] L. J. Bellamy, The infrared spectra of complex molecules (John Wiley & Sons, Inc., New York, N. Y., 1954).

[14] J. Linnig and J. E. Stewart, J. Research NBS **59,** 27 (1957) RP2771.

WASHINGTON, July 24, 1957.

U. S. GOVERNMENT PRINTING OFFICE: 1958

THE NATIONAL BUREAU OF STANDARDS

The scope of activities of the National Bureau of Standards at its headquarters in Washington, D. C., and its major field laboratories in Boulder, Colorado, is suggested in the following listing of the divisions and sections engaged in technical work. In general, each section carries out specialized research, development, and engineering in the field indicated by its title. A brief description of the activities, and of the resultant publications, appears on the inside of the front cover.

WASHINGTON, D. C.

Electricity and Electronics. Resistance and Reactance. Electron Devices. Electrical Instruments. Magnetic Measurements. Dielectrics. Engineering Electronics. Electronic Instrumentation. Electrochemistry.

Optics and Metrology. Photometry and Colorimetry. Optical Instruments. Photographic Technology. Length. Engineering Metrology.

Heat. Temperature Physics. Thermodynamics. Cryogenic Physics. Rheology. Engine Fuels. Free Radicals Research.

Atomic and Radiation Physics. Spectroscopy. Radiometry. Mass Spectrometry. Solid State Physics. Electron Physics. Atomic Physics. Neutron Physics. Nuclear Physics. Radioactivity. X-rays. Betatron. Nucleonic Instrumentation. Radiological Equipment. AEC Radiation Instruments.

Chemistry. Organic Coatings. Surface Chemistry. Organic Chemistry. Analytical Chemistry. Inorganic Chemistry. Electrodeposition. Molecular Structure and Properties of Gases. Physical Chemistry. Thermochemistry. Spectrochemistry. Pure Substances.

Mechanics. Sound. Mechanical Instruments. Fluid Mechanics. Engineering Mechanics. Mass and Scale. Capacity, Density, and Fluid Meters. Combustion Controls.

Organic and Fibrous Materials. Rubber. Textiles. Paper. Leather. Testing and Specifications. Polymer Structure. Plastics. Dental Research.

Metallurgy. Thermal Metallurgy. Chemical Metallurgy. Mechanical Metallurgy. Corrosion. Metal Physics.

Mineral Products. Engineering Ceramics. Glass. Refractories. Enameled Metals. Concreting Materials. Constitution and Microstructure.

Building Technology. Structural Engineering. Fire Protection. Air Conditioning, Heating, and Refrigeration. Floor, Roof, and Wall Coverings. Codes and Specifications. Heat Transfer.

Applied Mathematics. Numerical Analysis. Computation. Statistical Engineering. Mathematical Physics.

Data Processing Systems. SEAC Engineering Group. Components and Techniques. Digital Circuitry. Digital Systems. Analog Systems. Application Engineering.

• Office of Basic Instrumentation.

• Office of Weights and Measures.

BOULDER, COLORADO

Cryogenic Engineering. Cryogenic Equipment. Cryogenic Processes. Properties of Materials. Gas Liquefaction.

Radio Propagation Physics. Upper Atmosphere Research. Ionospheric Research. Regular Propagation Services. Sun-Earth Relationships.

Radio Propagation Engineering. Data Reduction Instrumentation. Modulation Systems. Navigation Systems. Radio Noise. Tropospheric Measurements. Tropospheric Analysis. Radio Systems Application Engineering.

Radio Standards. High Frequency Electrical Standards. Radio Broadcast Service. High Frequency Impedance Standards. Calibration Center. Microwave Physics. Microwave Circuit Standards.

Recent Publications of the National Bureau of Standards

Periodicals

Journal of Research of the National Bureau of Standards, Volume 59, No. 6, December 1957 (RP2806 to RP2814 incl.). 60 cents. Annual subscription $4.00, $1.25 additional for foreign mailing.

Technical News Bulletin, Volume 41, No. 12, December 1957. 10 cents. Annual subscription $1.00, 35 cents additional for foreign mailing.

Basic Radio Propagation Predictions for March 1958. Three months in advance. CRPL-D 160. Issued December 1957. 10 cents. Annual subscription $1.00, 25 cents additional for foreign mailing.

Building Materials and Structures Reports

BMS151. Thermal resistance of airspaces and fibrous insulations bounded by reflective surfaces. 20 cents.*

Circulars

C587. Electroforming of waveguide components for the millimeter-wavelength range. 15 cents.*

Available from the Superintendent of Documents, U. S. Government Printing Office, Washington 25, D. C. The three NBS periodicals are available on a 1-, 2-, or 3-year subscription basis, although no reduction in rates can be made.

**Foreign postage, one-fourth additional.*

UNITED STATES
GOVERNMENT PRINTING OFFICE
DIVISION OF PUBLIC DOCUMENTS
WASHINGTON 25, D. C.

OFFICIAL BUSINESS

PENALTY FOR PRIVATE USE TO AVOID PAYMENT OF POSTAGE, $300 (GPO)

Journal of Research of the National Bureau of Standards Vol. 60, No. 2 February 1958

Contents

		Page
Energy spectra of cascade electrons and photons. Charles A. Olson and Lewis V. Spencer.	RP2824	85
Observer differences in color-mixture functions studied by means of a pair of metameric grays. Kenneth L. Kelly.	RP2825	97
Precise evaluation of surface area with indirectly calculated dead space. William V. Loebenstein.	RP2826	105
Sample calculations of gamma-ray penetration into shelters: Contributions of sky shine and roof contamination. Martin J. Berger and James C. Lamkin.	RP2827	109
Heat content of sodium borohydride and of potassium borohydride from 0° C to 400° C. Thomas B. Douglas and Ann W. Harman.	RP2828	117
Infrared spectra of crystalline polyphenyls. James E. Stewart and Max Hellmann.	RP2829	125
On the application of steam-driven water jets for propulsion purposes. J. M. Burgers and A. Ghaffari.	RP2830	137
Mass spectra and relative sensitivities of some polyphenyls. Paul Bradt and Fred L. Mohler.	RP2831	143
Infrared spectra of thermally degraded poly(vinyl chloride). Robert R. Stromberg, Sidney Straus, and Bernard G. Achhammer.	RP2832	147

[A list of recent NBS publications is given on page 3 of the cover.]

For sale by the Superintendent of Documents, U. S. Government Printing Office, Washington 25, D. C. Price 60 cents (single copy). Subscription price: $4.00 a year; $1.25 additional for foreign mailing.

UNITED STATES GOVERNMENT PRINTING OFFICE, WASHINGTON : 1958